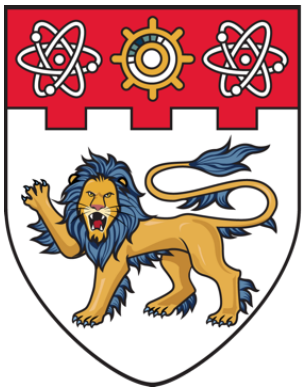

NANYANG TECHNOLOGICAL UNIVERSITY
SINGAPORE

Phase Separation in Active Matter: from Schematic to Realistic Models

Pin Nie

School of Physical and Mathematical Science

2019

Phase Separation in Active Matter: from Schematic to Realistic Models

Pin Nie

School of Physical and Mathematical Science

A thesis submitted to the Nanyang Technological University
in partial fulfillment of the requirements for the degree of
Doctor of Philosophy

2019

Statement of Originality

I hereby certify that the work embodied in this thesis is the result of original research done by me except where otherwise stated in this thesis. The thesis work has not been submitted for a degree or professional qualification to any other university or institution. I declare that this thesis is written by myself and is free of plagiarism and of sufficient grammatical clarity to be examined. I confirm that the investigations were conducted in accord with the ethics policies and integrity standards of Nanyang Technological University and that the research data are presented honestly and without prejudice.

05\12\2019 .....

Date

Pin Nie

Supervisor Declaration Statement

I have reviewed the content and presentation style of this thesis and declare it of sufficient grammatical clarity to be examined. To the best of my knowledge, the thesis is free of plagiarism and the research and writing are those of the candidates except as acknowledged in the Author Attribution Statement. I confirm that the investigations were conducted in accord with the ethics policies and integrity standards of Nanyang Technological University and that the research data are presented honestly and without prejudice.

05\12\2019

.....

Date

.....

Prof. Massimo Pica Ciamarra

Authorship Attribution Statement

This thesis does not contain any materials from papers published in peer-reviewed journals or from papers accepted at conferences in which I am listed as an author.

05\12\2019

.....

Date

.....

Pin Nie

Abstract

Large density fluctuations are commonly observed in biological systems of self-propelling particles. Examples we are all familiar with include fish schools, bird flocks, herds of animals. These density fluctuations are frequently interpreted as the manifestation of phase separation, despite the underlying system being out of thermal equilibrium. The active elements consume energy to self-propel. Due to the absence of a thermodynamic description, a question of great interest concerns the identification of the microscopic processes that induce these density fluctuations, as well as to develop of a non-equilibrium theory to predict the phase diagram of these systems.

Research in this direction follows two paths. On one side, we might assume these density fluctuations originate from underlying physical processes that are universal across different biological systems. Hence, to rationalize the microscopic origin of these fluctuations, one might devise simple models which are able to reproduce them and then investigate these models in detail. On the other side, one might acknowledge that different biological systems are different, and hence try to understand a particular system. In my research work, I have followed both approaches to some extent.

The most significant part of my research work, and hence of this thesis, focused on the investigation of a prototypical schematic model of the active particle, known as Active Brownian Particles (ABPs). This model describes a collection of particles interacting via short-range repulsive forces, experiencing thermal noise and self-propelling force.

The self-propulsion results from an active force acting on each particle, which differs across particles, whose directions are persistent on nature. This active force induces a velocity, known as the active velocity of the particles. At high enough particle density and high enough active velocity, ABPs undergo a transition from a

homogeneous to a phase-separated state. How does this happen? How it is possible that, in the absence of attractive forces, a group of particles condense?

The ABPs model is by-far the most investigated model of active particles. And indeed, when I started my thesis, I assumed the microscopic origin of its motility-induced phase separation to be clear. It was not the case. In literature, there are two competing theoretical approaches, one based on a kinetic description and the other on a hydrodynamic-like formulation. Apart from being in contradiction regarding to the identification of underlying physical processes driving the phase separation, these models are unable to make accurate quantitative predictions.

In this line of research, my main contribution has been in developing a theoretical model to predict the limit of stability of ABPs, as a function of the density of the particles and the motility strength. I have then numerically validated my theoretical model, in both two and three spatial dimensions, and as a function of different control parameters involved. My theoretical model results from a novel understanding of the underlying mechanism which is missed by the community before. In particular, I have identified a previously unreported physical process that promotes the destruction of the density fluctuations and formalizes its dependence on the different control parameters. In the kinetic description of ABPs, the decay of the density fluctuation has been associated to the diffusivity of the self-propelling direction. In the continuum approach, it was attributed to the particle diffusivity. I have shown that the motility also induces the decay of the density fluctuations.

This novel motility-induced physical process is fundamental to correctly predict the spinodal line, which results from the balance of physical processes promoting and suppressing density fluctuations.

As an extension of this project and partially motivated by the desire of understanding the phase separation occurring in systems of self-propelled colloidal particles, I have investigated how friction affects the motility induced phase separation. Indeed, friction is certainly present in dry experiments of active matter, and might also be relevant in wet experiments, where the active particles are suspended in a fluid. Recent experiments on colloidal suspensions under shear have indeed demonstrated the unexpected relevance of frictional forces. I have numerically demonstrated and theoretically rationalized, how friction affects the different physical mechanisms promoting and suppressing density fluctuations in active Brownian

particles. As a consequence, I have streamlined the physical origin of the qualitatively marked differences between the phase diagram of frictionless and frictional particles.

Another line of research, I have developed during my Ph.D. concerned the physics of a specific biological system of active particles: microbial biofilms. This is a research activity carried out in collaboration with SCELSE, the Singapore Centre for Environmental Life Sciences Engineering. The goal has been that of rationalizing all of the relevant processes influencing the early-stage biofilm formation, to develop a particle-resolved numerical model with that would help investigate the underlying physics. This is, therefore, a more interdisciplinary project, which required some understanding of the biological processes occurring in biofilms. In literature, there are just a few numerical models describing this process, and all of them seem to neglect what appears to be key biofilm features.

In this line of research, my main contribution has been the identification of all the relevant physical processes, and the developing of a numerical model able to describe the early stage biofilm formation. This has been a very complicated task, as bacteria move, grow and divide, leave a trail as they move and interact with it, like ants. In addition, they extrude polymers, known as extracellular polymeric substances, to which they may bond and ends up to be embedded in a protective gel-like polymeric matrix. The level of complexity is enormous, when compared to the schematic ABPs model. After developing the model, tailoring the many free parameters using available experimental data on the pathogen Pseudomonas Aeruginosa, I have investigated a few aspects of particular interests. My numerical results well compare with experimental data, which however are scarce, and shed light on the role and of the interplay of different parameters. For instance, I have demonstrated competition between the typical velocity of the bacteria and their reproduction rate, as well as the possibility of an auto-limited growth induced by the production of extracellular polymeric substances.

Summarizing, in my thesis, I fully rationalized the physic of the most studied schematic model of active particles, the active Brownian particles model. Also, I have developed a more realistic model to describe the early stage formation of biofilm, using it to investigate how different parameters affect the forming of a biofilm.

Acknowledgements

First of all, I would like to give my most enormous gratitude to my supervisor, Professor Massimo Pica Ciamarra, for his kindness and patience in guiding me throughout my Ph.D. study. His ability to explain abstract concepts in simple terms helped me understand the complex soft matter topic. His confident attitude impressed me and motivated me. From him, I learned how numerical simulations could work as a powerful tool to study and examine physical problems. I also wish to give my deepest gratitude to Professor Ran Ni for his help in supervising me in the later part of my Ph.D. study. His provocative questions have been inspiring.

I enjoyed collaborating with Dr. Joyjit Chattoraj, who always answers my questions with great competence. He provided a lot of help and guided my patiently. I also enjoyed discussing with Dr. Yanwei Li, appreciating his detailed knowledge of the physics of phase transitions. I enjoyed the company of Dr. Sudhir. His cheerful spirit inspired me up and generated a friendly environment in the lab. The arrival of these three postdocs has been crucial in my second year of Ph.D. study. At that time, I was depressed and lost in direction. They made the office a more delightful place to stay, with fun and meaningful discussions. I learned a lot from them. I also enjoyed the time with the rest Ph.D. students who joined in the following years, Shivam, Anshuman, Emma, Yuanjiang, and Xinyang.

I want to thank Ms. Alison for her professionalism as the manager of Student Development Office at NTU. Her supportive manners and the careful management of Graduate Students' Associations facilitated the organization of many interesting events. I developed my leadership skills and made many friends. My involvement in the Graduate Students' Association has been important to me, as it brightened my life and helped me gaining more confidence. We become close friends and maintain contact after I left the director position.

I also appreciate the time that I have spent with my friends in school activities, exercises and traveling, which made my stay in NTU so joyful and memorable.

Mainly, I enjoyed the friendship of my fellow Ph.D. students Wang You and Jia Guichong as we walk through Ph.D. struggles together.

My special thanks to the University Well-being Centre, the staffs, and consultants working there. During a hard time of my Ph.D., they helped me to think positively towards the difficulty in life, although sometimes you cannot change it. With their help, I gradually controlled my depression state.

Last but not least, I want to thank my beloved husband Dr. Bo En, my wise father, and my caring mother. Without their unconditional love, support, and understanding, I could not managed to achieve these results.

Contents

List of Figures

Part I

Introduction and Background

Chapter 1

Introduction

1.1 Background and motivation

The term 'active matter' indicates systems of particles that can transduce energy to self-propel. This field originated from the interest in the behavior of living systems like bird flocks, fish schools, bacteria swarms, cell tissues, and so on [1]. Since particles consume energy to self-propel, active systems are far from thermal equilibrium, and their collective behaviors cannot be directly explained by equilibrium statistic mechanics. Hence, the study of active matter systems is closely tied to the development of non-equilibrium statistical mechanics.

Active matter models were initially designed to study the swarm behavior of animals at the macroscale. Reynolds' Boid model [2] was introduced to simulate the collective motion of flocks of birds, schools of fish and herds of land animals. The Boids model contains three significant rules, including separation, alignment, and cohesion rules. A particular Boids model, which become extremely popular in literature, is the Vicsek model [3], where particles move at a constant speed. Particles have a so-called aligning interaction, as the direction of the self-propelling velocity of each particle aligns to the average self-propelling direction of the neighboring particles. Boids model and Vicsek model have been proven useful in describing the collective behavior of many systems of active particles. Also, these models are routinely used in applications like graphic computer simulations, unmanned ground vehicles, and self-assemble robotics.

The term 'active matter' also refers to systems of biological self-propelling particles influenced by stochastic forces, like bacteria, eukaryotic cells, filaments, and microtubules. These elementary particles not only self-propel but are also under the influence of thermal fluctuations. Their self-organizing phenomena and complex movements have been closely investigated by the physics and biophysics communities, in recent years. For instance, it is known that bacteria on a surface move diffusing via a run-and-tumble motion. While diffusing, they reproduce and perform other complex biological processes, and could also detach from the surface. Then, the bacteria stick to the surface in small groups, known as microcolonies. The emergence of these microcolonies appears to coincide with the transition from reversible to irreversible attachment of the bacteria, and is the initial state of development of a biofilm. There is considerable interest in the understanding of these complex biophysical process, which are frequently described by using a language borrowed from the statistical mechanics community, e.g. identifying the microcolonies with the critical nuclei that seed crystallization. Many researchers explore this and similar analogies between out-of-equilibrium and equilibrium thermal systems.

Experimentalists working in this area do not limit themselves to the observation of the collective behavior of systems of active biological particles. On the contrary, they have been remarkably able to fabricate artificial microswimmers which self-propel. This allowed for the emergence of well-controlled and reproducible experiments, used as a benchmark by the emerging theoretical approach. The experimental and theoretical research in this field is also complemented by numerical simulations.

My Ph.D. research project started within a collaboration with SCELSE, the Singapore Centre for Environmental Life Sciences Engineering. The original goal was that of developing a model to describe the early stage biofilm formation. The result of this investigation is described in the second part of my thesis. While trying to rationalize how individual bacteria agglomerate in the early stage of biofilm formation and form the so-called microcolonies, I explored concepts and methods to understand the so-called motility induced phase separation [4]. In doing that, I realized that the physical process underlying this phase separation were not clear, not even in the case of the much investigated Active Brownian Particles (ABPs)

model. Since I do believe that, without a clear understanding of the physics of simple models, there is little hope to understand complex ones, I started considering the ABPs model. The result of this investigation is in the first part of the thesis.

Physicists always try to find simple models to describe the general features of a class of systems. In the active matter context, the de-facto standard model is that of active Brownian particles (ABPs). In this model, particles undergo translational and rotational Brownian diffusion, while subject to a constant force whose direction rotates with the particles. Isolated particles thus perform a persistent random walk, whose persistence time set by the rotational diffusion coefficient. Despite its simplicity, this model allowed for a number of insight into the physics of active systems. For instance, the model allowed for the clear observation of a motility induced phase separation, in systems of particles interacting via steric repulsive forces. Indeed, at high enough density and self-propelling force, active Brownian particles phase separate in coexisting gas-like and liquid-like phases, in the absence of an attractive interaction between the particles. Such a motility-induced phase separation (MIPS) [5, 6] reminds of the gas-liquid phase separation where normally attractive interaction is required. In the absence of attraction, MIPS originates from a positive feedback mechanism that couples the self-propelling velocity to the local density, whereby particles are slower in a dense environment [4]. The positive feedback originates from the fact that particles in high density region hinder their respective motion, and are thus slower than the other particles. This causes a reduction of the pressure in the dense regions, and hence a flux of particles from low- to high-density regions. Density fluctuations are therefore enhance themselves.

Two approaches have been proposed in the literature to rationalize the motility induced phase separation of ABPs, a continuum approach [4] and a kinetic one [7]. Both approaches correctly predict only few features of the motility induced phase separation (MIPS) of ABPs, which indicates that a clear understanding of the underlying physics is missing. The kinetic theory starts from assuming the system to be phase-separated and derives an equation for the evolution of the size of a dense cluster. This equation considers the existence of an influx of particles moving from the low-density phase to the cluster, and of an opposite outflux. In Redner's theory [7], phase separation is promoted by the active velocity, and the homogeneous phase is promoted by rotational diffusion of the particles. The theory favorably compares to numerical simulations for the coexistence curve close

to the critical point. However, it fails to predict a U-shaped coexistence/spinodal line in the density-activity plane. Also, the theory introduces some ad-hoc scaling factors whose physical origin is ambiguous. The alternative continuum description of ABPs [6, 8, 9] predicts a U-shape phase diagram, but it underestimates the smallest value of the activity at the critical point by at least a factor 10. In the continuous theory, phase separation is also promoted by mobility, while the homogeneous phase is promoted by translational diffusion.

In this line of research, my main contribution has been that of introducing a theory that correctly describes the phase diagram of ABPs, which are considered the 'Ising' model for active systems. I have uncovered a physical process that promotes the destruction of dense clusters, neglected by both the kinetic and the continuous approaches. Specifically, I have demonstrated that a dense cluster of active particles rotates and that this rotation makes it unstable. The cluster dissolves into individual gas particles. This physical process can be related to the way two colliding active particles in the homogeneous gas phase can resolve their collision. In particular, it has not been considered in previous works that particles can slide one-past the other. By formalizing this physical process, I was able to derive a simple theoretical prediction for the spinodal line, which favourably compares to numerical simulations.

The novel physical process I have uncovered is at work in ABPs as the self-propelling directions of the particles is not affected by the interparticle collisions. Recent works have suggested that even for colloidal scale particles [10], the interparticle interaction could be affected by frictional forces. In particular, in the case of colloidal particles under shear, friction appears to be responsible for a drastic increase of the shear viscosity, a phenomenon known as discontinuous shear-thickening.

Surprisingly, and despite the existence of experimental systems where the active particles are macroscopic objects [11, 12], the effect of frictional forces has not been investigated in the context of active systems. I have performed this investigation and found out that friction changes the dynamics of the active particles in both the dense phase and the dilute regime when the motility is strong enough. Besides, friction strongly affects the physical processes inducing the phase separation of active systems, and hence, qualitatively changes the motility induced phase diagram.

In the last part of my thesis, I move away from the investigation of simple schematic models of active systems, and report the study of a model for bacteria. The aim is that of investigating the early stage of biofilm formation, and particularly the factor that might influence the formation of small bacterial colonies, known as microcolonies. Biological systems are infinitely more complex than the schematic ones. The motility of bacteria on a surface is a complex process. Bacteria can reproduce, die, attach, and detach from the surface, produce the so-called extracellular polymeric matrix and bind to it, etc. The complexity is enormous. The experimental investigation of the role of all of these factors is challenging, as it is difficult to tune them. In this line of research, my contribution has been that of developing a numerical toolbox which allows for the investigation of the role of these factors on biofilm growth. In the thesis, I will present applications of this toolbox, e.g., to investigate how the formation of a biofilm is affected by the motility of the bacteria, the reproduction rate, psl. etc. My results indicate that bacteria reproduction is a key ingredient promoting density fluctuations. In this respect, the physics governing bacteria systems appears to be quite distinct from that controlling simple model of self-propelled particles.

1.2 Objective and scope

My thesis aims at better rationalization of the physical processes responsible for the phase separation of systems of active particles, considering both schematic models and more realistic ones. The scope of this thesis is:

1. Rationalize the physical processes responsible for the phase separation of the prototypical Active Brownian Particle model.

2. Investigate how the frictional interaction affects the dynamics and phase diagram in active Brownian sphere model.

3. Develop a useful toolbox to investigate the early-stage biofilm formation, and the role of key biological processes, such as reproduction and production of extracellular matrix on microcolonies formation.

1.3 Novelty and significance

1. I have identified a previously unreported physical mechanism, which is responsible for the instability of fluctuation of the density (clusters) in the prototypical system of Active Brownian Particles. I have formalized this mechanism in a theoretical framework which can correctly predict the phase boundary of this system, as well as its dependence on the various control parameters.

2. I have performed first investigation of the role of friction in the motility induced phase separation of active systems. I have clarified that friction strongly affects the physical process, by inducing phase separation and qualitatively affecting the motility induced phase diagram.

3. I have developed a toolbox for the investigation of the early stage formation of biofilm. Bacteria are modeled as realistically as possible, and the different control parameters have been chosen to reproduce available experimental data, when possible. Using this toolbox, I have investigated the formation of microcolonies, uncovered an interplay between the growth rate of the bacteria and their motility. I also investigated the role of self-produced adhesion psl on the formation of microcolonies through attractive interactions.

1.4 Outline of thesis

Chapter 1 briefly reviews key aspects of the active matter field and the scope of the thesis and describes the physical problems that have motivated this research work. Much of the literature work on active matter focused on the prototypical model of Active Brownian Particles. Chapter 2 describes this model, discusses the equation of motion to the role of the inter-particle interaction, previous results on the dynamical properties of the model and on its Motility Induced Phase Separation (MIPS). Following chapters also review the current leading theories developed to describe MIPS in these systems, as well as their limitations. Chapter 3 discusses my numerical investigation of frictionless ABPs, in both two and three dimensions. The chapters also highlight a novel mechanism being responsible for the suppression of phase-separated state, and a theoretical model being able to correctly describe the

phase diagram of this system and overcome the limitations of previous approaches. Chapter 4 is dedicated to the first investigation of the effect of friction in active systems. I demonstrate that the friction drastically affects the features of the motility induced phase separation and rationalize by considering how friction affects the rotational motion of the particles as well as their ability to slide one past the other. Chapter 5 reviews the current state of research on the early-stage biofilm formation, and the relevance of this investigation. The chapters highlight some experimental observations which will guide the development of a model to describe the formation of a biofilm. This model is described in Chapter 6, where I introduce a useful toolbox to study the growth of bacteria colony on a surface. The chapter describes how different key biological factors are taken into account, including run-and-tumble motion, reproduction, self-produced adhesion psl. By using this toolbox, the chapters investigate how the growth of a microcolony is affected by the reproduction rate and motility of bacteria. Finally, Chapter 7 concludes this thesis and presents some potential ideas for future work.

References

[1] Clemens Bechinger, Roberto Di Leonardo, Hartmut Löwen, Charles Reichhardt, Giorgio Volpe, and Giovanni Volpe. Active particles in complex and crowded environments. *Reviews of Modern Physics*, 88(4):045006, 2016.

[2] Craig W Reynolds. *Flocks, herds and schools: A distributed behavioral model*, volume 21. ACM, 1987.

[3] Tamás Vicsek, András Czirók, Eshel Ben-Jacob, Inon Cohen, and Ofer Shochet. Novel type of phase transition in a system of self-driven particles. *Physical review letters*, 75(6):1226, 1995.

[4] Michael E Cates and Julien Tailleur. Motility-induced phase separation. *Annu. Rev. Condens. Matter Phys.*, 6(1):219–244, 2015.

[5] Adam Wysocki, Roland G Winkler, and Gerhard Gompper. Cooperative motion of active brownian spheres in three-dimensional dense suspensions. *EPL (Europhysics Letters)*, 105(4):48004, 2014.

[6] Yaouen Fily and M Cristina Marchetti. Athermal phase separation of self-propelled particles with no alignment. *Physical review letters*, 108(23):235702, 2012.

[7] Gabriel S Redner, Michael F Hagan, and Aparna Baskaran. Structure and dynamics of a phase-separating active colloidal fluid. *Physical review letters*, 110(5):055701, 2013.

[8] Joakim Stenhammar, Adriano Tiribocchi, Rosalind J Allen, Davide Marenduzzo, and Michael E Cates. Continuum theory of phase separation kinetics for active brownian particles. *Physical review letters*, 111(14):145702, 2013.

[9] Thomas Speck, Julian Bialké, Andreas M Menzel, and Hartmut Löwen. Effective cahn-hilliard equation for the phase separation of active brownian particles. *Physical Review Letters*, 112(21):218304, 2014.

[10] Takeshi Kawasaki and Ludovic Berthier. Discontinuous shear thickening in brownian suspensions. *Physical Review E*, 98(1):012609, 2018.

[11] Julien Deseigne, Olivier Dauchot, and Hugues Chaté. Collective motion of vibrated polar disks. *Physical review letters*, 105(9):098001, 2010.

[12] Chiao-Peng Hsu, Shivaprakash N Ramakrishna, Michele Zanini, Nicholas D Spencer, and Lucio Isa. Roughness-dependent tribology effects on discontinuous shear thickening. *Proceedings of the National Academy of Sciences*, 115(20):5117–5122, 2018.

Part II

Active Brownian Particles

Chapter 2

Active Brownian particles: overview

2.1 Introduction

Systems of self-propelled particles give rise to a variety of collective phenomena. Most frequently, these involve the spontaneous agglomeration of the particles, i.e., the spontaneous growth of density fluctuations. We are indeed all familiar with the observation of flocks of birds, schools of fishes, herds of animals. How does this spontaneous phase separation emerge? Several physical and biological processes may be involved, and these processes may depend on the specific system one considers. However, there is certainly a common theme in all of these processes that demand an explanation. From a physical perspective, the convenient thing to do to investigate this question is that of resorting to the simplest model able to reproduce this observed behavior, in an attempt to grasp the underlying physical processes at work. In the case of the active system, this model appears to be the Active Brownian Particles (ABPs) model. The ABPs model was introduced initially to model motile microorganisms, and has been heavily investigated both numerically and theoretically. Experimentally, this model is related to the behavior of self-propelled synthetic swimmers, although there are significant differences. In this chapter, I will review the basic physical features of this model. The model will be defined first, and the phenomenology observed in previous works described. After that, I will detail the theoretical approaches developed to rationalize the

observed phenomenology, highlighting their strong points and their weaknesses. Finally, I will revisit some relevant artificial ABPs experiments and discuss some open questions.

2.2 Active Brownian particles: model definition

By Active Brownian Particles, one refers to a system of particles that are subject to thermal noise, being therefore Brownian, while they self-propel, being therefore active. The self-propelling force acts along a direction, which changes as the particles revolve while undergoing rotational diffusion. The dynamics of this system is described by a Langevin equation to which an active force is added. In their most general form, the equations of motion for the translational $\mathbf{X}$ and the rotational θ degrees of freedom are the following:

$$M\ddot{\mathbf{X}} = -\nabla U(\mathbf{X}) + \mathbf{F_a} - \gamma\dot{\mathbf{X}} + \sqrt{2\gamma k_B T}\mathbf{R}(t) \tag{2.1}$$

$$I\ddot{\theta} = \mathbf{\Omega} - \gamma_r\dot{\theta} + \sqrt{2\gamma_r k_B T}\mathbf{R}(t) \tag{2.2}$$

Eq. (2.1) is the equation of motion for the translational degrees of freedom. Here γ is a damping parameter, $U(\mathbf{X})$ is the interparticle interaction potential, $\mathbf{F_a}$ is the active force, k_B is Boltzmann's constant, T is the temperature. $\mathbf{R(t)}$ is the Gaussian white noise, $\langle R_\alpha(t)R_\beta(t')\rangle = \delta(t-t')\,\delta_{\alpha\beta}$, α, β spacial indexes.

Eq. (2.2) is the equation of motion for the rotational degrees of freedom. Here I is the moment of inertia, γ_r is a damping parameter, Ω is the torque on particle, which can be expressed as $\mathbf{\Omega} = \mathbf{r} \times \nabla U(\mathbf{X})$. The noise terms in translation and rotation are uncorrelated.

The above equations have been considered only recently [1]. Indeed, most biological and synthetic active systems generally comprise colloidal scale particles, such as bacteria (0.5μm-5μm) or Janus particles (10nm-5μm), in a wet environment. In this condition, the inertia of the particles is negligible. When inertia is negligible, the equation of motion is the overdamped limit of Eq. (2.1) and Eq. (2.2). These equations are conveniently expressed in the following form:

$$\dot{\mathbf{X}}(t) = \frac{-\nabla U(\mathbf{X})}{\gamma} + \mathbf{v}_a + \sqrt{2D}\mathbf{R}(t) \tag{2.3}$$

$$\dot{\theta} = \frac{\mathbf{\Omega}}{\gamma_r} + \sqrt{2D_r}\mathbf{R}'(t) \tag{2.4}$$

where

$$\begin{aligned} \gamma &= 6\pi\eta r & D &= \frac{k_B T}{6\pi\eta r} \\ \gamma_r &= 8\pi\eta r^3 & D_r &= \frac{k_B T}{8\pi\eta r^3} \end{aligned} \tag{2.5}$$

The above equations describe overdamped ABPs, considering that the direction $\mathbf{n}$ of the self-propelling velocity rotates with the particle. That is, $\mathbf{v_a} = v_0\mathbf{n}$, where the director of particle i is $\hat{\boldsymbol{n}}_i = (\cos\theta_i, \sin\theta_i)$. D and D_r are the translational and the rotational diffusion of the passive suspension, where $\mathbf{v_a} = 0$, in the dilute limit in which the interparticle interaction can be neglected. Notice that D_r as the units of a frequency. $\tau_r = D_r^{-1}$ is the Brownian time, the decorrelation time needed of the angular velocity. In the following, we will use τ_r and D_r^{-1} interchangeably.

These above equations are those most often considered in the literature. We note, however, that the noise in translation is frequently neglected, e.g., as in [2]. Hence, D is set zero, in violation of the above Stokes-Einstein relation. We will discuss in the course of this thesis when this approximation is meaningful.

2.3 Interparticle interaction

The equation of motion for ABPs depends on the interparticle interaction. Inspired by colloidal scale experiments, as well as for the sake of simplicity, the vast majority of works considered purely repulsive finite ranged interaction potentials, which mimic the steric hindrance of a macroscopic object. Typical interaction potential are the Weeks-Chandler-Anderson (WCA), which is a Lennard-Jones potential truncated in its minimum

$$V(r) = 4\epsilon\left[\left(\frac{r}{\sigma}\right)^{-12} - \left(\frac{r}{\sigma}\right)^{-6}\right] + C; r \leq \sigma 2^{1/6} \tag{2.6}$$

$$V(r) = 0; r \geq \sigma 2^{1/6} \tag{2.7}$$

where the constant C is chosen so that assure the continuity of the potential, $V(\sigma 2^{1/6}) = 0$. Another common choice, which is one we will also consider, is the Harmonic interaction,

$$V(r) = \frac{1}{2}\epsilon(r-\sigma)^2; r \leq \sigma \tag{2.8}$$

$$V(r) = 0; r \geq \sigma \tag{2.9}$$

where σ is readily interpreted as the diameter of the particles.

These interaction potentials mimic frictionless spherical particles and do not lead to any torque acting on the particles. When these potentials are used, $\mathbf{\Omega} = 0$ in Eq. 2.4.

2.4 Control parameters

2.4.1 Length scales: volume fraction

The rotational and the translational diffusivity, which are related, give rise to a timescale, D_r^{-1}, which is the correlation time of the self-propelling direction. Another relevant timescale which characterizes the equation of motion is that time particles need to move a distance of the order of their diameter, in the dilute regime, σ/v_a. The ratio of these two parameters defines an important non-dimensional control parameter, the Peclet number

$$\mathrm{Pe} = \frac{v_a}{\sigma D_r}. \tag{2.10}$$

Notice that the alternative definitions of Peclet number are possible, which differ from the one above by a proportionality constant. This needs to be taken into account when comparing results from the literature.

Another timescale of ABPs might be, in principle, derived from the energy scale of the interaction potential. However, as already mentioned, the interaction potentials which are considered in the literature are stiff, mimicking an hard-sphere like repulsion, so that this additional time scale is most often neglected.

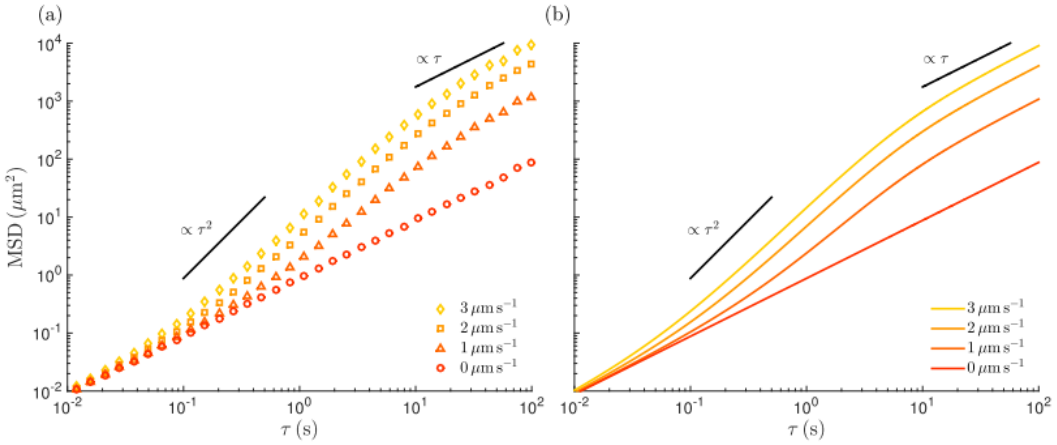

FIGURE 2.1: Mean square displacement (MSD) of active Brownian particles and effective diffusion coefficients. (a) Numerically calculated and (b) theoretical calculated. For passive Brownian particles (v = 0 ms1, circles) the motion is always diffusive ($MSD(\tau) \propto \tau$), while for active Brownian particles the motion is diffusive with diffusion constant D at very short time scales (MSD(τ) $\propto \tau$ for $\tau \ll \tau_r$), ballistic at intermediate time scales (MSD(τ) $\propto \tau^2$ for $\tau \approx \tau_r$), and again diffusive but with an enhanced diffusion constant at long time scales (MSD(τ) $\propto \tau$ for $\tau \gg \tau_R$).[3]

In the literature, it is also common to compare the above two time scales introducing a persistent length, $l_p = v_a/D_r$. This is the length a particle travels before its self-propelling direction decorrelate due to its rotational diffusion. The Peclet number is persistent length measured in units of the particle size, σ.

The Peclet number can be seen as a measure of how far from thermal equilibrium the system is driven by the active force. In the limit Pe $\to$ 0, activity plays no role, and the system behaves as a thermal one. It is therefore of interest to investigate how the properties of a system change as it is increasingly driven out of thermal equilibrium as Pe varies.

2.5 Very dilute regime: active gas

We start discussing the behavior of ABPs in the dilute regime, i.e., in the limit in which the interparticle interaction can be neglected, $\phi \ll 1$. Fig.2.1 illustrates numerical (panel a), and theoretical (panel b) results for the mean square displacement of ABPs, in the dilute limit. Different curves refer to different value of the active velocity, or equivalently of the Peclet number. The theoretical prediction of

the time dependence of the mean square displacement, in two dimensions, is [4–6].

$$\mathrm{MSD}(t) = [4D + 2v_a^2\tau_r]t + 2v_a^2\tau_r^2[e^{-t/\tau_r} - 1]. \tag{2.11}$$

At short and intermediate times, $t \ll \tau_r$, the rotational diffusion of the self propelling direction of the particles can be neglected. Taylor expanding the above equation up to the second order, one finds $\mathrm{MSD}(t) = 4Dt + v_a^2t^2$. Hence, the mean square displacement results from the superposition of the diffusive motion induced by the thermal noise and of the ballistic motion induced by the activity. Hence, the mean square displacement exhibits a crossover from a diffusive to a super-diffusive behavior at time $2dD/v_a^2$, d is the dimension. At long times, $t \gg \tau_r$, the self-propulsion of the particles leads to a random walk motion, with step size $v_a\tau_r$, and number of steps t/τ_r. Hence, the mean square displacement is $\mathrm{MSD}(t) = [4D + v_a^2\tau_r]t$. That is, particles undergo standard diffusion with an effective diffusion coefficient $D_{eff} = D + \frac{1}{4}v_a^2\tau_r$. Analogous results are found in three dimensions.

2.6 Phase separation

At higher density, the increase of the Peclet number induces the phase separation of the system. What is remarkable is that, contrary to what occurs in systems of passive particles, numerical results clarify that this phase separation occurs in the absence of any attractive interactions between the particles [7, 9, 10]. The phase separation is also observed in experiments of synthetic microswimmers, although one cannot exclude the existence of an attractive interaction between the particles [11, 12], which might have different physical origins. The examples of phase separate states are illustrated in Fig. 2.2. Panel a is a snapshot taken from a two-dimensional simulation of ABPs, taken from Ref. [7], while panel b is a slice of a three-dimensional simulation, taken from Ref. [8].

The motility induced phase separation of ABPs has been first reported by Fily *et al.* [10] in 2012. In this work, they considered a system two-dimensional repulsive disks and demonstrated the coexistence of a gas and liquid-like phases at volume fraction $\phi = 0.4$, for high enough Peclet number. In a related study, Redner *et al.* [7] investigated the complete phase diagram of two-dimensional ABPs, as a

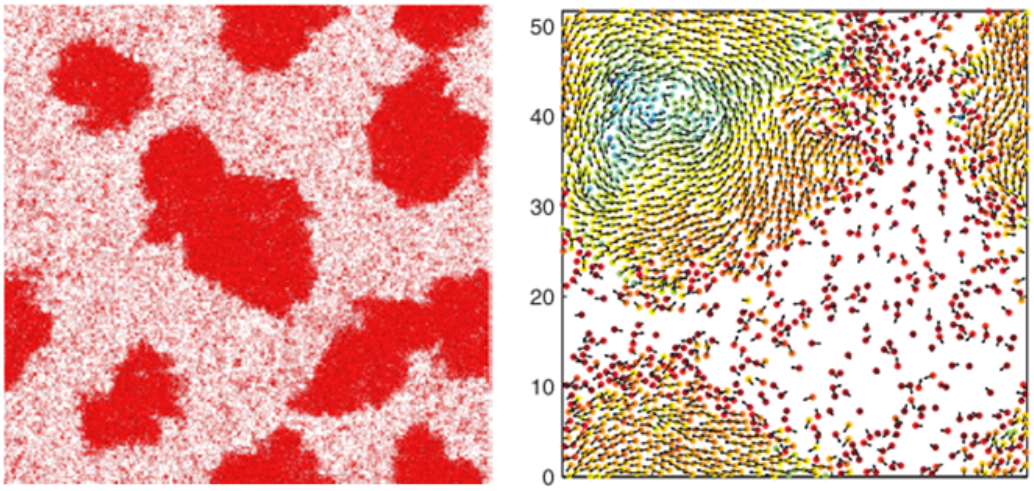

FIGURE 2.2: Motility-induced phase separation. Left: 2D system [7]. Right: slice of 3D system [8]. The vector represent the displacement of each particle and the color represent the ratio between displacement and the Pe number of this system. Red means fast particles and Blue means slow particles.

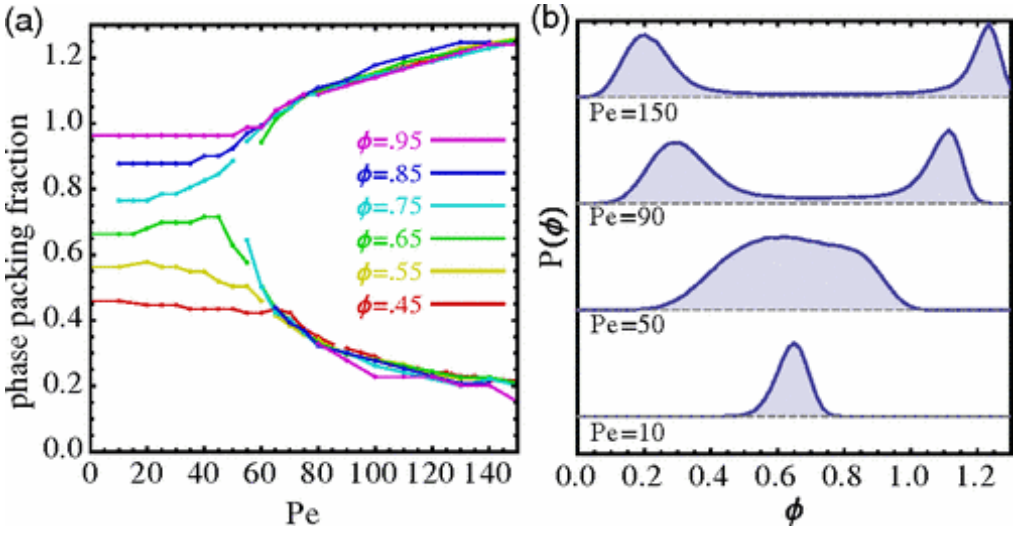

FIGURE 2.3: Panel (a) illustrates the coexistence line of two dimensional ABPs. For each value of the volume fraction ϕ, at high enough Peclet number the distribution of the local volume fraction becomes bimodal, as in panel b. The two peaks of this bimodal distribution identifies the coexisting densities, which are illustrated in panel a. From Redner *et al.* [7].

function of the volume fraction and of the Peclet number, ϕ-Pe. The phase diagram is illustrated in Fig. 2.3. We note here that the definition of Pe used in this works differ by a factor 3 from the one of Eq. 2.10. Note also that the particles considered

in this work are soft, which is why the volume fraction acquires large values, well above one.

At the same time, experiments on synthetic microswimmer reported an analogous phenomenon [11, 12] even if, as we already mentioned, in the experiments attraction between the particles might play a role [13]. In the following years, many numerical investigations have reported phase diagrams consistent with those of Fig. 2.3, and have investigated different aspects of it. Ref. [8] has considered three-dimensional active Brownian particles, evidenced the presence of finite size effects on the high density side of the coexistence line, as well as the emergence of spatio-temporal correlation between the particles. Ref.s [14, 15] reproduced the two-dimensional phase diagram and tried to rationalize the spinodal line via an effective Canh-Hilliard approach, starting from a continuous description of active matter we will review in the following. Stenhammar *et al.* [16] compared two and three-dimensional phase diagrams of ABPs and clarified that they are qualitatively analogous but quantitatively different. Levis *et al.* [17] performed a numerical investigation of two-dimensional ABPs, investigating the pressure across the phase boundaries. They found that, as in thermal system and for no fundamental reason, the pressure in active systems behaves as the pressure of passive ones, e.g., it does not depend on the density in the coexistence region. Digregorio *et al.* [18] also reproduced the phase diagram of 2d ABPs, working in the hard sphere limit, investigating the equation of state. Also, they investigated the relationship between the motility induced phase separation, and the hexatic phase, which is observed at smaller Peclet number. They observed that, on increasing the Peclet number, first the liquid-hexatic coexistence region found in thermal hard disks disappears, and the liquid-gas motility induced coexistence regions open. That is, the two coexistence regions are well separated in the $\phi - \mathrm{Pe}$ plane. Fily *et al.* [2] investigated the phase diagram of two-dimensional ABPs, considering the translational and the rotational diffusion coefficient to be independent, and not related to each other by the Stokes-Einstein relations as in Eq. 2.5. Bruss and Glotzer [19] investigate ABPs in the limit of infinite persistent time, i.e., ballistic particles, and showed that in this limit phase separation occurs when the mean duration between interparticle collisions is smaller than the collision time.

All of these results indeed prove that ABPs phase separate, and give insight on the features of the motility induced phase diagram. But what it the physical origin of

this phase separation? Is it possible to predict the coexistence and the spinodal lines? The next section reviews theoretical attempts in this direction.

2.7 Theoretical approaches

In the absence of a thermodynamic formalism to describe the phase separation of driven systems, existing theoretical approaches have followed two paths. In the kinetic approach, one tries to determine the coexistence (and later the spinodal) lines by balancing the flux of particles moving from the dense phase to the gas phase, and the reverse flux. In the continuum approach, the spinodal line is determined via a linear stability analysis of effective hydrodynamic equations of active particles. I will describe these two approaches, highlighting their strong and weak points. The theoretical model I developed, which is introduced in the next chapter, overcomes the limitations of these approaches.

2.7.1 Kinetic theory

A kinetic approach to rationalize the physical origin of the motility induced phase diagram has been put forward by Redner *et al.* [7, 20]. In their first paper [7], the author set-up a model to predict the coexistence line. When two phases coexist, the flux of particles moving from the less dense to the more dense phase, or influx, balances the reverse outflux of particles moving from the dense to the less dense phase. The rate k_{in} at which particles move from the gas to the liquid phase is proportional the density of the gas phase, to the velocity of the particles in the gas, they assumed to equal the active velocity in the dilute regime. Hence, the assumed

$$k_{in} = \frac{\rho_g v_p}{\pi}, \tag{2.12}$$

where the factor π arises from geometrical consideration. What is the physical process that controls the flux of particles from the liquid to the gas phase? Redner *et al.* [7], along the line of previous speculations [21], assumed that a particle in the rim of a dense cluster remains bound to the cluster until its self-propelling direction points away from the cluster center. In this picture the physical process controlling the outflux is the rotational diffusion of the self-propelling direction,

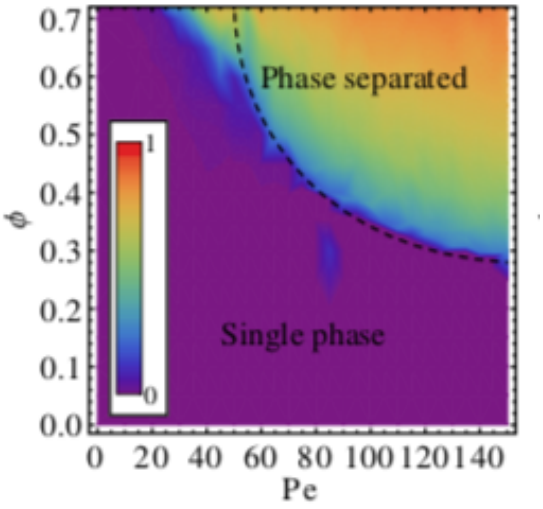

FIGURE 2.4: Contour plot of the density of particles in the largest cluster. The dashed line is the theoretical prediction of Eq. 2.14. From Redner *et al.* [7].

controlled by the rotational diffusion coefficient D_r, and the outflux is

$$k_{out} = \frac{\kappa D_r}{\sigma}, \tag{2.13}$$

where κ is a constant introduced to take into account the possibility that several particles leave the cluster in a single event. Notice that in this model, the outflux does not depend neither on the density of the dense phase nor on the active velocity. By equating k_{in} and k_{out} this model provides an estimation for the density of the gas phase along the coexistence curve,

$$\rho_g = \frac{\pi \kappa D_r}{\sigma v_p}. \tag{2.14}$$

To validate their model, Redner *et al.* [7] have estimated the coexistence line by investigating the fraction of particles that belong the large cluster, as a function of the volume fraction and the Peclet number. This fraction is small in the gas phase, while it grows in the phase separate phase. The contour plot of this fraction illustrated in Fig. 2.4, leads to the identification of a clear boundary between the homogeneous and the separate phases. This boundary is well described by Eq. 2.14. Hence, the numerical results support the kinetic model. We note, however, that this model predicts a coexistence line varying as 1/Pe. That is, it does not predict a U-shaped coexistence line and the existence of a critical point, which are conversely

critical features of the motility induced phase separation, as in the phase diagram of Fig. 2.3.

In a sequel paper [20], the same authors extended the kinetic approach to attempt to predict both the coexistence and the spinodal line. Interestingly, they have done within a kinetic description of the nucleation process, a form which they also obtained a description of the phase separation in terms of an equivalent thermodynamic system.

The starting point of this approach is a master equation for the evolution of the density of cluster with n particles, ρ_n:

$$\partial_t \rho_n = J(n-1) - J(n) \tag{2.15}$$

$$J(n) = j_{\text{in}}(n)S(n)\rho_n - j_{\text{out}}(n+1)S(n+1)\rho_{n+1}. \tag{2.16}$$

Here $J(n)$ is the flux of particles going from a cluster of size n to a cluster of size $n+1$, and it is assumed that only single particles move from a cluster to a different one. Clusters are assumed to be circular, with volume $V(n) = n/\rho_{\text{c}}$ and surface area $S(n) = \sqrt{4\pi n/\rho_{\text{C}}}$. $j_{\text{in}} = (\rho_{\text{g}} v_{\text{p}}/\pi)$ and $j_{\text{out}}\,(n) = (D_{\text{r}}/\sigma)\,[\pi/2\alpha(n)]^2$ are the flux of particles moving from the dense to the less-dense phase, and vice versa. These fluxes have been modeled as previously described, Eqs. 2.12-2.13. The only difference is the presence of more accurate estimations of geometrical factors involved, which, however, do not change the qualitative picture.

The steady-state corresponds to the case $J = 0$. In the absence of phase separation, in this state free monomers coexist with small, transient clusters. The steady-state cluster size distribution (CSD) $P(n)$ can be calculated by iterating Eq. 2.16,

$$\rho_n = \rho_1 \prod_{m=1}^{n-1} \frac{j_{\text{in}}(m)S(m)}{j_{\text{out}}(m+1)S(m+1)} \equiv \rho_1 P(n). \tag{2.17}$$

Given the models for j_{in} and j_{out}, one finds

$$P(n) = \frac{(z\rho_{\text{g}})^{n-1}}{\sqrt{n}} P_0(n) \tag{2.18}$$

where $z = \frac{v_p \sigma}{\pi D_r}$, and $P_0(n) = \left[\prod_{m=1}^{n-1} \left(\frac{2\alpha(m+1)}{\pi}\right)\right]^2$ accounts for the geometric effects.

In order to access the nucleation dynamics, the system is assumed to be in a quasi-stationary state, with $\partial_t \rho_n = 0$, but allowed for a small nonzero flux $J(n)$. The existence of this regime, according to Ref. [20], is supported by simulations that show a regime in which the nucleation is slow with respect to the time needed for the cluster size distribution to reach its steady-state. Under this condition, the fluxes J result not to depend on the cluster size [20] and are given by

$$J = \rho_1 \left(\sum_{n=1}^{\infty} \frac{1}{j_{\text{in}}(n) S(n) P(n)} \right)^{-1} \tag{2.19}$$

The mean nucleation time in a system with volume V is then given by $\tau_{\text{nucl}} = (JV)^{-1}$.

Importantly, this theoretical approach allows to map ABPs on a thermodynamic system with an effective free energy $G(n)$ for a cluster of size n. Indeed, the theoretical approach predicted by ρ_n, with in an equilibrium system is given by $\rho_n \propto \exp\left[-G(n)/\left(k_{\text{B}}T\right)\right]$. Hence, $G(n)$ can be obtained inverting this relation. One finds

$$G(n) = -k_{\text{B}}T \left\{ n \ln\left(z\rho_9\right) - 1/2 \ln(n) + \ln\left[P_0(n)\right] \right\}. \tag{2.20}$$

As illustrated in Fig. 2.5, $G(n)$ is monotonically increasing for $z\rho_{\text{g}} < 1$. In this limit, the stable phase is that of cluster of size $n = 1$, i.e. the homogeneous gas phase. When $1 < z\rho_g < \sqrt{2}(2\alpha(2)/\pi)^2 \approx 2.42$, $G(n)$ has a maximum. In this region, therefore, the system is metastable. Finally, for $z\rho_g \geq 2.42$, $G(n)$ monotonically decreases, which indicates that the system is in the unstable region of the phase diagram. Hence, the equation for the coexistence and for the spinodal line are $z\rho_g = 1$ and $z\rho_g = 2.42$. Given the definition of $z = \frac{v_p \sigma}{\pi D_r}$, both lines scale as $\text{Pe} \sim 1/\phi$.

As the original one, also this refined kinetic approach does not predict the existence of a critical point. In addition, it predicts a spinodal line which diverges in the limit $\phi \to 0$. Hence, according to this model, the system is unstable if the Peclet number is high enough, regardless of the volume fraction. This contradicts numerical observations. Studies that have considered the behavior of the spinodal line also investigating high values of the Peclet number, such as Ref. [15] and later ones, have demonstrated that the spinodal lines diverge at a finite ϕ value.

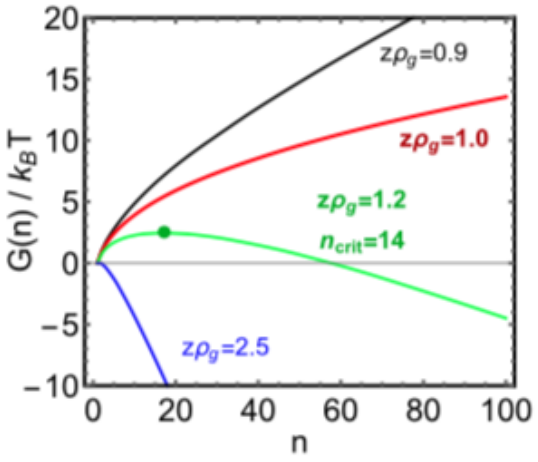

FIGURE 2.5: Dependence of the effective free energy on the cluster size, for different value of $z\rho_g$. From Redner *et al.* [20].

2.7.2 Continuous theory

The continuous description of active matter started from a seminal paper by Toner and Tu [22], who introduced a hydrodynamic description of the Vicsek model [23]. This is a trendy model whose key ingredients are, besides the presence of motility, that of an alignment interaction. Specifically, the self-propelling direction of each particle does not diffuse, as in the ABPs model, but instead tries to align to the self-propelling direction of nearby particles. As a result, the model nicely reproduces the flocking behavior of birds, for instance, and predicts flocking to be a non-equilibrium phase transition.

The continuum approach to the motility induced phase separation has been developed for a system characterized by an explicit coupling between the self-propelling direction and the density. For instance, if the motility is driven by the consumption of food, or by a local chemical reaction, different particles might compete for the 'food', so that they slow down in a dense environment. See Ref. [24] for a review of this approach. In the case of Active Brownian Particles, such an explicit dependence of the particle velocity on the local density does not exist. However at finite volume fraction, in the homogeneous phase, ABPs are characterized by an affected density dependence swimming speed

$$v_e = v_a \left(1 - \frac{\phi}{\phi^*}\right). \tag{2.21}$$

This has been demonstrated numerically [10], then related to the anisotropy of the pair-correlation function [25] and rationalized in term of the collision rate [16]. The dependence of the active velocity on the local density gives rise to a positive feedback mechanism that promotes phase separation, as the pressure becomes smaller on increasing the density.

This scenario can be formalized solving effective continuum equation for the evolution of the relevant coarse-grained parameters. These are the local density $\rho(\mathbf{r},t)$, and the local polarization $\mathbf{p}(\mathbf{r},t) = \rho(\mathbf{r},t)P(\mathbf{r},t)$. We remind that in ABPs each particle has a self-propelling velocity $v\mathbf{n}$. Coarse-graining this self-propelling velocity one can associate to each point in space a polarization density field, a vector whose magnitude and direction correspond to the typical particle velocity in the considered point. Hence, in the above expression $P(\mathbf{r},t)$ is the orientational order parameter, the average self-propelling direction of the particles in $\mathbf{r}$ at the considered time.

The relevant dynamical equations are [2, 10, 16, 26]

$$\partial\rho_t = -\nabla[v(\rho)\mathbf{p} - D(\rho)\nabla\rho] \tag{2.22}$$

$$\partial_t\mathbf{p} = -D_r\mathbf{p} - \frac{1}{2}\nabla[v(\rho)\rho] + K\nabla^2\mathbf{p} \tag{2.23}$$

Eq. 2.22 is the continuity equation. The current $J = v(\rho)\mathbf{p} - D(\rho)\nabla\rho$ has an advection term, due to the self-propelling motion with velocity $v(\rho)$ in the polarization direction. $D(\rho)$ is a density dependence diffusivity, in principle depending on the density. There is not any first-principle evaluation of this diffusivity. But it is common practice to assumed $D(\rho)$ to be the density-independent diffusivity of the passive suspensions, given by Eq. 2.5. We will argue later on that this common assumption made in the literature needs to be revised.

Eq. 2.23 described the evolution of the polarization density fields. This is governed by a diffusive term, with diffusion coefficient set by the rotational diffusion constant. This term described the fact that the polarization tends to decrease, as particles diffuse independently. The second term describes the effect of spatial inhomogeneities of the particle density. Finally, the last term describes polarization diffusion.

To solve these equations, it is assumed that at large time the time dependence of the polarization can be neglected. Dropping the nonlinear terms, from Eq. 2.23 the polarization results

$$\mathbf{p} = -\frac{1}{2D_r}\nabla[v(\rho)\rho]. \tag{2.24}$$

Substitution in Eq. 2.22 leads to a diffusion equation for the density, $\partial\rho_t = \mathcal{D}\nabla\rho$ where $\mathcal{D}$ is an effective diffusivity given by

$$\mathcal{D} = D(\rho) - \frac{v^2(\rho)}{2D_r}\left[1 + \frac{d\log v}{d\log\rho}\right]. \tag{2.25}$$

When $\mathcal{D} < 0$, the system is unstable as particles move towards regions of higher density. Hence,

$$\mathcal{D} = 0 \tag{2.26}$$

determines the spinodal line.

To make progress, one needs the explicit dependence of the diffusion coefficient $D(\rho)$ and of the self-propelling velocity $v(\rho)$ on the density. For the density, the coarse grained velocity is assumed to behave as the effective velocity, Eq. 2.21, e.g. $v(\rho) = v_a(1-\rho/\rho^*)$. The diffusion coefficient, as we already mentioned, is identified with the density independent diffusion coefficient of the passive suspension in the dilute limit, $D = D_r\sigma^2/3$. With these assumptions, the spinodal line is found to be

$$\mathrm{Pe} = \left[\frac{3}{2}\left(1 - \frac{\phi}{\phi^*}\right)\left(1 - \frac{2\phi}{\phi^*}\right)\right]^{-1/2}. \tag{2.27}$$

This continuum approach has the merit of correctly prediction a U-shaped spinodal line. The spinodal line diverges at the maximum density ϕ^*, as well as at a finite density $\phi^*/2$. The existence of a finite value is in agreement with the numerical observations and was not captured by the kinetic approach. The critical point is at $\phi_c = 3\phi^*/4$, $\mathrm{Pe}_c = \sqrt{4/3}$.

As previously noticed [24], this prediction largely underestimates the critical Peclet number. The theory predicts the critical Peclet number to be of order 1, while the numerical results suggest this to be of order 10. Here, we also notice that it predicts $\phi_m = \phi^*/2$, overestimating the actual value. A better agreement between the prediction of the continuum model and of the numerical results could be obtained treating ϕ^* [2] (or ϕ_m [15, 27]) as free parameters, and allowing for a presence of a scale factor possibly associated to an effective diffusivity.

2.7.3 Kinetic vs. continuous approach

As we have seen, both the kinetic and the continuous approach have their strength and weaknesses. The kinetic approach quantitatively predicts a fraction of the low-density coexistence line. It is, however, unable to predict the existence of a critical point, and hence the high-density coexistence/spinodal lines. The continuum approach correctly described the U-shaped spinodal line, but it is quantitatively off by a factor 10, which suggests that it is not capturing some fundamental aspects of the physics [24].

It is also of interest to consider that the two approaches attribute the shape of the phase diagram to different physical processes. In the kinetic theory, the equilibrium between coexisting phases is that between an influx, promoted by the motility, and an outflux, promoted by the rotational diffusion. Hence, motility promotes phase separation, and rotational diffusion promotes the homogeneous phase. In the continuum approach, conversely, as apparent from Eq. 2.25, the motility promotes phase separation, but the translational rather than the rotational diffusion promotes the homogeneous phase.

In the next chapter, I will demonstrate that there is a physical process not described by these theoretical approaches that also promotes the homogeneous phase, related to the motility itself.

2.8 Related experiments

Active systems are common at both the macroscopic and the microscopic scale. Experimental investigations of these systems are therefore common and are becoming increasingly popular. See Ref. [3, 28] for recent reviews. The Active Brownian Particle model we have been considering so far corresponds to an idealized experiment, where spherical particles self-propel performing a persistent random walk, and interact via purely repulsive forces. Here I would like only to discuss *wet* and *dry* experiments of self-propelled colloidal scale particles, which are those most related the idealized ABPs scenario. There are, however, significant differences, I will also highlight.

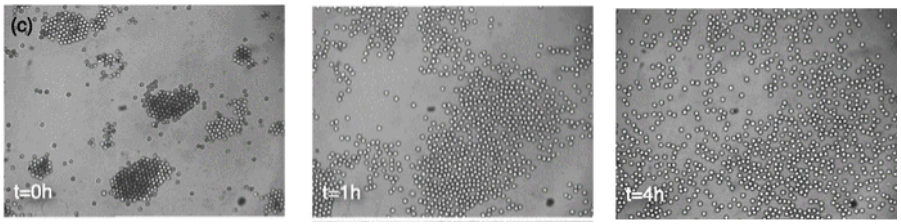

FIGURE 2.6: (a) Motility induced phase separation of phoretic particles. The motility derives from local heating processes induced by laser light. Panel a-c shows that the system evolves towards the homogeneous phase as the laser light is switched off at a time $t = 0$. From Ref. [11].

2.8.1 Wet experiments

In these experiments, colloidal scale particles self-propel via diffusion phoresis, i.e., because of the presence of a concentration gradient in their environment. This concentration gradient is created by the particles themselves. Two this end, different approaches have been considered in the literature, all of them involving Janus particles, spherical particles whose two hemispheres are coated with different materials. This is needed to induce asymmetry in the particles, and a preferential direction of motion. Experiments that have followed this approach are in Ref.s [12, 21, 29, 30].

As an example, Buttinoni *et al.* [11] have considered $rmSiO_2$ colloidal scale particles (radius $\sim 2.13\mu m$) with graphite coating one hemisphere. The particles settle under gravity in a two-dimensional monolayer, in the water-lutidine mixture. When illuminated via a laser beam whose wavelength is properly tuned, the carbon coated-side of the particles absorbs the light and locally heat the mixture above the critical temperature. Hence, locally water and lutidine demix. Since water and lutidine have a different affinity towards the two hemispheres, this demixing induced a phoretic force.

So far, experiments have not investigated the complete phase diagram of these systems, as a function the volume fraction and of the motility strength. However, as illustrated in Fig. 2.6a, the phase separated steady state appear to comprise a number cluster of different sizes, suggesting the presence of microphase separation, rather than of the phase separation of ABPs. Note the cluster are dynamic: they continually rotate, break, and reform.

In particular, Ref. [30] has investigated the properties of the rotational motion of the clusters. The experimental results suggest that the particles in the cluster

approximately points in a random direction. Indeed, under this approximation, one can evaluate the typical rotational speed of the cluster as a function of the cluster size. The results of this estimation agree with the experimental measures. We remark here that this observed rotational motion will be important to us, as related to the novel instability mechanisms for ABPs we will introduce.

As concern these experimental approaches, we notice that stable rotating clusters are not observed in ABPs. This suggests that in the experiments, there is an additional attraction, which only acts when the particles are made active. Indeed, in the absence of activity, the equilibrium state experimentally observed is the homogeneous one, as in Fig. 2.6 (but see also [12]). The presence of this motility induced attraction is controversial. For instance, according to Ref. [29] there is not, while more recent theoretical works suggest that this is indeed present [13]. Let me finally mention that another important difference between these experiments and the ABPs model concern the hydrodynamic interaction. This long-range interaction is undoubtedly present in the experiments, while it is not modeled in the ABPs approach.

2.8.2 Dry experiments

Hydrodynamic interactions are negligible in granular scale experiments of active particles, which are conducted in air. The most relevant experiments in this line of research is that of Deseigne, Dauch out and Chaté [31–33], which have engineered a system of active disks that self-propel when vibrated. The self-propulsion is achieved endowing the disks with asymmetric mechanical properties: each time a vibrated disks collide with the substrate, it experiences a net force pointing in a specific direction associated to its orientation. The disks have been observed to perform a persistent random walk, and the persistence length was partially tunable by acting on the amplitude of the vibrational motion. Disks are in a petal-shaped container, which allows the particle that agglomerate on the sides to be re-injected in bulk. Experimental difficulties prevented the investigation of the phase diagram as a function of the volume fraction and the persistent length.

Fig. 2.7 illustrates that this experimental setup reproduces the emergence of giant number fluctuations. Interestingly, it also reproduces a flocking type behavior, where particles collectively move. This behavior is not observed in ABPs, while it

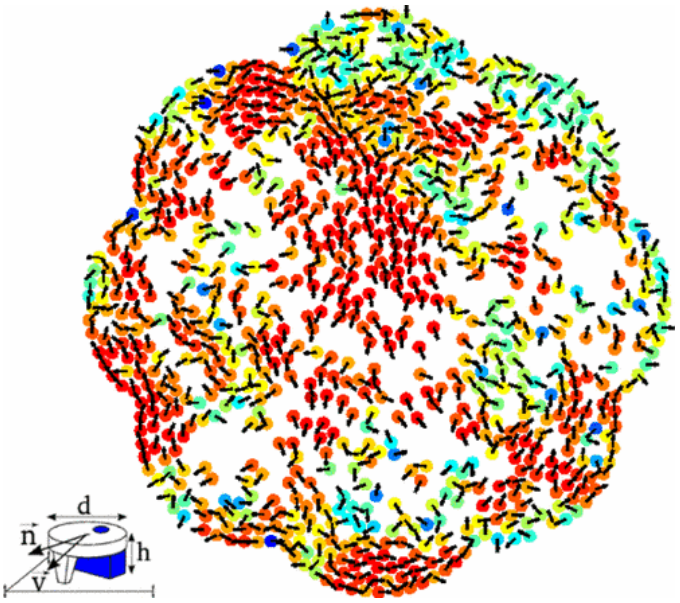

FIGURE 2.7: Experiments of vibrated polar disks, exhibiting clustering and collective behavior. From Ref. [31].

is commonly observed in the presence of interactions that induce alignment of the self-propelling directions. This alignment does not seem to be promoted in most of the collisions [32], and hence, the emergence of the flocking behavior in this model has not been fully understood.

References

[1] Suvendu Mandal, Benno Liebchen, and Hartmut Löwen. Motility-induced temperature difference in coexisting phases. *arXiv preprint arXiv:1902.06116*, 2019.

[2] Yaouen Fily, Aparna Baskaran, and Michael F Hagan. Dynamics of self-propelled particles under strong confinement. *Soft matter*, 10(30):5609–5617, 2014.

[3] Clemens Bechinger, Roberto Di Leonardo, Hartmut Löwen, Charles Reichhardt, Giorgio Volpe, and Giovanni Volpe. Active particles in complex and crowded environments. *Reviews of Modern Physics*, 88(4):045006, 2016.

[4] K Franke and H Gruler. Galvanotaxis of human granulocytes: electric field jump studies. *European Biophysics Journal*, 18(6):334–346, 1990.

[5] K Martens, L Angelani, R Di Leonardo, and L Bocquet. Probability distributions for the run-and-tumble bacterial dynamics: An analogy to the lorentz model. *The European Physical Journal E*, 35(9):84, 2012.

[6] Jonathan R Howse, Richard AL Jones, Anthony J Ryan, Tim Gough, Reza Vafabakhsh, and Ramin Golestanian. Self-motile colloidal particles: from directed propulsion to random walk. *Physical review letters*, 99(4):048102, 2007.

[7] Gabriel S Redner, Michael F Hagan, and Aparna Baskaran. Structure and dynamics of a phase-separating active colloidal fluid. *Physical review letters*, 110(5):055701, 2013.

[8] Adam Wysocki, Roland G Winkler, and Gerhard Gompper. Cooperative motion of active brownian spheres in three-dimensional dense suspensions. *EPL (Europhysics Letters)*, 105(4):48004, 2014.

[9] Hugues Chaté, Francesco Ginelli, Guillaume Grégoire, and Franck Raynaud. Collective motion of self-propelled particles interacting without cohesion. *Physical Review E*, 77(4):046113, 2008.

[10] Yaouen Fily and M Cristina Marchetti. Athermal phase separation of self-propelled particles with no alignment. *Physical review letters*, 108(23):235702, 2012.

[11] Ivo Buttinoni, Julian Bialké, Felix Kümmel, Hartmut Löwen, Clemens Bechinger, and Thomas Speck. Dynamical clustering and phase separation in suspensions of self-propelled colloidal particles. *Physical review letters*, 110(23):238301, 2013.

[12] Jeremie Palacci, Stefano Sacanna, Asher Preska Steinberg, David J Pine, and Paul M Chaikin. Living crystals of light-activated colloidal surfers. *Science*, 339(6122):936–940, 2013.

[13] Benno Liebchen and Hartmut Löwen. Which interactions dominate in active colloids? *The Journal of chemical physics*, 150(6):061102, 2019.

[14] Julian Bialké, Jonathan T Siebert, Hartmut Löwen, and Thomas Speck. Negative interfacial tension in phase-separated active brownian particles. *Physical review letters*, 115(9):098301, 2015.

[15] Thomas Speck, Julian Bialké, Andreas M Menzel, and Hartmut Löwen. Effective cahn-hilliard equation for the phase separation of active brownian particles. *Physical Review Letters*, 112(21):218304, 2014.

[16] Joakim Stenhammar, Davide Marenduzzo, Rosalind J Allen, and Michael E Cates. Phase behaviour of active brownian particles: the role of dimensionality. *Soft Matter*, 10(10):1489–1499, 2014.

[17] Demian Levis, Joan Codina, and Ignacio Pagonabarraga. Active brownian equation of state: metastability and phase coexistence. *Soft Matter*, 13(44):8113–8119, 2017.

[18] Pasquale Digregorio, Demian Levis, Antonio Suma, Leticia F Cugliandolo, Giuseppe Gonnella, and Ignacio Pagonabarraga. Full phase diagram of active brownian disks: From melting to motility-induced phase separation. *Physical review letters*, 121(9):098003, 2018.

[19] Isaac R Bruss and Sharon C Glotzer. Phase separation of self-propelled ballistic particles. *Physical Review E*, 97(4):042609, 2018.

[20] Gabriel S Redner, Caleb G Wagner, Aparna Baskaran, and Michael F Hagan. Classical nucleation theory description of active colloid assembly. *Physical review letters*, 117(14):148002, 2016.

[21] Ivo Buttinoni, Giovanni Volpe, Felix Kümmel, Giorgio Volpe, and Clemens Bechinger. Active brownian motion tunable by light. *Journal of Physics: Condensed Matter*, 24(28):284129, 2012.

[22] John Toner and Yuhai Tu. Long-range order in a two-dimensional dynamical xy model: how birds fly together. *Physical review letters*, 75(23):4326, 1995.

[23] Tamás Vicsek, András Czirók, Eshel Ben-Jacob, Inon Cohen, and Ofer Shochet. Novel type of phase transition in a system of self-driven particles. *Physical review letters*, 75(6):1226, 1995.

[24] Michael E Cates and Julien Tailleur. Motility-induced phase separation. *Annu. Rev. Condens. Matter Phys.*, 6(1):219–244, 2015.

[25] Andreas Zöttl and Holger Stark. Hydrodynamics determines collective motion and phase behavior of active colloids in quasi-two-dimensional confinement. *Physical review letters*, 112(11):118101, 2014.

[26] Joakim Stenhammar, Adriano Tiribocchi, Rosalind J Allen, Davide Marenduzzo, and Michael E Cates. Continuum theory of phase separation kinetics for active brownian particles. *Physical review letters*, 111(14):145702, 2013.

[27] Thomas Speck. Stochastic thermodynamics for active matter. *EPL (Europhysics Letters)*, 114(3):30006, 2016.

[28] M Cristina Marchetti, Jean-François Joanny, Sriram Ramaswamy, Tanniemola B Liverpool, Jacques Prost, Madan Rao, and R Aditi Simha. Hydrodynamics of soft active matter. *Reviews of Modern Physics*, 85(3):1143, 2013.

[29] I Theurkauff, C Cottin-Bizonne, J Palacci, C Ybert, and L Bocquet. Dynamic clustering in active colloidal suspensions with chemical signaling. *Physical review letters*, 108(26):268303, 2012.

[30] F Ginot, I Theurkauff, F Detcheverry, Christophe Ybert, and C Cottin-Bizonne. Aggregation-fragmentation and individual dynamics of active clusters. *Nature communications*, 9(1):696, 2018.

[31] Julien Deseigne, Olivier Dauchot, and Hugues Chaté. Collective motion of vibrated polar disks. *Physical review letters*, 105(9):098001, 2010.

[32] Julien Deseigne, Sébastien Léonard, Olivier Dauchot, and Hugues Chaté. Vibrated polar disks: spontaneous motion, binary collisions, and collective dynamics. *Soft Matter*, 8(20):5629–5639, 2012.

[33] Christoph A Weber, Timo Hanke, J Deseigne, S Léonard, Olivier Dauchot, Erwin Frey, and Hugues Chaté. Long-range ordering of vibrated polar disks. *Physical review letters*, 110(20):208001, 2013.

Chapter 3

The stability phase diagram of active Brownian particles

In the previous chapter, we have discussed the two main theoretical approaches that have been developed to rationalize the features of the motility induced phase separation of Active Brownian Particles, the kinetic, and the continuous one. Both approaches assume that the phase separated state is driven by the motility. However, the two approaches suggest that different physical processes promote the homogeneous phase. According to the kinetic approach, the phase separated state is promoted by the rotational diffusion of the self-propelling directions of the active particles, while according to the continuous one it is promoted by the translational diffusion. As a consequence, the models make different predictions. When compared to the numerical results, the prediction of both models appears to be inaccurate. The kinetic model only predicts the low-density side of the coexistence line. It does not predict the U-shaped coexistence/spinodal line, and hence the existence of a critical point in the Peclet number, volume fraction plane. The continuous approach does predict a critical point, but underestimate the critical value of the Peclet number by a large factor, around 10. In addition, in the hard-sphere limit, it predicts the U-shaped spinodal line to diverge at ϕ^*, which essentially coincides with the random close packing volume, and at $\phi^*/2$. This last prediction is not supported by the experimental data. The weakness of this model is well described in Ref. [1].

In this chapter, I develop a novel theoretical model to rationalize the spinodal line of ABPs, and validate it against numerical simulations conducted in both two and three spatial dimensions. This novel theoretical approach clarifies what are the physical forces that promote the homogeneous phase. The rotational diffusion coefficient is found to have a role, as suggested by the kinetic model. The translational diffusion of the passive suspensions is conversely demonstrated to be irrelevant, which contrast with what suggested by the continuous model. In addition, my theoretical development clarifies that there is a novel physical process, related to the ability of two particles to resolve their collision by sliding one past the other, which has been neglected so-far.

The chapter is structured as follows. Sec. 3.1 quickly reviews the numerical model. We review the model as we have considered a more general form of the usually considered equations of motion, to allow for a more stringent test of our theoretical predictions. Sec. 3.2 develops my novel theoretical model. Sec. 3.3 validates the model against numerical simulations. In Sec. 3.4, I explore further the role of diffusion in the phase separation of ABPs, to identify what is the assumption made in the continuum model that fails. The theoretical model I developed to describe the instability of the homogeneous phase is built on the novel understanding of the role of the rotational motion of density fluctuation of homogeneous systems. The same rotational motion occurs in the phase separated state, where the density fluctuations correspond to macroscopic clusters. In Sec. 3.5, I demonstrate how the novel mechanism I have uncovered allows rationalizing the cluster dynamics in phase separated state. A discussion of the results of this chapter is in Sec. 3.6. I note here that this chapter is related to the article 'The stability phase diagram of active Brownian particles' by Pin Nie, Joyjit Chattoraj, Antonio Piscitelli, Patrick Doyle, Ran Ni, Massimo Pica Ciamarra, https://arxiv.org/abs/1907.04464, currently under review.

3.1 Model and simulation methods

3.1.1 Numerical model

We aim at describing the motility induced phase diagram of self-propelled ABPs particles, which evolves according to the following equation of motion:

$$\boldsymbol{v}_i = \frac{\boldsymbol{F}_i}{\gamma} + \frac{F_a}{\gamma}\hat{\boldsymbol{n}}_i + \sqrt{2D_t}\boldsymbol{\eta}_i^t \tag{3.1}$$

$$\boldsymbol{\omega}_i = \sqrt{2sD_r}\boldsymbol{\eta}_i^r. \tag{3.2}$$

Here sD_r and $D_t = D_r\sigma^2/3$ are the rotational and the translational diffusion coefficients, $\gamma_r = \gamma\frac{\sigma^2}{3}$, η is Gaussian white noise variable with $\langle\eta\rangle = 0$ and $\langle\eta(t)\eta(t')\rangle = \delta(t-t')$, F_a the magnitude of the active force acting on the particle and $\hat{\boldsymbol{n}}_i$ its direction, $\boldsymbol{F}_i = \sum \boldsymbol{f}_{ij}$ the forces arising from the interparticle interactions.

The above equation are essentially does of Eq. 2.4, 2.4. There are two differences. First, in the angular equation of motion, there is not a torque originating from the interparticle interaction. This is because we are going to consider frictionless spherical particles. Secondly, in Eq. 3.2 we have multiplied the rotational diffusion coefficient D_r by a factor s. Hence, the effective rotational diffusion will be sD_r. By varying s, we are therefore in the position of independently tuning the rotational and the translational diffusion coefficient. This will allow for a more stringent test of our theoretical approach, and of the previous ones.

For the interparticle interaction, we use the Harmonic model,

$$\begin{aligned} V(r) &= \frac{1}{2}k_n(r-\sigma)^2 \text{ if} r \leq \sigma \\ V(r) &= 0 \text{ otherwise,} \end{aligned} \tag{3.3}$$

where $\sigma = 1/2(\sigma_i + \sigma_j)$ is the average diameter of the interacting particles, r their distance. This potential is essentially a one-sided spring, as the particles only experience a repulsive interaction when they overlap. k is a spring stiffness. In my investigations, the value of k plays no role, as I work in the hard-sphere limit. Precisely, I have set k to such a high value that for all investigated parameters, no particle ever experiences a relative deformation $1 - r/\sigma$ larger than 10^{-4}. Note

that previous investigation has not always considered this limit. Softer particles may highly deform due to the presence of the active force; a feature speculated to induce a re-entrance in the phase diagram [2].

In the absence of interaction and noise, particles move with velocity of $v_a = F_a/\gamma$ and do not rotate. The control parameters are the volume fraction ϕ, and the Peclet number $\mathrm{Pe} \equiv \frac{v_a}{D_r \sigma}$, with σ the average particle diameter. For Brownian spheres $s = 1$ in Eq. 3.2.

3.1.2 Numerical method

I have investigated the collective behavior of a system of particles interacting via Eq. 3.2, with the described interaction potential, via Molecular Dynamics Simulations. Essentially, this tantamount to solving the numerically solving Newton's equation of motion.

The simulations have been performed via the open-source code LAMMPS [3]. This package is commonly used in this research community. LAMMPS is a highly optimized numerical simulation, which allows solving the equation of motion in parallel. To this end, I made extensive use of resources provided by the National Supercomputing Center Singapore, NSCC, through a grant for computer hours I secured.

Note that LAMMPS has been designed to solve Newton's equation of motion, nor their overdamped limit, which is relevant to our purpose. Exploiting the fact that LAMMPS is open-source and highly customizable, I have developed the code (C++) needed to solve the overdamped equations of motion, and integrated into the LAMMPS package. In this part of my work, I benefited from the interaction with a Post. Doc. that worked in the group, Dr. J. Chattoraj that had relevant experience.

3.2 Stability phase diagram of ABPs: theoretical prediction

3.2.1 Goal and approach

I intend to develop a model to predict the spinodal line of ABPs, in the Peclet number, volume fraction plane. This will be a U shaped line, $\mathrm{Pe}(\phi)$. For every value of the volume fraction ϕ, the system is unstable towards phase separation as soon as the Peclet number overcomes the spinodal limit, i.e., for $\mathrm{Pe} > \mathrm{Pe}(\phi)$. Accordingly, the spinodal line can be identified as the limit of stability of the homogeneous phase.

To determine the spinodal line, also partially guided by previous approaches, I will identify the physical process that promotes the growth of density fluctuation in a homogeneous system, a small cluster of particles. This process will have a timescale τ_g. At the same time, I plan to identify the physical processes by which a density fluctuation is able to decay, τ_d. The spinodal line will then result from the balance of these two timescales.

In doing this, let me stress that I will consider as a density fluctuation, not just region containing more particle than the rest of the system. Indeed, I will also demand that the particle involved in these density fluctuations to have to oppose self-propelling directions. It is indeed the collision of particles moving in opposite directions that gives rise to the induced phase separation.

3.2.2 Growth of a density fluctuation

We consider as a density fluctuation the emergence of a small cluster, two particles, that collide having roughly opposite self-propelling directions. This definition excludes the possibility that we consider as density fluctuations a cluster of particles that simply collide due to their Brownian motion.

To estimate the associated timescale, we consider that particles have been shown to move along their self-propelling direction with an effective density dependent

active velocity, as

$$v_e = v_a \left(1 - \frac{\phi}{\phi^*}\right) \tag{3.4}$$

as we discussed in recapped in Sec. 2.7.2. This has been demonstrated numerically [4], then related to the anisotropy of the pair-correlation function [5] and finally rationalized in term of the collision rate [6]. In the limit of stiff particles, ϕ^* can be identified with the close packing volume fraction. Taking into account that the number of collisions scales with the volume fraction, the typical inverse agglomeration time results

$$\tau_{\mathrm{g}}^{-1} = a\phi\frac{v_a}{\sigma}\left(1 - \frac{\phi}{\phi^*}\right), \tag{3.5}$$

where a is a constant of order one.

τ_{g}^{-1} vanishes for $\phi \to 0$. This is as expected, as in this limit, there is no collision. Similarly, $\phi \to \phi^*$. This might seems strange. However, we are here looking for the timescale associated with the collisions induced by the self-propulsion of the particles. In the $\phi \to \phi^*$ particles are jammed, and the collisions are just due to crowding.

It is interesting to note that this density induced effect has not been considered in previous kinetic approaches to the motility induced phase separation. Indeed, if this density dependence is neglected, which is formally done assuming $\phi^* \to \infty$, then τ_{g} essentially reduces to the flux of particles assumed to move from the homogeneous to the dense in previous works [1, 7–10].

3.2.3 Decay of a density fluctuation

We identify two physical mechanisms possibly responsible for the decay of density fluctuations. These are illustrated in Fig. 3.1 and described below.

3.2.3.1 Rotational detaching mechanism

One physical process responsible for the decay of density fluctuations has been recognized in previous works. Suppose that two particles collide their self-propelling

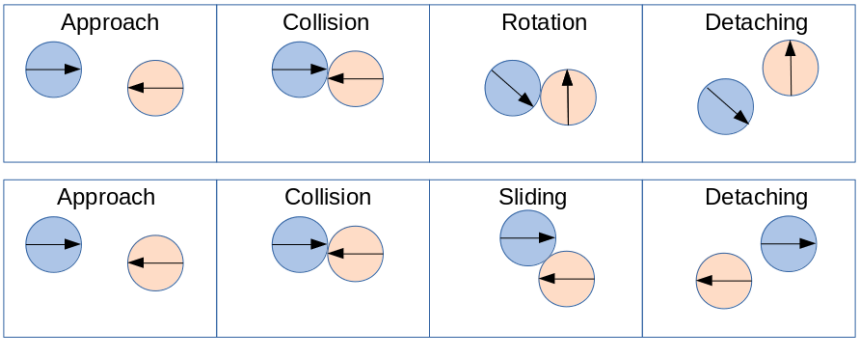

FIGURE 3.1: Physical processes allowing for the decay of a density fluctuation. The top row illustrates the rotational detaching mechanism, the bottom one the sliding detaching mechanism.

direction, pointing against each other. Given that the self-propelling direction undergoes Brownian diffusion, according to Eq. 3.2, after a time of order D_r^{-1} the self-propelling directions will no longer oppose each other, as illustrated in Fig. 3.1 (top row). The associated inverse timescale of this rotational detaching mechanisms, which is fixed by the rotational diffusion coefficient, is

$$\tau_{\mathrm{rd}}^{-1} = bsD_r, \tag{3.6}$$

with b a constant of order one.

This physical process is essentially the mechanisms by which particles on the rim of an active cluster have been assumed to detach from it [1, 7–9]. Here, however, we assume this mechanism to be at work in the homogeneous phase, not in the phase separated ones.

3.2.3.2 Sliding detaching mechanism

There exist an alternative process that allows for two colliding particles to resolve their collision. Indeed, as illustrated in Fig. 3.1 (bottom row), two particles may slide apart without any change in the orientation of their self-propelling direction, effectively rotating around their center of mass. This existence of this process was noticed in previous works but never formalized [10, 11]. This process is promoted by the interparticle repulsive force, proportional to the active velocity, and hindered by the surrounding particles which slowdown motion (not shown in the figure). We,

therefore, assume particles to slide off each other with a velocity proportional to the effective active velocity. The inverse timescale associated to this sliding detaching mechanisms thus result

$$\tau_{\rm sd}^{-1} = c\frac{v_a}{\sigma}\left(1-\frac{\phi}{\phi^*}\right), \tag{3.7}$$

where c is a constant of order one.

3.2.4 Theoretical prediction for the spinodal line

The spinodal line is fixed by the balance of the above time scales. Precisely, we balance the associated frequencies, $\tau_{\rm g}^{-1} = \tau_{\rm rd}^{-1} + \tau_{\rm sd}^{-1}$, to take into account that the fastest detaching mechanism dominates the overall detaching time. The resulting spinodal line is,

$$\begin{aligned} {\rm Pe} &= \frac{As}{(\phi^*-\phi)(\phi-\phi_m)},\ s\neq 0 & (3.8)\\ \phi &= \phi_m,\ s=0 & (3.9)\end{aligned}$$

with $\phi_m = \frac{c}{a}$ and $A = \frac{b\phi^*}{a}$.

Given that a, b and c are of order one, so are ϕ_m and A, in both 2d and 3d. The critical point is at

$$\begin{aligned} \phi_c &= \frac{1}{2}(\phi^*+\phi_m) & (3.10)\\ {\rm Pe}_c &= \frac{4A}{(\phi^*-\phi_m)^2}. & (3.11)\end{aligned}$$

Notice that, since $\phi^*-\phi_m \simeq 1/2$, the Peclet number at the critical point is of order 10. We also remark that, at large Pe, the rotational detaching mechanism becomes negligible, so that the spinodal line diverges at ϕ_m, which is set by the balance of $\tau_{\rm g}$ and of $\tau_{\rm sd}$. Hence, ϕ_m is set by the balance of two competing processes, both of them driven by the activity. As we discussed in Chapter 2.7, the two proposed theories attributed the promotion of the homogeneous phase to either to the rotational or to the translational diffusivity. This finding has its conceptual novelty as we first point out activity also promote the homogeneous phase.

We finally note that our model reduces to the one introduced by Redner *al.* [7, 10] for the binodal, if one neglects the density dependence of τ_g Eq. 3.5, as well as the

sliding detaching mechanism Eq. 3.7. The corresponding theoretical prediction, which is formally derived from Eq. 3.9 setting $c = 0$ and taking the $\phi^* \to \infty$ limit, is

$$\mathrm{Pe} = \frac{b/a}{\phi}. \tag{3.12}$$

3.3 Numerical validation of theoretical model

3.3.1 The standard ABPs model

To validate our theoretical prediction, we perform numerical simulations of ABPs in both two and three spatial dimensions, for a system of particles (polydispersity 2.9%) interacting via a Harmonic potential. We use periodic boundaries in all spatial directions. As mentioned, we work in the hard-sphere limit considering stiff particles, the maximum relative deformation of a particle being $\leq 10^{-4}$ for the range of parameters we have considered. In this subsection, we focus on what we call the standard ABPs model, for which the rotational and the translational diffusion are related with $s = 1$.

After having inserted into the simulation box the particles at the desired value of the volume fraction, we perform long simulations in the presence of the active force to drive the system in its steady state. Precisely, the equilibrium time is at least $50/D_r$. Examples final configurations are illustrated in Fig. 3.2 (2D) and Fig. 3.3 (3D).

At this point, we need to decide if the final configuration of the system is in the homogeneous or in the phase separated state. The direct visualization of the system is undoubtedly enough to make this decision in some cases, but in general, it is not.

To this end, we have therefore decided to study the distribution of the coarse-grained density field, $\rho_{cg}(r)$. This distribution is indeed expected to have a single peak in the homogeneous phase, and two peaks in the phase separate one, the location of the two peaks occurring at the volume fraction of the coexisting densities.

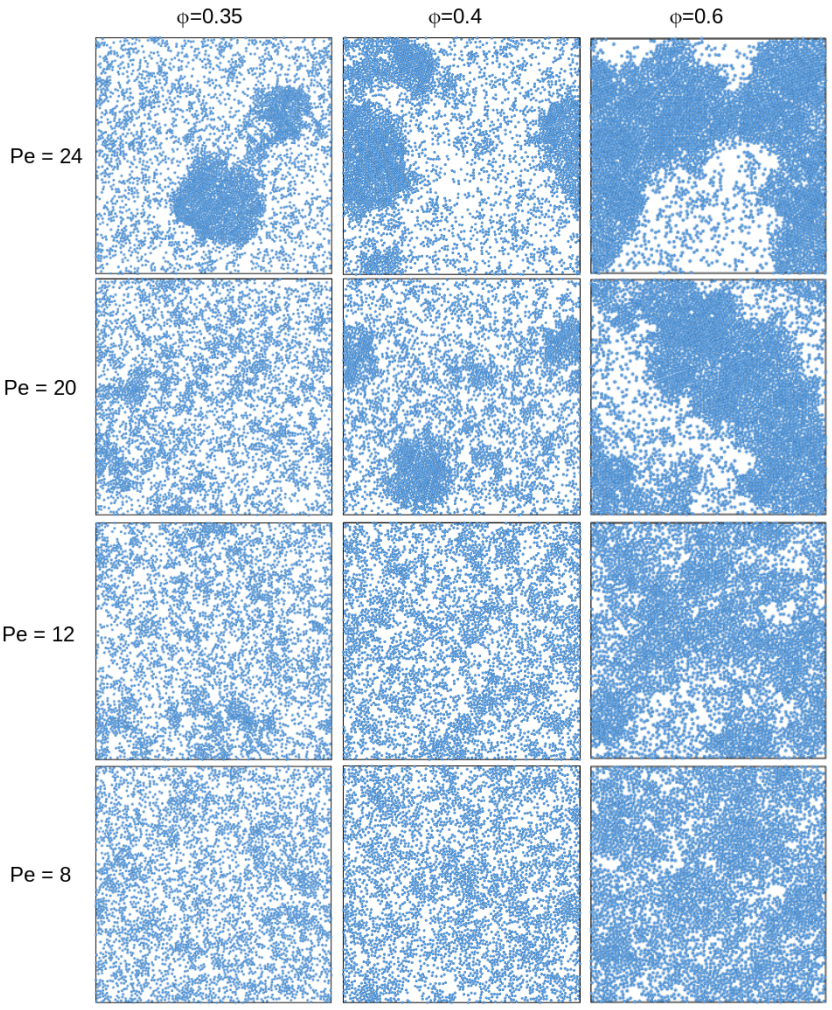

FIGURE 3.2: Example steady state configurations for different values of the volume fraction ϕ and of the Peclet number Pe, for two dimensional systems with $N = 4000$ particles.

The coarse-grained density field can be defined in several different ways. Here we follow the approach of Ref. [12], and define the coarse-grained density by convoluting the number density $\sum_i \delta(\mathbf{r} - \mathbf{r_i})$ with $f(\mathbf{r}) = Z \exp[-1/(1 - r^2/w^2)]$, where Z is a normalization factor. That is,

$$\rho_{cg}(\mathbf{r}) = \int \sum_i \delta(\mathbf{r}' - \mathbf{r_i}) f(|\mathbf{r} - \mathbf{r}'|) d\mathbf{r}'. \tag{3.13}$$

The coarse-graining function depends on a length scale, we fix to $w = 3.5$ particle diameters, following Ref. [12]. We have checked that if w varies, withing reason, the phase diagram does not substantially changes.

Example distributions of the local volume fraction are in Fig. 3.4a,b. Figs. 3.4c,d

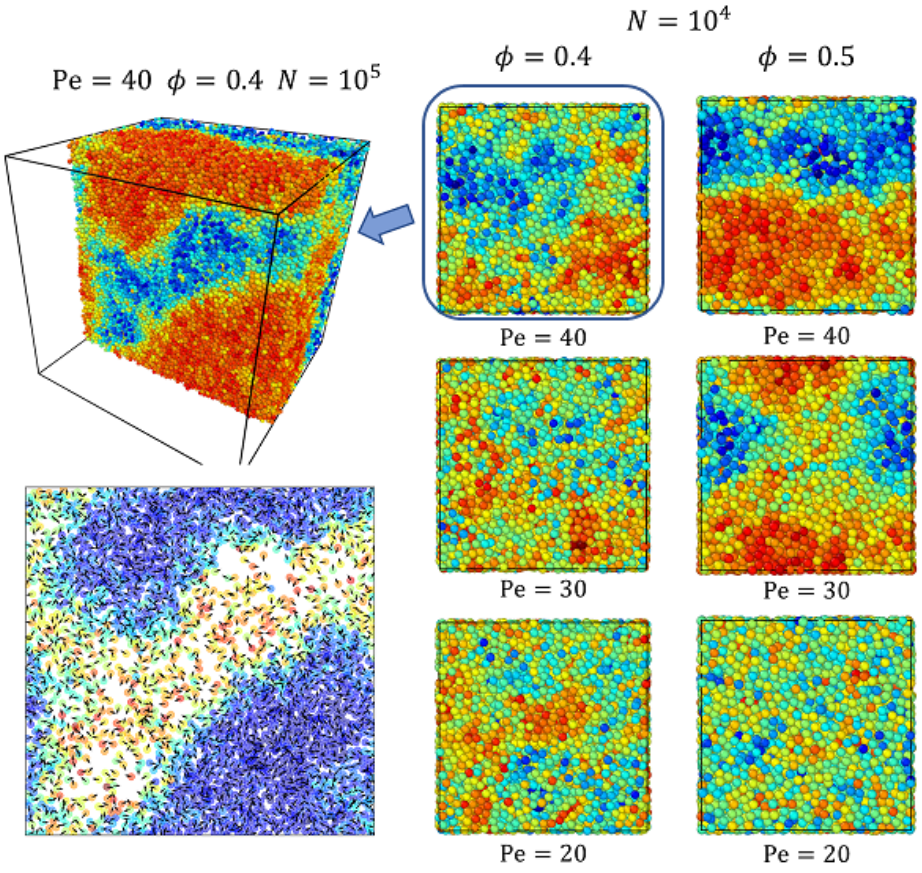

FIGURE 3.3: Examples of steady-state configurations for different values of the volume fraction ϕ and of the Peclet number Pe, for three dimensional systems with $N = 10^4$ and $N = 10^5$ particles. The color code is jet type, which tells the local density from higher density (red) to lower density(blue). The color bar is auto ranged within each configuration; thus, it only shows the difference in density within each configuration. At the boundary of the phase diagram when phase separation is hard to determine from $N = 10^4$, we will move to a larger system size. The configuration on the button right is a slice of 3D configuration with color-coded by the magnitude of displacement.

show the resulting phase diagram, respectively in 2d and in 3d, for standard Brownian particles ($s = 1$), which are consistent with those previously reported in the literature as concern the critical value of the Peclet number and the typical values of the volume fractions. We assign a point in the $\phi-$Pe to a phase-separated phase only if we can spot bimodal density probability distribution. Sometimes when the state is not clear as the density probability distribution showed in Fig. 3.4b and the configuration in Fig. 3.3 at $Pe = 40, \phi = 0.4$, we will go to larger system. In two dimensions, we consider systems with N up to 32000, in three dimensions with N up to 10^6.

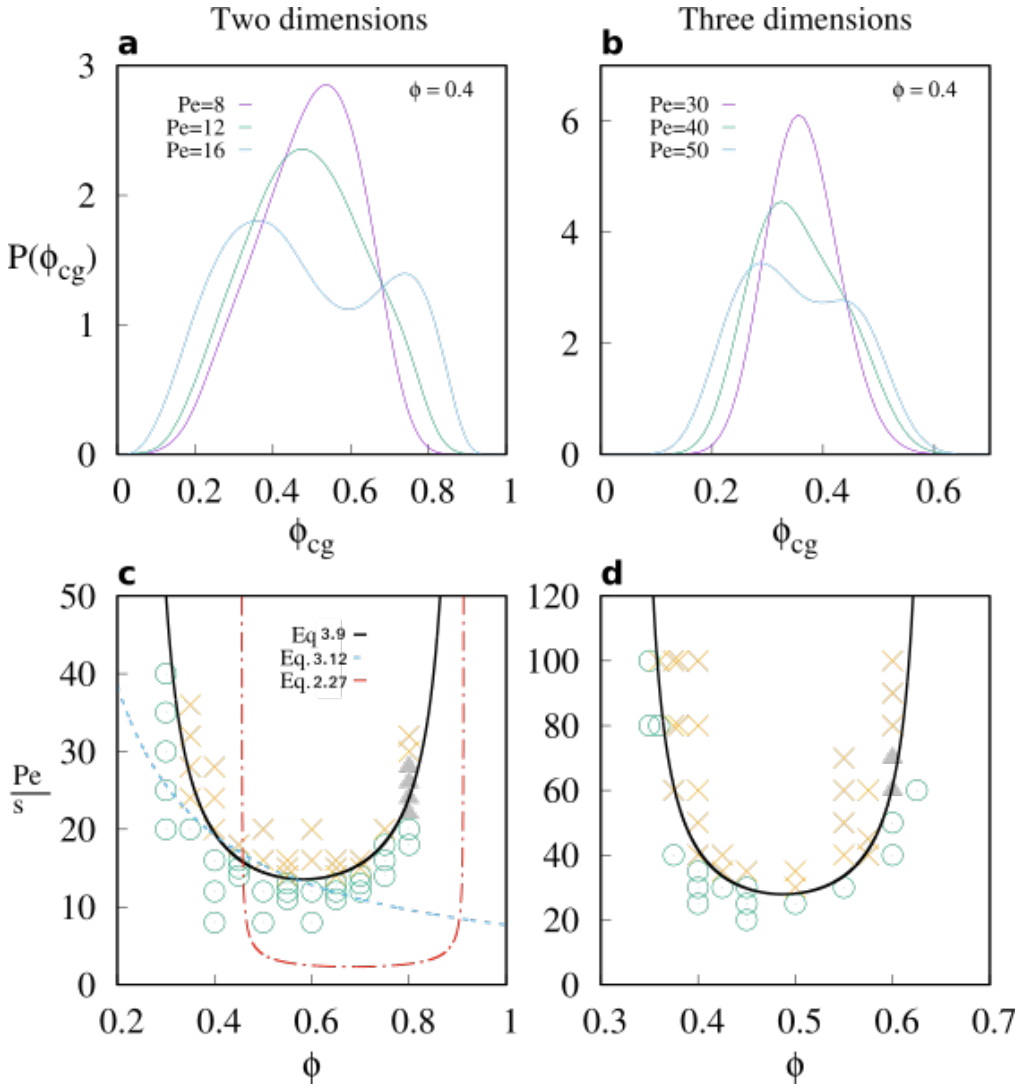

FIGURE 3.4: Panel **a** illustrates the probability distribution of the coarse-grained volume fraction at $\phi = 0.4$ for different values of the Peclet number, in two dimensions, for $N = 4000$. Panel **c** shows the resulting phase diagram, where crosses identify phase-separated configurations, circle homogeneous ones, and triangles state points at which we were unable to conclusively asses the phase. The full line is a fit to the functional form of our theoretical model, Eq. 3.9, with $\phi^* = 0.91$, $\phi_m = 0.25$ and $A = 1.47$, the blue line is prediction of the kinetic approach for the coexistence line, Eq. 3.12 with $b/a \simeq 7.5$, while the red line line is the prediction of the continuum model, Eq. 2.27. Panels **b** and **d** illustrate analogous three dimensional results, for $N = 10000$. In this case, $\phi^* = 0.645$, $\phi_m = 0.345$ and $A = 0.60$.

In Fig. 3.4, my theoretical prediction of Eq. 3.9 is the full black line. Clearly, our model correctly identifies the spinodal line. The parameter values are $\phi^* = 0.91$, $\phi_m = 0.25$ and $A = 1.47$: they are all of order one as expected. This result certainly strongly support the physical scenario we have hypothesized.

In the figure, we also illustrated the predictions of the kinetic theory for the coexistence line, as the blue dashed-dotted line. As mentioned, this prediction does not describe the existence of a critical point. However, the coexistence line is expected to be close to the spinodal line, at least close to the critical point, and indeed we see that this is the case at least as concern the low-density side, $\phi \leq \phi_c$. Finally, in the figure, we also illustrate the prediction of the continuum theory, as a red line. This prediction corresponds to Eq. 2.22, in which the diffusion coefficient is fixed to the value of the passive suspensions in the dilute limit. As previously noticed [1], this prediction largely underestimates the critical Peclet number. Here, we also notice that it predicts $\phi_m = \phi^*/2$, overestimating the actual value. A better agreement between the prediction of the continuum model and of the numerical results could be obtained treating ϕ^* [2] (or ϕ_m [13, 14]) as free parameters, and allowing for a presence of a scale factor possibly associated to an effective diffusivity.

3.3.2 A more stringent test

Our theoretical model has three free parameters and correctly describe the data. Conversely, the continuum description, which does not describe the data, has none. Somehow artificially, one might introduce free parameters also in the continuum model, for instance, by assuming that the diffusivity is an effective diffusivity. In this way, one can translate the red curve in Fig. 3.4c, and hence describe the numerical data reasonably well.

To perform a more stringent comparison between the different theoretical predictions, we consider that according to our model, the spinodal line is proportional to the constant s. We remind that the rotational diffusion coefficient is sD_r, the translational one $D_t = D_r\sigma^2/3$. The continuum model prediction [2, 4, 13, 15], which we have derived in Sec. 2.7.2, can easily be generalized to the case in which the rotational diffusion is scaled by a factor s. In this case, the effective diffusivity results

$$\mathcal{D} = D - \frac{v_{\rm cg}^2(\rho)}{2sD_r}\left[1 + \frac{d\log v_{\rm cg}}{d\log\rho}\right], \tag{3.14}$$

and the spinodal line

$$\mathrm{Pe}_s^{\rm cont} = -s^{1/2}\left[\frac{3}{2}\left(1-\frac{\phi}{\phi^*}\right)\left(1-\frac{2\phi}{\phi^*}\right)\right]^{-1/2}. \tag{3.15}$$

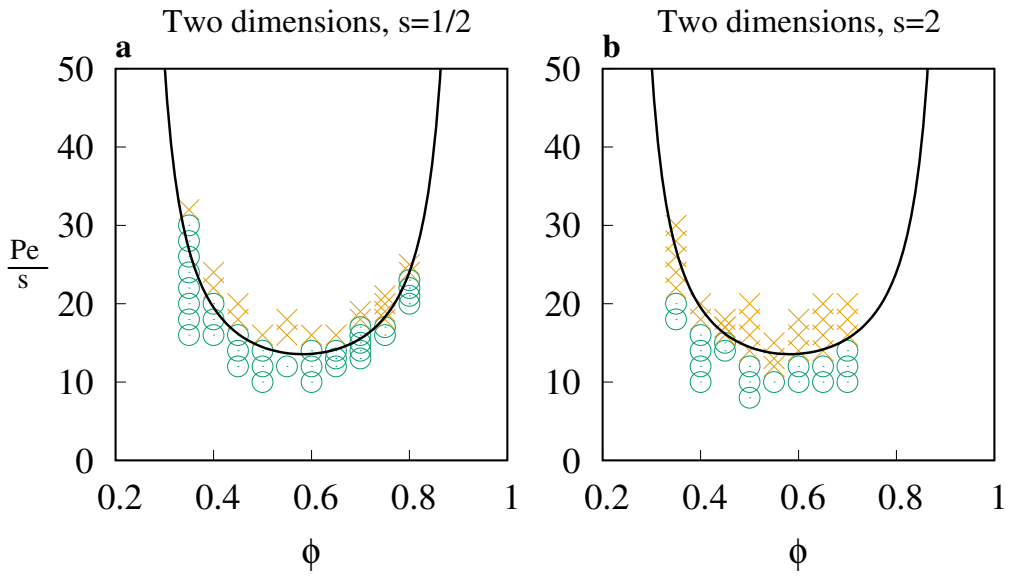

FIGURE 3.5: Phase diagram (spinodal lines) of ABPs, in two dimensions. With respect to its standard value, the rotational diffusion coefficient is changed by a factor $s = 1/2$ in **a**, and by a factor $s = 2$ in **b**. This does not affect the phase diagram, if the Peclet number is also rescaled by a factor s.

Hence, out theoretical prediction and the prediction of the continuum model predicts a different scaling of the critical line with s. The critical line is proportional to s in our model, while it scales as $s^{1/2}$ in the continuum approach. This implies that a stringent test between the two models can be numerically performed investigating the s dependence of the spinodal line.

I have performed this investigation in two dimensions, considering $s = 1/2, 1$ and 2. The phase diagram for $s = 1$ is in Fig. 3.4c, while the results for $s = 1/2$ and $s = 2$ and in Fig. 3.5a and b, respectively. In all cases, we are plotting on the y-axis the Peclet number over the constant s. Hence, according to our theoretical model, all of these diagrams should be essentially equal, while according to the continuum model, we should observe a marked difference. For instance, on the y axis Fig. 3.5a and b should differ by a factor 4. The numerical results demonstrate that the phase diagram in the Pe/s vs ϕ plane is s independent, strongly supporting the validity of our theoretical model.

To further compare the different model, we consider the limiting case $s = 0$. In this limit, there self-propelling directions of the particles do not diffuse but are constant. This limiting case has been previously investigated by Fily *et al.* [2, 4]. These works have demonstrated that, in the hard-sphere limit, the absence of angular noise leads to a vertical phase boundary, $\phi_s(\mathrm{Pe}) = \phi_m$, in agreement with

our theoretical prediction of Eq. 3.9. Notice that the continuum model predicts a vertical phase boundary in the absence of translational noise [2], regardless of the rotational noise. All of these results appear to support the validity of the proposed theoretical model strongly.

3.4 The role of the translational diffusivity

The theoretical prediction of the continuum approach does not appear to describe the spinodal line of ABPs well. However, the underlying formalism appears to be exact, also considering that the continuum hydrodynamic equation has been recently re-derived starting from the many-body Smoluchowski equation. Hence, the equation for the effective diffusivity derived within the continuum approach, we repeat here for completeness, appear to be correct,

$$\mathcal{D} = D - \frac{v^2(\rho)}{2D_r}\left[1 + \frac{d\log v}{d\log \rho}\right]. \tag{3.16}$$

So, how the theoretical predictions may be wrong?

The answer to this question, I suspect, is in the absence of a theoretical prediction for the diffusion coefficient D, which in the above equation is the only positive term, i.e., the only 'force' promoting the homogeneous phase. The spinodal line of the continuum model we have discussed so far corresponds to the solution of $\mathcal{D} = 0$ under the assumption that D is the translational diffusion coefficient of the passive suspension, in the dilute limit, $D = D_r\sigma^2/3$. This is the standard assumption in the literature [4, 13, 15, 16]. Here I demonstrate that this assumption is certainly wrong and that some other expressions for the diffusivity need to be found.

To prove that the thermal diffusivity plays a negligible role, I compare the diffusion coefficient of the passive suspension to effective diffusion coefficients induced by the activity. I have determined the diffusivity of the passive suspension by performing simulations in which the active velocity is set to zero, i.e., purely Brownian Dynamics simulations. In two dimensions, I have found the diffusion coefficient to approximately scale as $D_p(\phi) = D(1 - \phi/\phi_d)$ with $\phi_d \simeq \phi^*$, in the volume fraction range considered. This is inconsistent with the expectation for the low-density behavior of Brownian particles [17].

For active suspension, I considered two diffusivities. Indeed, the motion of a particle in the homogeneous phase can be described as resulting from a sequence of steps alternatively taken from distributions corresponding to two different stochastic processes, describing the motion in between collisions and during a collision. The stochastic process describing the motion resulting from the steps performed in between the collisions is that of a persistent random walk, with persistence time $1/sD_r$. The corresponding diffusivity $D_\parallel$ is evaluated, following previous works [4, 6], considering the steps to have length $l = v_a s^{-1} D_r^{-1} \left(1 - \frac{t_c}{t_c + t_{\rm mf}}\right)$, where t_c and $t_{\rm mf}$ are the mean duration of a collision, and the mean time between collisions. At low density $t_{\rm mf} \propto (v_a \sigma^{d-1} \rho)^{-1} \gg t_c$, and $t_c/t_{\rm mf} = \phi/\phi^*$ [6], so that

$$D_\parallel - \frac{D_p(\phi)}{d} \simeq \frac{\sigma^2 D_r {\rm Pe}^2}{s} \left(1 - \frac{\phi}{\phi^*}\right)^2 . \tag{3.17}$$

In the above equation, I have taken into account the contribution of the thermal diffusivity, which is divided by a factor d accounting for the fact that $D_\parallel$ is effectively a one-dimensional diffusivity. The stochastic process describing the motion resulting from the steps performed during the collisions is that of a simple random walk, with step size $\propto \sigma$ and step frequency $1/(t_c + t_{\rm mf}) \sim 1/t_{\rm mf} \propto v_a \phi/\sigma$, so that

$$D_\perp - \frac{D_p(\phi)}{d} \simeq \sigma^2 {\rm Pe} D_r \phi \tag{3.18}$$

To numerically validate these theoretical predictions, we decompose the instantaneous velocity of particle i in the components parallel and perpendicular to its self-propelling direction, $\mathbf{v}_i(t) = \mathbf{v}_i^\parallel(t) + \mathbf{v}_i^\perp(t)$, with $\mathbf{v}_i^\parallel = (\mathbf{v_i} \cdot \mathbf{n_i})\mathbf{n_i}$. The time integration of these velocities defines a normal and a tangential displacement, $\mathbf{\Delta r}_{\parallel,\perp}^i(t) = \int_0^t \mathbf{v}_i^{\parallel,\perp}(t) dt$, from which we estimate the diffusion coefficients, $D_{\parallel,\perp} = \lim_{t\to\infty} \langle \mathbf{\Delta r}_{\parallel,\perp}^2(t) \rangle / 2t$. Fig. 3.6 shows that these numerical estimates well compare with the theoretical predictions. The theoretical predictions fail at small Pe, where the collisional description of the dynamics is no longer appropriate.

Importantly both diffusion coefficients, and in particular $D_\perp$ which describes a physical process promoting the homogeneous phase, grow with the Peclet number, and are much larger than the diffusivity of the passive suspension, which is therefore negligible. This demonstrates that the thermal diffusivity does not generally play any role in the motility induced phase separation. Shortly, the diffusion coefficient

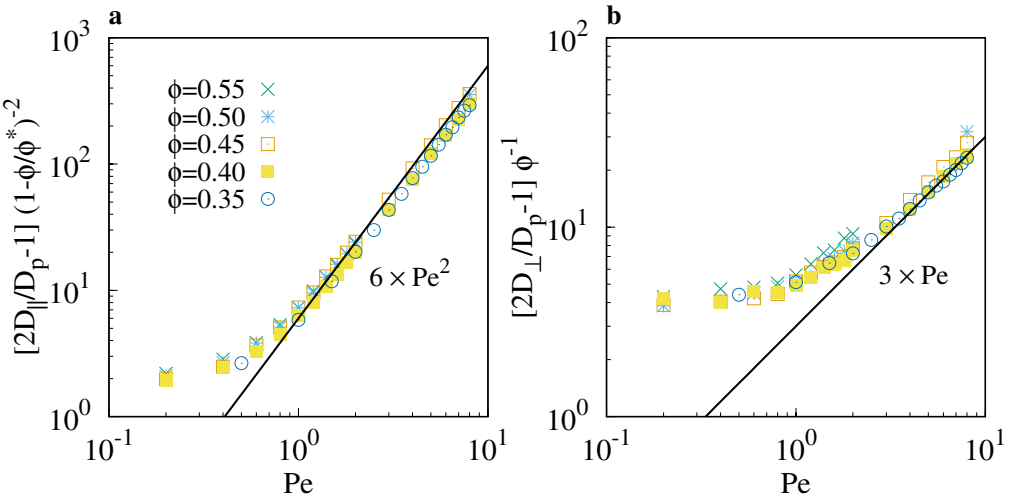

FIGURE 3.6: Peclet number dependence of rescaled diffusion coefficients associated to the motion parallel and perpendicular to the self-propelling direction of each particle.

that needs to be considered in the continuum description should be an effective Peclet number dependent one. Which one, I do not know.

As a final note, I remark that the investigation of the diffusion coefficients clarifies that the thermal diffusion coefficient could play a role, but only if the rotational diffusion is small, i.e., if $s \ll 1$. As s decreases, the value of the Peclet number at the critical point decreases and becomes smaller than 1, the value at which thermal effects are expected to play a role. The investigation of the motility induced phase diagram for small values of s could be of interest to study the interplay between the MIPS coexistence region, and the liquid-hexatic coexistence region of the passive suspensions [18].

3.5 Cluster dynamics in the phase separated state

3.5.1 Rotational motion of active clusters

The sliding detaching mechanism illustrated in Fig. 3.1(lower panel), which is a crucial ingredient of our theoretical model for the spinodal line, can be described as resulting from the rotation of two colliding particles around their center of mass, in the absence of changes in their self-propelling directions.

Cluster comprising not two, but many particles, are observed inside the coexistence region. In particular, in the coexistence region, the steady-state is highly dynamic, as clusters are seen to break and reform continuously. How do cluster break?

The common assumption in the literature is that cluster brake through the rotational detaching mechanism [7, 19, 20]. That is, it is expected that a particle in the rim of a cluster detaches from it as a consequence of the rotation of its self-propelling direction, which might point away from the cluster center.

The existence of the sliding detaching mechanisms suggests that large cluster might break through a different physical process. In particular, it is possible that a cluster rotates, without the self-propelling directions of the particles changing. As in the simple case of a two-particle cluster, the rotation of the cluster makes the self-propelling direction parallel to the cluster surface. This is expected to induce instability, and we call rotational instability.

Before demonstrating this instability, let me mention that in a related experimental contest, the rotational motion of the clusters has been observed. In particular, Ref. [21] has recently performed a careful investigation of the cluster dynamics, demonstrating that cluster does rotate. In particular, it has been demonstrated that the angular velocity of the cluster is a Gaussian random variable, with typical scale

$$\omega \propto \frac{1}{N_c}\frac{v_a}{\sigma} \propto \frac{1}{N_c}\frac{Pe}{\tau_B}, \tag{3.19}$$

where N_c is the number of particles of the cluster. This results, including the dependence on N_c, is rationalized considering that the overall torque acting on the cluster is the sum of the torques exerted by the particles, which are uncorrelated random variables [21]. Let me remind however that in the experiments there is cohesion between the active particles [22]: hence, even if the self-propelling directions become parallel to the cluster surface and promote the instability, the instability is prevented by the attractive interaction between the particles.

A similar scenario has been reported in numerical simulation of Active Brownian dumbbells. In this systems, the active velocity acts along the long edge of of the dumbbell. Due to their elongated shape, particles now exerts a torque on each other. As a consequence, the rotation of a cluster induces the rotation of the particles, and hence of their self propelling directions. Because of this, in the active dumbbells, the rotation of a cluster does not make the self -propelling direction

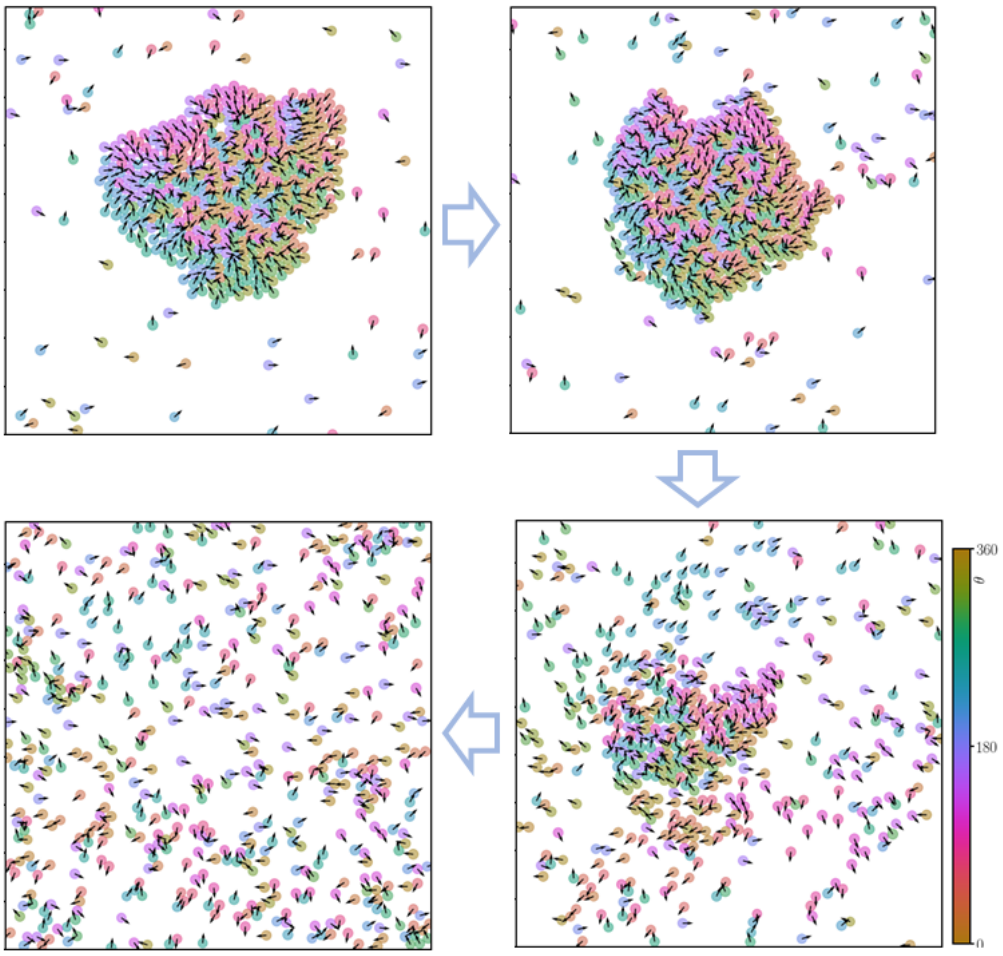

FIGURE 3.7: Evolution of a cluster of ABPs, with color-code and arrows indicating the self-propelling directions. As the cluster rotates, it becomes unstable and disintegrate. The corresponding video could be find in the link: https://youtu.be/Vt66x0dsGLE

parallel to the cluster surface promoting the instability. It follows that cluster of active dumbbells may perform the long-lived rotational motion, as numerically reported [23].

3.5.2 Rotational instability of active clusters in ABPs

According to the consideration above, in ABPs the rotational motion of a cluster should induce its instability. We do show that this is actually the case in Fig. 3.7, where we illustrate the time evolution of a cluster. We do see that as the cluster rotates, it becomes unstable, and then disintegrate. Notice that the timescale of this process is set by the typical rotational angular velocity of the cluster, Eq. 3.19.

This scales with the active velocity, and hence with the Peclet number. At high Peclet number, this is a fast process.

However, the angular velocity is also inversely proportional to the cluster size. Hence, this is a slow mechanism for large clusters. In this case, we have observed that the instability develops at the cluster surface, as a group of particles starts sliding over the cluster. This leads to detachment of the small cluster from the large one 3.8, or to the fragmentation of a large cluster in smaller ones 3.9. Characterization of these processes would be interesting, but it is left for further studies.

3.6 Discussion and conclusion

In this chapter, I have developed a theoretical approach to predict the spinodal line of ABPs, in the Peclet number, volume fraction plane. This approach is based on our kinetic description of the time evolution of the density fluctuations, the spinodal resulting from the balance between the time needed for a fluctuation to form, and the time it needs to decay. Some of the involved timescales have been evaluated following previous works, modifying earlier predictions to take into account the density induced slowdown of the dynamics. More importantly, however, I have identified a previously unreported mechanism for the decay of the density fluctuations and evaluated its timescale. This is the sliding detaching mechanism, illustrated in Fig. 3.1 (lower panel). The theoretical prediction compares very well with the numerical simulations, in both two and three dimensions. It also clearly outperforms earlier theoretical studies. This is clearly illustrated in Fig. 3.4c, and also results from the additional investigations I have reported. Overall, it appears that these results solve a longstanding issue in the literature, and clarify the physical processes at work in the prototypical active matter system.

In addition, I have investigated the reason why the prediction of the first-principle continuum description of ABPs appears to fail. The conclusion is that the prediction fails as based on an inappropriate assumption made on the role of the diffusion coefficient, which is not derived from first principles. Finally, I have investigated the role of the sliding detaching mechanism in the dynamics occurring in the phase separated state, inside the spinodal line. I have shown that this mechanism gives

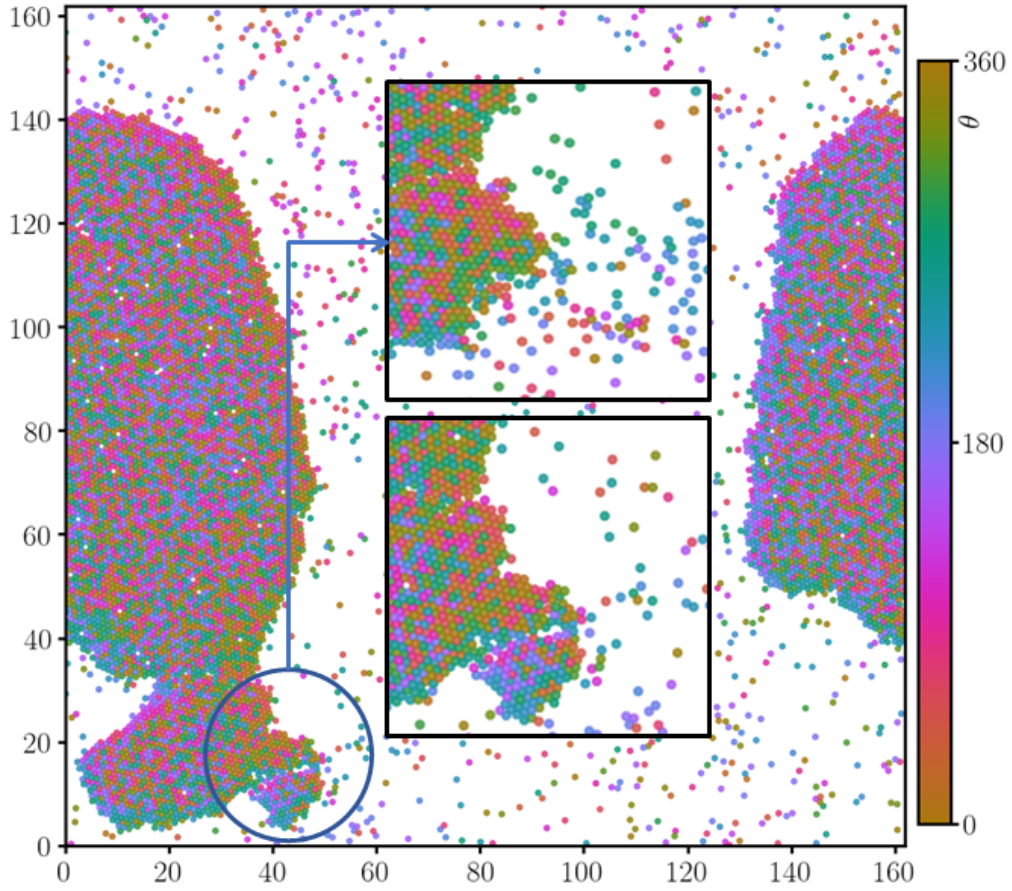

FIGURE 3.8: The rotational motion of a huge cluster could be slow, as the angular velocity is inversely proportional to the cluster size. The large cluster may therefore not disintegrate when rotation, as in the case illustrated in Fig. 3.7. Rather, an instability may develop on the surface, leading to the detachment of a small cluster from the main one, as illustrated in this figure. The corresponding video could be find in the link: https://youtu.be/jjFI9tJowA8

rises to a rotational instability of the clusters, whereby small clusters quickly dissolves upon rotation and illustrated how this instability manifests in large clusters, whose rotational motion is slow.

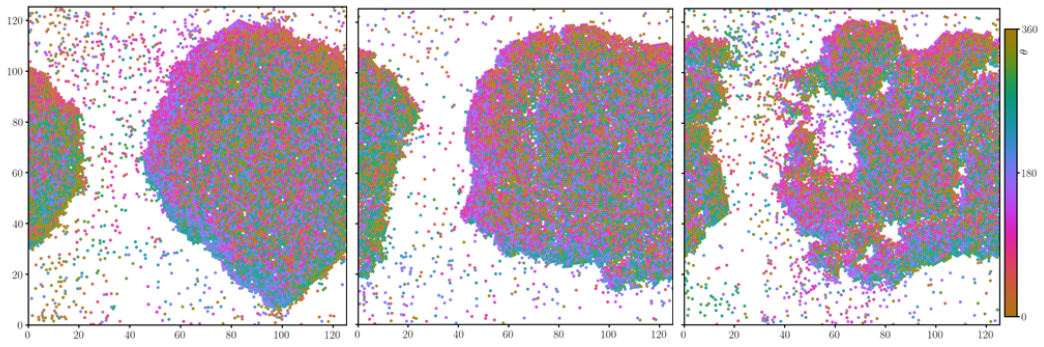

FIGURE 3.9: The rotational motion of large clusters might also induce its fracturing in a number of smaller clusters, which then disintegrate through the rotational instability mechanism (Fig. 3.7). This figure illustrates the developing of this fracturing process. The corresponding video could be find in the link: https://youtu.be/EaFHmjNlebg

References

[1] Michael E Cates and Julien Tailleur. Motility-induced phase separation. *Annu. Rev. Condens. Matter Phys.*, 6(1):219–244, 2015.

[2] Yaouen Fily, Aparna Baskaran, and Michael F Hagan. Dynamics of self-propelled particles under strong confinement. *Soft matter*, 10(30):5609–5617, 2014.

[3] Steve Plimpton. Fast parallel algorithms for short-range molecular dynamics. *Journal of computational physics*, 117(1):1–19, 1995.

[4] Yaouen Fily and M Cristina Marchetti. Athermal phase separation of self-propelled particles with no alignment. *Physical review letters*, 108(23):235702, 2012.

[5] Andreas Zöttl and Holger Stark. Hydrodynamics determines collective motion and phase behavior of active colloids in quasi-two-dimensional confinement. *Physical review letters*, 112(11):118101, 2014.

[6] Joakim Stenhammar, Davide Marenduzzo, Rosalind J Allen, and Michael E Cates. Phase behaviour of active brownian particles: the role of dimensionality. *Soft Matter*, 10(10):1489–1499, 2014.

[7] Gabriel S Redner, Michael F Hagan, and Aparna Baskaran. Structure and dynamics of a phase-separating active colloidal fluid. *Physical review letters*, 110(5):055701, 2013.

[8] Ivo Buttinoni, Julian Bialké, Felix Kümmel, Hartmut Löwen, Clemens Bechinger, and Thomas Speck. Dynamical clustering and phase separation in suspensions of self-propelled colloidal particles. *Physical review letters*, 110(23):238301, 2013.

[9] Adam Wysocki, Roland G Winkler, and Gerhard Gompper. Cooperative motion of active brownian spheres in three-dimensional dense suspensions. *EPL (Europhysics Letters)*, 105(4):48004, 2014.

[10] Gabriel S Redner, Caleb G Wagner, Aparna Baskaran, and Michael F Hagan. Classical nucleation theory description of active colloid assembly. *Physical review letters*, 117(14):148002, 2016.

[11] Isaac R Bruss and Sharon C Glotzer. Phase separation of self-propelled ballistic particles. *Physical Review E*, 97(4):042609, 2018.

[12] Michael E Cates and Julien Tailleur. When are active brownian particles and run-and-tumble particles equivalent? consequences for motility-induced phase separation. *EPL (Europhysics Letters)*, 101(2):20010, 2013.

[13] Thomas Speck, Julian Bialké, Andreas M Menzel, and Hartmut Löwen. Effective cahn-hilliard equation for the phase separation of active brownian particles. *Physical Review Letters*, 112(21):218304, 2014.

[14] Thomas Speck. Stochastic thermodynamics for active matter. *EPL (Europhysics Letters)*, 114(3):30006, 2016.

[15] Julian Bialké, Jonathan T Siebert, Hartmut Löwen, and Thomas Speck. Negative interfacial tension in phase-separated active brownian particles. *Physical review letters*, 115(9):098301, 2015.

[16] Elijah Flenner, Grzegorz Szamel, and Ludovic Berthier. The nonequilibrium glassy dynamics of self-propelled particles. *Soft matter*, 12(34):7136–7149, 2016.

[17] Jan KG Dhont. *An introduction to dynamics of colloids*, volume 2. Elsevier, 1996.

[18] Pasquale Digregorio, Demian Levis, Antonio Suma, Leticia F Cugliandolo, Giuseppe Gonnella, and Ignacio Pagonabarraga. Full phase diagram of active brownian disks: From melting to motility-induced phase separation. *Physical review letters*, 121(9):098003, 2018.

[19] Ivo Buttinoni, Giovanni Volpe, Felix Kümmel, Giorgio Volpe, and Clemens Bechinger. Active brownian motion tunable by light. *Journal of Physics: Condensed Matter*, 24(28):284129, 2012.

[20] I Theurkauff, C Cottin-Bizonne, J Palacci, C Ybert, and L Bocquet. Dynamic clustering in active colloidal suspensions with chemical signaling. *Physical review letters*, 108(26):268303, 2012.

[21] F Ginot, I Theurkauff, F Detcheverry, Christophe Ybert, and C Cottin-Bizonne. Aggregation-fragmentation and individual dynamics of active clusters. *Nature communications*, 9(1):696, 2018.

[22] Benno Liebchen and Hartmut Löwen. Which interactions dominate in active colloids? *The Journal of chemical physics*, 150(6):061102, 2019.

[23] Isabella Petrelli, Pasquale Digregorio, Leticia F Cugliandolo, Giuseppe Gonnella, and Antonio Suma. Active dumbbells: Dynamics and morphology in the coexisting region. *The European Physical Journal E*, 41(10):128, 2018.

Chapter 4

Frictional active Brownian particles

In this chapter, I present the first numerical and theoretical investigation of the effect of friction in active matter, focusing on a model of frictional active Brownian particles(ABPs). I will show that friction qualitatively affects the features of the motility induced phase diagram. In particular, while in the absence of friction the low density side of the U-shaped spinodal line diverges at a finite density, with friction it only diverges in the zero density limit. In this respect, the $\mathrm{Pe} - \phi$ phase diagram of frictional ABPs qualitatively differ from its frictionless counterpart, and results similar to the $1/T - \phi$ liquid-gas phase diagram.

This chapter is structured as follows. In Sec.s 4.1 and 4.2 I will illustrate the experiments that suggest frictional forces might play a role in active matter, overview the basic features of the frictional interactions, as well as the numerical model we use to model the frictional interaction. Friction qualitatively affect the features of the motility induced phase diagram. I demonstrate this in Sec. 4.3, where I present results for the frictional dependence of the phase diagram. In Sec. 4.4 I investigate the dynamical features of ABPs in the presence of friction, so as to gain insights allowing to develop a model for the phase separation in the presence of friction. In the following Sec. 4.4.5 I demonstrate that, in general, friction affects the rotational dynamics of the particles, but it does not align the self-propelling directions. Hence, frictional active matter does not display flocking, as for instance schools of fish do, and more generally active matter of elongated particles. In this

respect, frictional ABPs are similar to the frictionless ones. Finally, discussion and perspective are presented in Sec. 4.5.

4.1 Why friction in active matter?

4.1.1 Overview

To my knowledge, all previous numerical investigations of active matter systems, for instance as reviewed in Chapter 2.6, are focused on frictionless systems. In the ABPs model, particles are assumed to interact via spherically symmetric repulsive potentials, such as the Harmonic repulsion we have also considered, Yukawa-like potential [1], the WCA potential [2], and similar ones. In these models, the interaction forces are always along the line that joining the center of the two interacting particles. That is, no torque acts on the particles during their collisions. As a consequence, the self-propelling direction of the particles is not affected by their collision, but simply diffuses with diffusion coefficient D_r. Such kinds of modelling make the rotational dynamics of the self-propelling directions a purely diffusive one. This might be a really special case in nature as torques occurs in the interaction of elongated particles,which is more common, or torque could be generated from the friction force which exist almost everywhere in nature.

Here below, we review two set of experimental observations that suggesting that friction might be at work in active systems. The considerations below will clarify that, even if the current experiments are unaffected by friction, it is in principle possible to engineer experiments in which the frictional interaction is relevant.

4.1.2 Friction in dry systems

Friction might be certainly guessed to play a role in experiments of dry active matter [3–5]. In these experiments, a flocking behavior has been observed, which is not commonly found in ABPs. Such a behavior has been rationalized invoking [5] a coupling between the polarity of the particles and their velocity, mediated by the interaction with the bottom substrate. The role of the frictional interaction between the particle, conversely, has not been explored. More generally, we are

certainly all familiar with the existence of friction in the interaction between two macroscopic objects, and it is therefore of interest to understand how this affects particle dynamics. People in a crowd, for instance, are subject to frictional forces.

4.1.3 Friction in wet systems

Experiments on synthetic colloidal scale active particles are performed in wet conditions. That is, the particles self-propel while in a liquid. In these circumstances, one might think friction in the interparticle interaction not to be relevant. Indeed, direct inter-particle interactions in a fluid are generally screened by a fluid layer trapped in between the colliding particles.

However, in a different context, it has been recently demonstrated that direct frictional inter-particle contacts do actually occur in colloidal suspensions. In particular, in colloidal suspensions under shear, at high shear rates particles might overcome their hydrodynamic repulsion entering into physical contact. It is currently believed that this is the mechanism responsible for the so-called discontinuous shear thickening [6–9], a sudden jump in the dependence of the shear viscosity on the shear rate.

In the case of active colloidal particles one might therefore suspect that, at high Peclet numbers, two colliding particles may likewise overcome their hydrodynamic repulsion and enter into physical contact. Thus, active forces could be in principle at work in experiments with thermophoretic active particles [10–12]. To check if this is the case, one may investigate the rotational motion of the particles in dense clusters, as in the presence of friction particles will certainly not undergo free rotational diffusion. This experimental study has not yet been carried out.

Regardless, even if friction is not actually relevant in the current experimental realizations of active matter, it might be in the future. Indeed, recent works have demonstrated that it possible to engineering colloidal particles with very rough surfaces, whose frictional interaction is readily observed [8, 13]. These considerations make certainly of interest the investigation of the role friction in active matter.

4.2 Friction: basic concepts and modeling

4.2.1 Frictional interaction

Frictional forces are extremely complex, and have been studied for more than 500 year. Friction is clearly a topic of great relevance, with applications in engineering, physics, material science, biology and so on. The modern name of the discipline investigating frictional forces is 'tribology'. Perhaps, this discipline originated in 1493, when Leonardo da Vinci observed that the frictional resistance between two objects only depends on their area of contact, in an unpublished notebook. da Vinci also observed that the friction resistance opposing the relative motion of two different objects of the same weight but difference area of contact is the same. Finally, da Vinci noticed that when the weight of the objects doubles, the force needed to overcome friction and put the objects in relative motion doubles. These observations are currently known as are the first and second law of friction, as published by Guillaume Amontons, a pioneer in the subject, in 1699. These laws were further developed by Charles-Angustin de Coulomb in 1785, who noticed that the static friction force may depend on the contact time and the dynamic friction may depends on sliding velocity, normal force and contact area. Today, the investigation of the properties and of the microscopic origin of the frictional forces is still a topic of intense research. For instance, Coulomb friction coefficient, we are all familiar with, is usually assumed to depend on surface material, ranging from low friction coefficient material ice (0.02) to high friction coefficient material rubber (1.0), silver (1.5) etc. However, in a recent paper Oded and Fineberg have experimentally demonstrated that the friction is not a material constant, as it depends on the loading conditions [14].

Here we do not dwell in these complex and not yet settled features of the frictional interaction, and simply assume as customary that the properties of the frictional interaction are well described by the following laws:

1. First Law of Amontons: Friction is independent of the apparent area of contact;

2. Second Law of Amontons: The frictional force is directly proportional to the normal load;

3. Third Law of Coulomb: Dynamic friction is independent of the relative sliding speed.

4.2.2 Model frictional interaction

To numerically take into account the effect of friction, one needs to consider that the microscopic origin of the frictional force is in the deformation of their interface. Numerically, this deformation, $\mathbf{\Delta s}_t$, is measured as the integral of the relative velocity of the two objects. We are considering here the relative velocity at the point/area of contact, a quantity that is also affected by the rotational motion of the two objects.

In the numerical simulations, we describe the frictional interaction between two objects using the Mindlin model [15], according to which the tangential force acting at the interface between two contacting objects is

$$\mathbf{F}_t = -k_t \Delta \mathbf{s_t} \quad \text{if } |\mathbf{F_t}| < |\mu \mathbf{F_n}| \tag{4.1}$$

$$\mathbf{F}_t = -\mu |\mathbf{F}_n| \frac{\Delta \mathbf{s_t}}{|\Delta \mathbf{s_t}|} \quad \text{otherwise} \tag{4.2}$$

Eq. 4.1 essentially describes a spring that opposes the sliding motion of the objects. This equation admits a more general form including a viscous damping term $-m_{\text{eff}} \gamma_t \mathbf{v_t}$; Here we neglect this term to reduce the number of parameters, considering that our simulations will be performed in the overdamped limit. The two equations above also enforce Coulomb's friction law, as the magnitude of the tangential force is bounded by that of the normal one. Notice that the frictional force acts at the point of contact between the two contacting objects, and hence induces a torque making the particle rotate.

In the simulations reported in this Chapter, we use the above model for the tangential interaction between two particles, and the model of Eq. 3.3 for the normal one, fixing $k_t = \frac{2}{7} k_n$. This is the standard in the literature [16]. We remark that in the $\mu \to 0$ limit our frictional model reduces to the frictionless one investigated in the previous chapter.

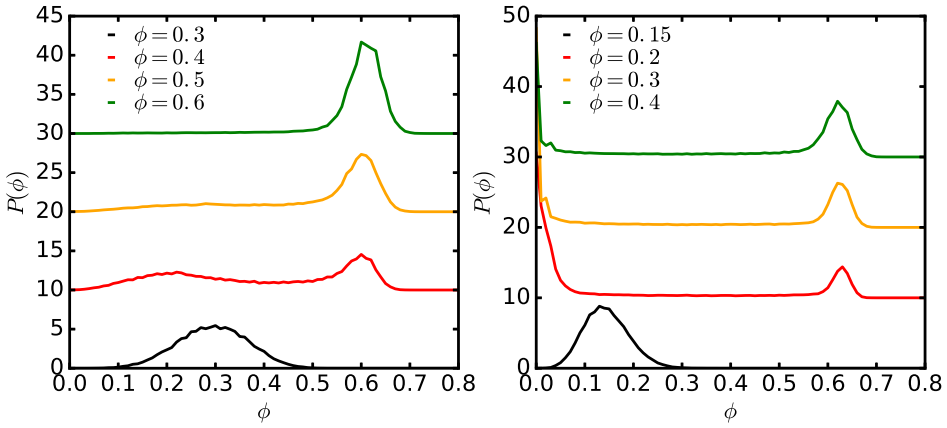

FIGURE 4.1: Probability distribution of the local volume fraction, for different values of the volume fraction, at Pe = 500. The curves are vertically shifted for clarity. In left panel $\mu = 0$, while in the right one $\mu = 0.9$.

4.3 Phase diagram

Here we focus on the investigation of the motility induced phase diagram of frictional active Brownian particles. As in the frictionless case, we determine the phase diagram by first running long simulations so that the system reaches the steady state, and then considering the probability distribution function of the local volume fraction of the steady state configurations. If the distribution is single peaked, we assumed the system to be in the homogeneous phase, while conversely we assume it to be in the phase separated one.

4.3.1 Local volume fraction distribution

For instance, we illustrate in Fig. 4.1 the probability distribution function of the local density in three-dimensions. Data are shifted for clarity. In the left panel we consider the frictionless case ($\mu = 0$) at Peclet number 500. The probability distribution is clearly unimodal at small and at high volume fractions, while two peaks are observed at intermediate volume fraction. On the right panel, the same quantity is investigated for $\mu = 0.9$ at the same Peclet number. The scenario is the same as before. But the phase separation occur between $\phi = 0.15$ $\phi = 0.2$,which is much smaller than no frictional case. Besides, in the presence of friction the first peak of the local volume fraction distribution occurs at $\phi = 0$.

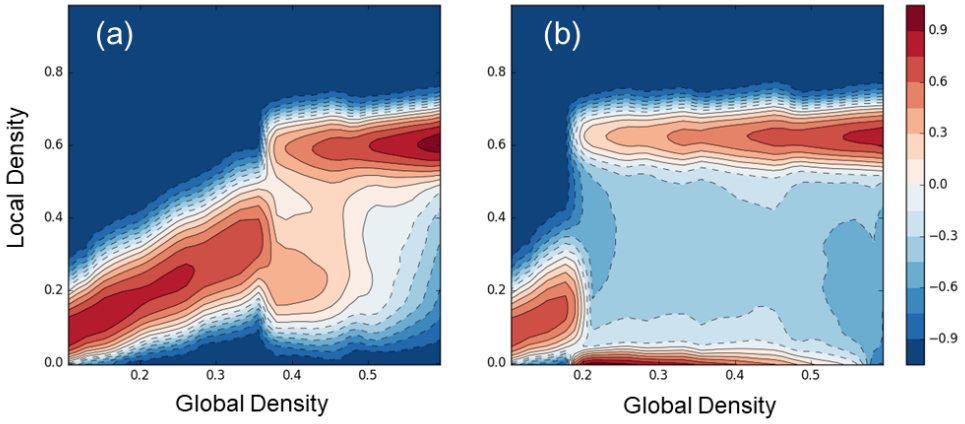

FIGURE 4.2: Colour plot of the local volume fraction distribution, as a function of the global volume fraction, for Pe = 500. Panel (a) refers to the frictionless case, $\mu = 0$, while panel (b) refers to the frictional one, $\mu = 0.9$. The transition from the homogeneous to the phase separated state occurs at $\phi \simeq 0.35$ in the absence of friction, at $\phi \simeq 0.19$ in the frictional case.

A more comprehensive comparison of the volume fraction dependence of the local volume fraction distribution of the frictionless and of the frictional case is provided in Fig. 4.2. The figure illustrates the contour plot of the local volume fraction distribution, at Pe = 500, in the frictionless case (panel a), and for $\mu = 0.9$. Clearly, the transition from the homogeneous to the phase separated state occurs at a smaller density in the presence of friction. Hence we can conclude that friction enhances the motility induced phase separation. In addition, confirming the previous observation, we notice that in the presence of friction the local volume fraction distribution has a peak at $\phi = 0$.

4.3.2 Phase diagram

Having investigated the probability distribution function of the local density as a function of global volume fraction ϕ, Peclet number Pe, and friction coefficient μ, we can now determine the frictional dependence of the phase diagram. This is shown in Fig. 4.3, where the spinodal line is plotted as a function of the volume fraction, for different values of the friction coefficient μ, for a three dimensional system.

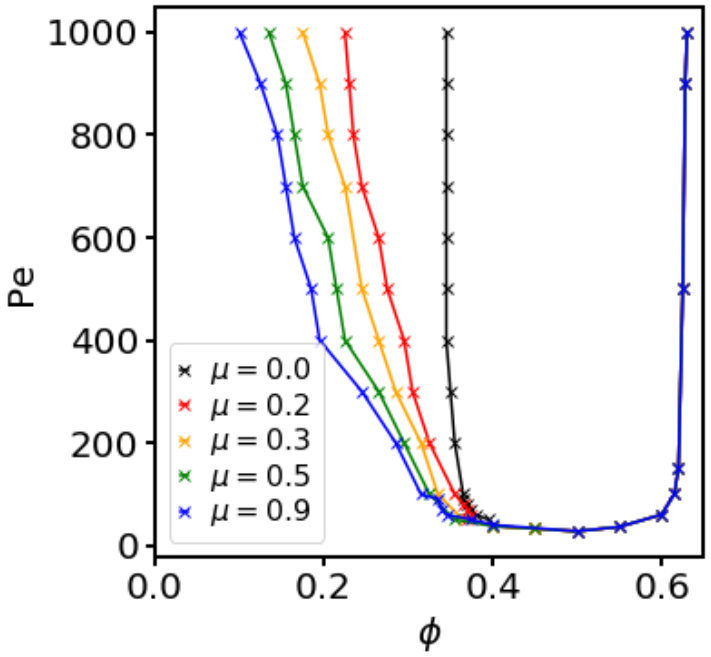

FIGURE 4.3: Phase diagram (spinodal line) of three dimensional active Brownian spheres, for different values of the friction coefficient μ. While in the absence of friction the low density spinodal line diverges at a finite density $\phi \simeq 0.345$, in the presence of friction it approaches $\phi \to 0$ as Pe increase. The approach depends on the friction coefficient.

The data for $\mu = 0$ are well fitted by our theoretical prediction of Eq. 3.9,

$$\mathrm{Pe} = \frac{A}{(\phi^* - \phi)(\phi - \phi_m)}, \tag{4.3}$$

with $\phi_m \simeq 0.345$, $\phi^* \simeq 0.645$ and $A \simeq 60$. We note, in particular, that for $\mu = 0$ the spinodal line diverges at $\phi_m > 0$.

As the friction coefficient increases, the low density spinodal line changes qualitatively: regardless of the friction coefficient ($\mu > 0$), the spinodal line diverges at $\phi = 0$. Hence, the frictionless case appears to be a singular limit. The exist of friction could change the phase diagram dramatically. For frictional coefficient $\mu = 0.9$, we could find the system phase-separated in density as low as $\phi = 0.1$.

To further characterize the friction dependence, we have investigated the dependence of the volume fraction of the spinodal line $\phi_c(\mathrm{Pe}, \mu)$ on the friction coefficient at a fixed large value of the Peclet number, Pe = 1000. Hence, we are essentially

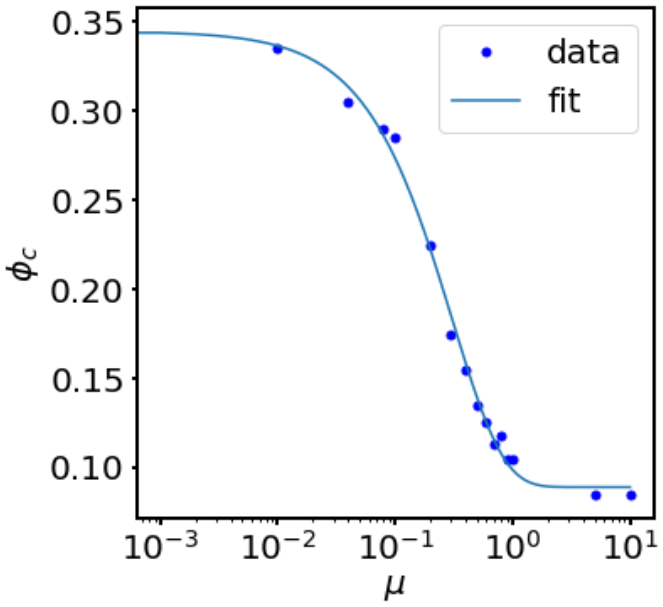

FIGURE 4.4: At $\mathrm{Pe} = 10^3$, the volume fraction of the spinodal line varies exponentially from the frictionless to the frictional limit. The full line if a fit with Eq. 4.4.

moving horizontally in the phase diagram of Fig. 4.3. We illustrate the result of this investigation in Fig. 4.4. The spinodal line interpolates the frictionless limit, which is essentially attained for $\mu < 1e-2$, and a highly friction one, which is reached for $\mu > 1$. The fitting line illustrated in the figure is an exponential decay,

$$\phi_c(\mu) = \phi_c(\infty) + [\phi_c(0) - \phi_c(\infty)]e^{-\mu/\mu^*}, \tag{4.4}$$

where $\mu^* \sim 0.345$. In a different context, a similar exponential dependence of the properties of frictional systems on the value of the friction coefficient has been previously reported [17].

Our prediction for the frictionless phase diagram is clearly unable to describe the frictionless case. Given the results of Fig. 4.3, here I make two remarks:

1. First, the frictionless and the frictional spinodal lines approach each other in the limit of small Peclet number. In this limit, active forces are small, and thermal effects become more and more relevant. Hence, it is actually expected that in this limit, frictional forces are smaller enough to be negligible.

2. Secondly, we note that the prediction for the frictionless spinodal line does not qualitatively describe the frictional data. There is no way Eq. 4.3 could describe the frictional data, as this equation is invariant under reflection around the $\phi = 1/2(\phi_m + \phi^*)$ line. This invariance is not seen in the numerial data.

3. At high densities, there is not a clear difference in phase separation is observed between the frictionless and the frictional results.

4.4 Dynamics in frictional systems

4.4.1 Effect of friction on the dynamics: observations in dilute regime

To gain insight into why and how friction affects the stability line, I have investigated the dynamical properties of frictional active Brownian particles.

Fig. 4.5a compares the mean square displacement of the frictionless (full lines) and the frictional (symbols) simulations, for three different values of the Peclet number, as identified by the colors. Note that we are scaling the time by the rotational diffusion coefficient. Specifically, we are scaling it by D_r^0, where the superscript '0' is to remind that this is the bare rotational diffusion coefficient as measured in the absence of friction. Given the theoretical arguments discussed in Sec. 2.5, we expect in the lack of friction case, there is a crossover from a superdiffusive to a diffusive behavior at $tD_r^0 \simeq 1$. This is exactly what we observe in the figure. The frictional simulations appear to behave as the frictionless ones in short and intermediate time: the symbols and the full lines do indeed exhibit a prolonged transient collapse. At a long time, however, the two cases differ, as in the presence of friction the long-time diffusion coefficient is smaller.

We demonstrate that this is the case in Fig. 4.5b, where we investigate the Peclet dependence of the long-time diffusion coefficient ($r^2 = 2dDt$ at the long-time), for different values of the friction coefficient. In the frictionless case this diffusion coefficient is expected to grow quadratically with the Peclet number, Sec. 2.5, as we observe. In the presence of friction, the diffusion coefficient goes as Pe^2 at small

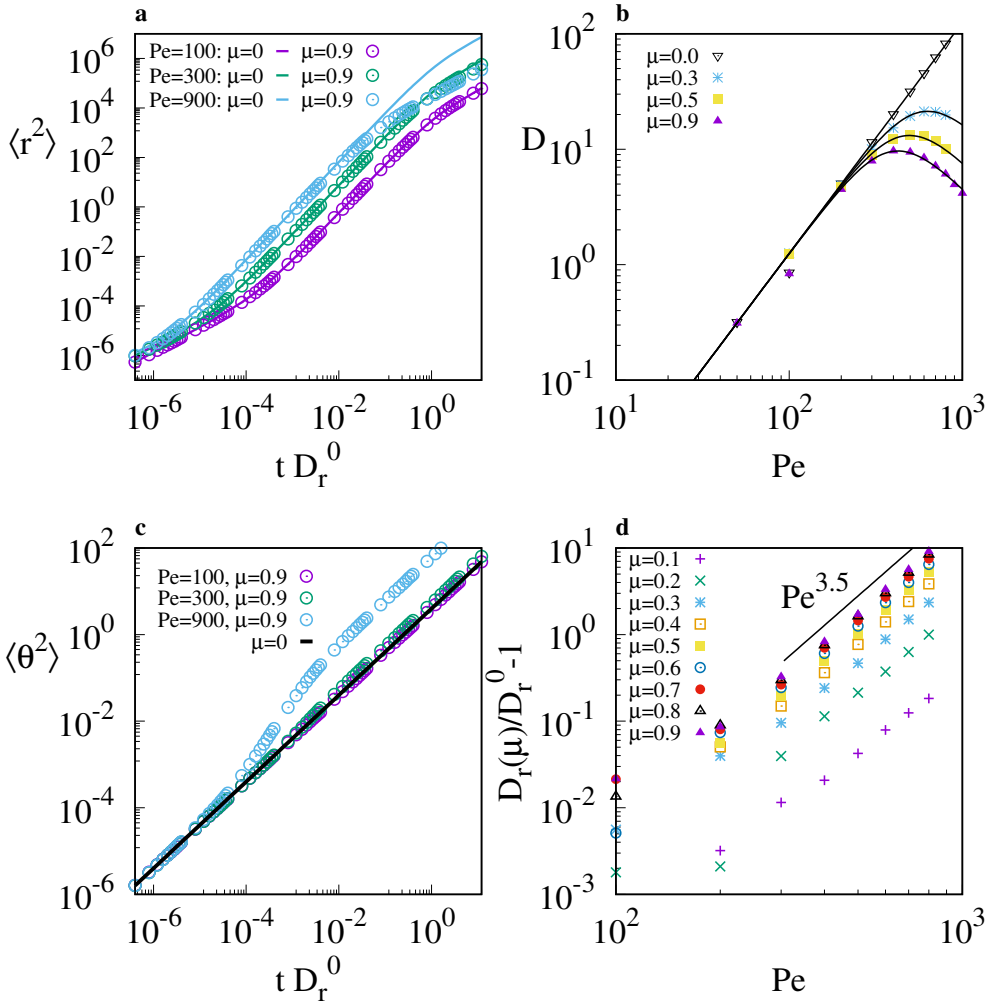

FIGURE 4.5: Mean square displacement (**a**) for the frictionless ($\mu = 0$, full lines) and the frictional dynamics ($\mu = 0.9$, symbols) for selected values of the Peclet number. At large Pe friction reduces the time at which the dynamics enters the asymptotic diffusive regime, and hence suppresses the diffusion coefficient (**b**). The full lines in panel b are from the theoretical prediction of Eq. 4.6. The mean square angular displacement (**c**) is enhanced by the frictional force, at times larger than the inter-particle collision time. This leads to an increase of the rotational diffusivity (**d**) scaling as $\mu^2 \mathrm{Pe}^x$, with $x \simeq 3.5$. Lines in (**b**) are one parameter fits to the theoretical prediction of Eq. 4.5 where $x = 3.5$ is held constant. In all panels, $\phi = 0.1$.

Peclet number, but then it reaches a maximum and decreases. Hence on increasing the activity of the particles, the dynamics slows down. This is undoubtedly a counter-intuitive result.

To rationalize these results, we have investigated the rotational dynamics of the

system. In Fig. 4.5**c**, we illustrate the time evolution of the mean square angular displacement of the particles. At short times, the mean square displacement is not affected by the friction coefficient. At longer times, we do see a crossover in the mean square displacement, which increases in the presence of friction. Hence frictional forces, which are generally associated with a slowdown of the dynamics, do speed-up the rotational motion. From the long-time limit of the mean squared angular displacement, we have measured the frictional dependent rotational diffusion coefficient, $D_r(\mu)$. This equals D_r^0 in the absence of friction. Hence, the enhancement in the rotational diffusivity of the particles induced by friction is measured by $D_r(\mu)/D_r^0 - 1$. We show the dependence of this quantity on the Peclet number in Fig. 4.5**d**, considering data taken at different values of the friction coefficient. In all cases, we do see the enhancement to grow as Pe^x with $x \simeq 3.5$. Before rationalizing these results, let me mention that for all friction coefficient μ, this trend is consistent. In particular, we understand that in the presence of friction the system enters the diffusive regime at a time $< tD_r^0$: this explain why the translational diffusivity of frictional systems (see panel a) is smaller than that of the frictionless ones.

4.4.2 Effect of friction on the dynamics: model

In Chapter 3 we have developed a model to predict the spinodal line of frictionless ABPs. This model is based on the balance of the timescales of the different physical processes that promote or suppress density fluctuations in Sec. 3.2. While I do not have an equivalent model able to account for the friction dependence of the spinodal line, I have investigated the frictional dependence of the different mechanism involved.

In particular, I focus here on the sliding-detaching mechanism (see Sec. 3.2) This is the most important of the mechanisms I have introduced, as it is the one describing the motility induced suppression of the density fluctuations. It is because of this mechanism that the in the absence of friction, the low-density spinodal line diverges at $\phi_m > 0$, and not at $\phi_m = 0$. At high density, in the phase-separated state, we have also seen that this mechanism leads to the rotation of active clusters and to their subsequent destruction.

Since the more immediate effect of friction is a speedup of the rotational motion of the particles, I start modeling this aspect. In the overdamped limit we are considering, the rotation $\Delta\theta_i$ induced by a collision is proportional to the induced torque, and to the duration of the contact. We assume the duration of a collision $t_{\rm coll}$ to scale as Pe^q. Assuming the contacts to be their critical Coulomb value, the typical torque magnitude is $\sigma F_t \propto \mu F_n \propto \mu \mathrm{Pe}$. We now consider that the mean squared angular displacement induced by a collision scales as $\langle \Delta\theta_i^2 \rangle \propto \mu^2 \mathrm{Pe}^{2+2q}$. At low density consecutive torques experienced by a particle are uncorrelated, and the numbers of collisions per unit time is proportional to Pe. From this, we predict for the rotational diffusivity

$$D_r(\mathrm{Pe}, \mu) = \mathrm{D_r^0} + \alpha \mu^2 \mathrm{Pe^x} \tag{4.5}$$

with α a constant and $x = 3 + 2q$. This prediction is a good agreement with the result of panel d, which suggests $x \simeq 3.5$, indicating that the average duration of an interparticle collision grows weakly with the Peclet number. This occurs as the torques experienced by two colliding particles tend to anti-align their self-propelling directions, hence protracting the contact.

The dependence of the rotational diffusion coefficient on Pe and μ allows us to rationalize the non-monotonic behavior of the diffusivity observed in Fig. 4.5**b**. Indeed, in the $\phi \to 0$ limit the long time mean square displacement of an active particle is $\Delta r^2(t) = 6 D_t^0 t + \frac{v_a^2}{D_r} t$, so that at low density we expect

$$D(\mathrm{Pe}, \mu) = c(\phi) \left[D_t^0 + \frac{\sigma^2}{6} \frac{(D_r^0)^2}{D_r(\mathrm{Pe}, \mu)} \mathrm{Pe}^2 \right] \tag{4.6}$$

with $c(\phi)$ a constant of order unit. This well describes the data of Fig. 4.5**b**, with $c(\phi = 0.1) \simeq 0.8$. Hence, the diffusivity grows as Pe^2 at small Pe, and decreases as Pe^{2-x} at large Pe.

These results clarify that in the gas phase the effect of friction on the dynamics is only apparent at long times, as it is the cumulative effect of many frictional collisions to induce a change in the diffusivity. Also, the dependence of the rotational diffusion on the friction coefficient clarifies that friction affects the dynamics when the Peclet number overcomes a threshold $\mathrm{Pe}^*(\mu) \propto \mu^{-4/7}$. Indeed, we show in Fig. 4.6**a** that, when plotted vs $\mathrm{Pe}/\mathrm{Pe}^*$, rotational diffusivity data corresponding to different values of the friction coefficient nicely collapse. The threshold Pe^*

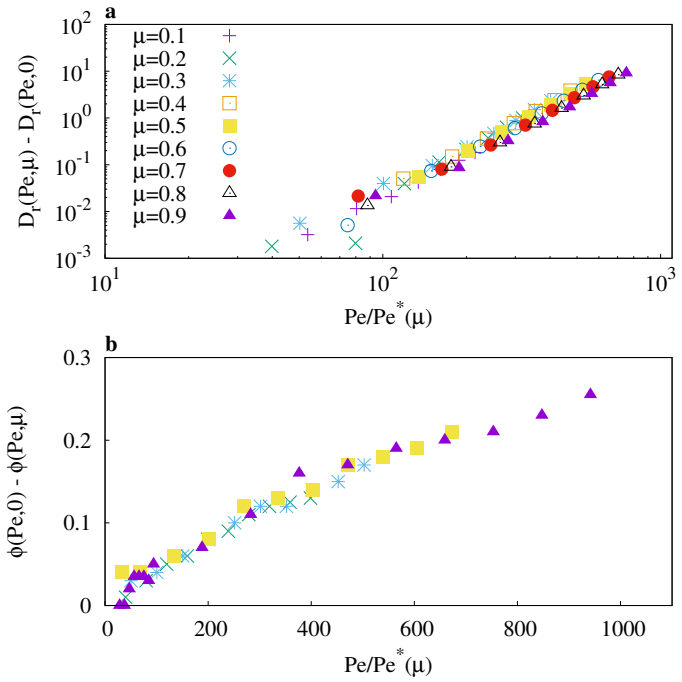

FIGURE 4.6: Friction leads to an increase of the rotational diffusivity scaling as $D_r(\mathrm{Pe},\mu) - D_r(Pe,0) \propto \mathrm{Pe}^* \propto \mu^{-4/7}$ (**a**). The difference between the frictionless and the frictional low density critical lines (see Fig.4.3**b**) is also controlled by Pe^* (**b**).

signifies that friction is only relevant when the frictional forces are strong enough with respect to the thermal ones. We confirm this expectation in Fig. 4.6**b**, which illustrates that the distance between the frictionless and the frictional critical lines, $\phi(\mathrm{Pe},0) - \phi_c(\mathrm{Pe},\mu)$ scales as $\mathrm{Pe}/\mathrm{Pe}^*(\mu)$. These power-law dependence on Pe and μ further emphasize that the change in Phase Diagram is related to friction-active induced enhancement in rotational dynamics.

4.4.3 Effect of friction on dynamics: dense regime

At low densities, friction enhances the rotational diffusivity, and consequently suppresses the translational one. What happens at high densities? Here I discuss the dependence of the dynamics on the Peclet number at very high densities, $\phi = 0.63$, in the homogeneous phase. Fig. 4.7a compares the mean square displacement of the frictionless and of the frictional simulations. While at low densities there are equal up to long times, at high densities differences are apparent also at very short times. Indeed, friction protract the long short-time subdiffusive transient which precedes the super-diffusive regime. Notice, in addition, that the larger the Peclet

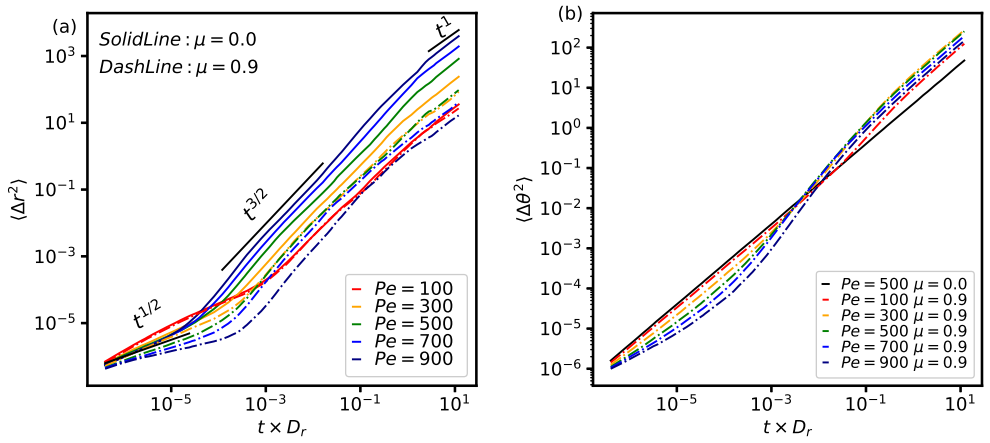

FIGURE 4.7: Mean squared translational (a) and rotational (b) displacements, for different values of the Peclet number, at high density: $\phi = 0.63$. Both panles compare frictionless data (full lines) and frictional ones (dashed lines).

number, the slower dynamics. This is understood as frictional effects become more and more relevant at high Peclet number. Similarly, Fig. 4.7b shows that friction gives rise to a subdiffusive transient in the mean square angular displacement. Also in this case, the higher the Peclet number, the slower the system, at short times. At longer times, conversely, as in the dilute case friction enhances the rotational diffusivity.

4.4.4 Effect of friction on the rotational stability process

In Chapter. 3, we have developed a model able to predict the spinodal line of frictionless active Brownian particles. The model identifies the spinodal by balancing the typical timescales of the different processes that either promote the growth of density fluctuations or suppress them. While it appears challenging to develop a similar model for the frictional case, we do have investigated the frictional dependence of the different phenomena involved.

In particular, here we focus on the frictional dependence of the sliding detaching mechanism, see Sec. 3.2.3.2. This is the crucial mechanism that leads to the main feature of the frictionless spinodal line: the presence of a finite volume fraction ϕ_m below which the homogeneous state is stable at all Peclet number. In the presence of friction, the phase diagram of Fig. 4.3 clarifies that $\phi_m \to 0$. Hence, friction must drastically affect this mechanism.

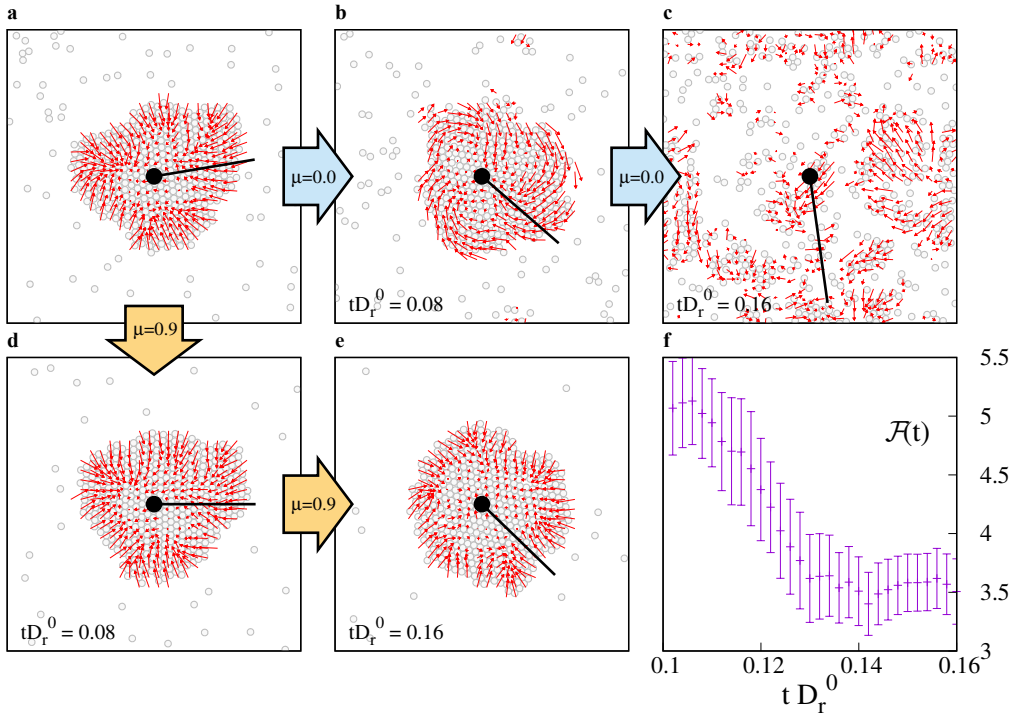

FIGURE 4.8: Evolution of a two dimensional cluster of ABPs in the absence (**a,b,c**) and in the presence (**a,d,e**) of frictional forces. The red arrows show the active force field (see methods). In all plots, the central black circle identifies the position of the particle, which is closer to the center of mass of the cluster, in the initial configuration. We emphasize the rotational motion of the cluster, drawing a line connecting the central particle and another particle of the cluster. Both with and without friction the cluster rigidly rotates around its center of mass. In the absence of friction, the rotation of the cluster makes the active velocities parallel to the cluster surface (**b**) inducing a cluster instability (**c**). Indeed, we see in panel **f** that, in the absence of friction, as the cluster rotates, the average interaction force that contrasts the motion along the direction of the self-propelling forces decreases, fluctuating around a value characteristic of the homogeneous phase once the cluster breaks. In the presence of friction, the cluster rotation induces that of the self-propelling directions, and the cluster remains stable (**d,e**). For these illustrative two-dimensional simulations $N = 500$, $\mathrm{Pe} = 500$, $\phi = 0.2$ and $\mu = 0.0; 0.9$. The corresponding frictionless video is the same as mentioned in previous chapter, and the frictional video could be find in URL : https://youtu.be/b_SgM9FS8Lg. Other links for simulations about frictional case could be find in the SI.

We investigate the frictional dependence of this mechanism considering that, in the phase-separated state, this mechanism is responsible for a rotational instability of the active clusters. We have discussed this instability in Sec. 3.5. Accordingly, here, we consider how friction affects this rotational instability.

To perform this investigation, we first consider a simulation of a frictional system,

for values of the parameters within the coexistence region. Specifically, we fix $\mu = 0.99$, $\phi = 0.2$ and $\mathrm{Pe} = 500$. Also, for the sake of visualization, we consider a relatively small two-dimensional system with $N = 500$ particles. The corresponding steady-state (but dynamic!) configuration is phase-separated. We illustrate this configuration in Fig. 4.8a. We assume this to be our $t = 0$ configuration. In the drawing, the red arrows indicate the direction of a coarse-grained self-propelling directions, we have define by averaging on a circle with radius 2.2σ. I only show the average velocity on grid points averaging over at least 5 particles. The thick black line connects the center of the cluster and a randomly selected particle of the cluster which I fix once and for all at $t = 0$. After having prepared this initial configuration, we follow its subsequent evolution in simulations, I have performed removing or keeping the frictional interaction.

Fig. 4.8a,b,c shows the evolution observed in the absence of friction. As the cluster rotates, the self-propelling directions become parallel to the cluster surface. Hence, particles on the surface become free to slide away, and indeed the cluster dissolves. This is the rotational instability mechanism we have already described in Sec. 3.5.2. Interestingly, notice that the cluster disappears for $tD_r^0 \ll 1$: this implies that this process is not influenced by the rotational diffusion of the self-propelling direction of the particles.

Fig. 4.8a,d,e illustrate the evolution in the presence of friction. In this case, the self-propelling directions are seen to rotate together with the cluster. This kills the rotational instability, making the cluster stable. In this respect, frictional systems behave as systems of elongated particles, that also exerts a torque on each other which couples their self-propelling directions. Indeed, clusters performing long-lived rotations are seen in systems of rod-shaped particles such as active dumbbells [18, 19].

Overall, this investigation clarifies that, at high Peclet number, the sliding detaching mechanism is either killed or strongly suppressed. This could also be explained from another approach. When frictional interaction exist, although the rotational dynamics due to thermos noise is suppressed by friction. The active rotation due to friction is enhanced, which explains the superdiffusive of angel in intermediate regime. This is also the same mechanism which drive the particle self-propelling direction followed the rotation of an active cluster. The active cluster is much

more stable when frictional force exist. This explains why the spinodal line of the frictionless system approaches $\phi_m \to 0$ in the $\mathrm{Pe} \to \infty$ limit.

4.4.5 Flocking & collective motion

4.4.5.1 Flocking: instantaneous alignment

Non-spherical active particles, such as active rods, are well known to give rise to flocking behavior. This occurs as, due to their shape, the interparticle interaction favors their nematic alignment. The same flocking transition can occur in systems of active spherical particles, in the presence of an aligning interaction. This occurs, for instance, in the famous Vicsek model [20, 21].

Such collective behavior is not seen in the standard ABPs model as the particle-particle interaction has no explicit alignment mechanism. In the presence of friction, however, particles exert a torque on each other and a flocking behavior may in principles occurs. We investigate the possible emergence of flocking via the investigation of a flocking order parameter. Specifically, for each particle i we define

$$\psi_i = \frac{1}{z_i} \sum_{j \in z_i} \mathbf{e_i} \cdot \mathbf{e_j}, \tag{4.7}$$

where e_k is the director of the active velocity of particle k, and the sum runs over all z_i neighbor of particle i. We consider two particles to be neighbor if their distance is smaller than 2σ, but have checked that this choice is not critical. This order parameter is defined so that $\psi = 1$ if a particle and its neighbor particles are self-propelled in parallel directions, i.e., if the particle is in a flock. $\psi = -1$ if the particle is anti-aligned with all of its neighbours, while $\psi = 0$ if the self-propelling directions are uncorrelated. Fig. 4.9 illustrates the probability distribution of ψ, for a three dimensional system with volume fraction $\phi = 0.63$ and Peclet number $\mathrm{Pe} = 500$. The figure compares frictionless and frictional ($\mu = 0.9$) data.

The two distributions are Gaussian-like, and are centered to values very close to zero. There is a small difference between the two cases, the average value being slightly larger in the presence of friction. In any case, the frictionless and the frictional simulations give very similar results. We have checked that the similar results are obtained as the Peclet number and the volume fraction are varied, in

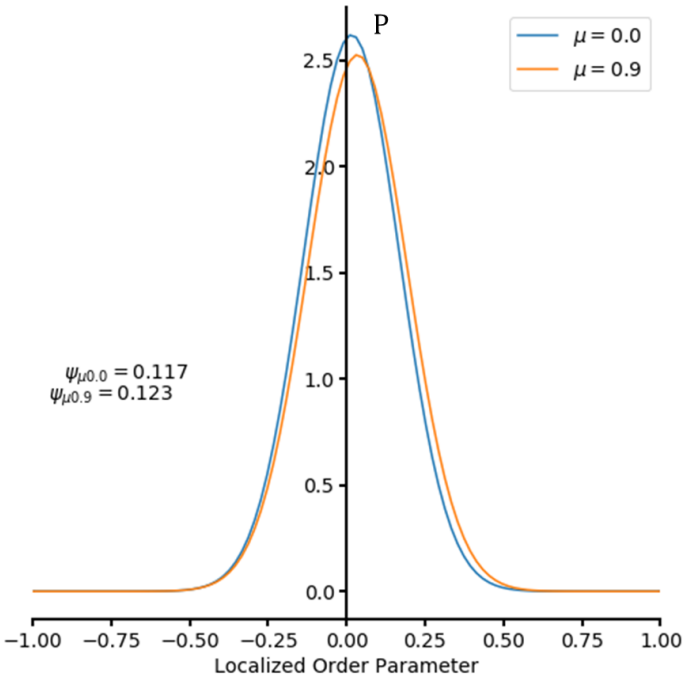

FIGURE 4.9: Distribution of local order parameter ψ_i, defined in Eq. 4.7, for a three dimensional system with $N = 10000$ particles and volume fraction $\phi = 0.63$. The figure compares frictionless and frictional data, which do not display noticeable differences. P in the y-axis denotes the Distribution of localized order parameter. The order parameter distribution range from -1 to 1.

both three and two spatial dimensions. In conclusion, we can safely conclude that friction does not induce alignment of the self-propelling directions and hence the flocking collective motion.

4.4.5.2 Collective motion: delayed alignment

While the self-propelling directions of close particles do not align, yet it is always possible that the particles move in the same direction. Indeed, in a dense environment, particles do not generally move in the direction of their self-propelling force. In the frictionless case, this collective motion has been reported in Ref. [1], and possibly in small systems also in Ref. [22]. Friction may affect this collective motion, by forcing particles to move together. To investigate the effect of friction on this collective motion, we measure a spatio-temporal correlation function

introduced in Ref. [1], which is defined as:

$$C_d(r,\Delta t) = \frac{\left\langle \sum_{i,j\neq i} \mathbf{d_i}\cdot\mathbf{d_j}\delta\left(\mathbf{r}-|\mathbf{r_i}-\mathbf{r_j}|\right)\right\rangle_t}{c_0\left\langle \sum_{i,j\neq i}\delta\left(r-|\mathbf{r_i}-\mathbf{r_j}|\right)\right\rangle_t}, \tag{4.8}$$

with $c_0 = \langle \sum_i d_i^2/N\rangle$ a normalization factor. In Fig. 4.10, I present results for the correlation function measured at different times, for the frictionless case, panel a, and for the frictional one, panel b. The simulation are at $\phi = 0.63$ and Pe $= 500$. Both in the absence and in the presence of friction, the correlation function decays over a distance which increases with time. We do expect the correlation to decrease at very long times. For the frictionless case, the decrease is observed in $t = 4$, while for frictional case, such decrease is not clearly seen but a saturation is observed. Comparing the two panels, we clearly see that friction strongly enhances correlated particle displacements at high densities.

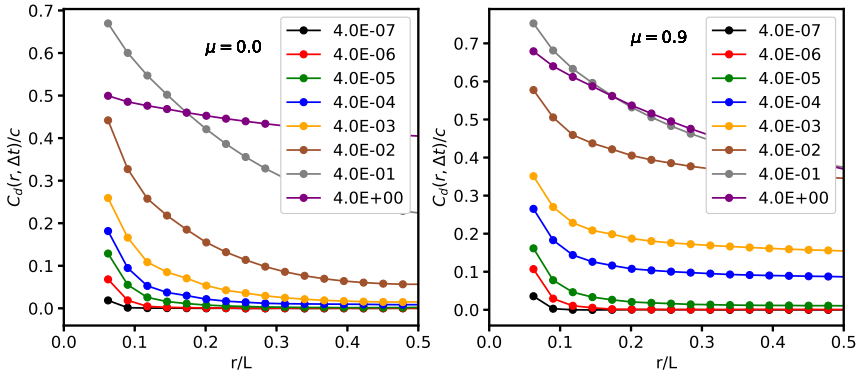

FIGURE 4.10: Spatial decay of the spatio-temporal correlation function of the particle displacements, at different times. Panel (a) and (b) show results for frictionless and frictional simulations, respectively. In both cases $\phi = 0.63$,Pe $=$ 500.

4.5 Discussion and conclusion

In this chapter, I have presented the first investigation of the motility-induced phase-separation of frictional active matter, focusing on the most straightforward frictional generalization of the active Brownian particle model. Frictional forces play an essential role in the presence of long lasting particle contacts. These frictional force generated from contacts are enhanced by the activity, which pushes

the particles against each other. But these contacts are disrupted by the thermal motion, which randomizes the position of the particles. As a consequence, as Peclet number increase, the frictional interaction become more visible.

The first significant result that I have achieved is investigating the motility-induced phase diagram in the $\mathrm{Pe} - \phi$ plane, for different values of the friction coefficient. My findings suggest that the frictionless case, in which the spinodal line diverges at a finite value of the volume fraction $\phi_m > 0$, is a singular point. Indeed, for every value of the friction coefficient, ϕ_m vanishes and the phase diagram in lower boundary approachs zero density as Pe number increase.

To have an insight into the physical origin of this observation, I have investigated the dynamics of frictionless systems in the dilute regime and dense regime. This study has clarified that the main effect of friction in long timescale is that of increasing the rotational diffusion coefficient, at high Peclet number. In turn, this leads to a reduction of the translational diffusion coefficient. There is no difference observed in short timescale for the dilute case, while in the dense regime, friction suppresses both the translational and rotational dynamics. From this, we could suggest that friction suppress the short-time rotation due to thermos noise, while from intermediate timescale, friction could transfer part of the active energy from translational to rotational, thus enhance the rotational diffusion coefficient in the long time. This mechanism could be understand from the simulations of the frictional active cluster, as friction force could let surface particles follow the rotation of the cluster, and make active cluster a much stable one by compare with non-friction case.

I have described the effect of friction on the rotational dynamics in a rotational random walk perspective by assuming that each collision induced torque on the particle and different collisions are uncorrelated. In addition, dynamical analysis clarifies that the torque magnitude scales with the Peclet number. As a consequence, I was able to predict the power-law dependence of the rotational diffusion on the Peclet number. I have then demonstrated that, when this dependence is taken into account, the spinodal lines corresponding to different values of the friction coefficient could be collapsed. Hence, it appears that friction affects the stability limit as it changes the rotational diffusion coefficient. I have considered the effect of friction on the rotational instability of active clusters, the physical processes which is responsible for the finite lower bound of the spinodal line in the frictionless case.

I have demonstrated that this instability mechanism is suppressed in the presence of friction, as the rotation of a cluster could induces following changes in the self-propelling directions of its particles. This explains why in the presence of friction, the spinodal line only diverges in the $\phi \to 0$ limit.

Finally, I clarify that friction despite introducing a torque on the particles during their collisions, does not induce alignment of the self-propelling directions. Because of this, in the frictional as in the frictionless case, no flocking behavior is observed.

Further work in this direction includes the direct investigation of the dependence of all processes that contribute to the instability of homogeneous suspensions on friction. This investigation might suggest how to develop a theory able to predict the spinodal line of the frictional system, which is currently lacking.

References

[1] Adam Wysocki, Roland G Winkler, and Gerhard Gompper. Cooperative motion of active brownian spheres in three-dimensional dense suspensions. *EPL (Europhysics Letters)*, 105(4):48004, 2014.

[2] Gabriel S Redner, Michael F Hagan, and Aparna Baskaran. Structure and dynamics of a phase-separating active colloidal fluid. *Physical review letters*, 110(5):055701, 2013.

[3] Julien Deseigne, Olivier Dauchot, and Hugues Chaté. Collective motion of vibrated polar disks. *Physical review letters*, 105(9):098001, 2010.

[4] Julien Deseigne, Sébastien Léonard, Olivier Dauchot, and Hugues Chaté. Vibrated polar disks: spontaneous motion, binary collisions, and collective dynamics. *Soft Matter*, 8(20):5629–5639, 2012.

[5] Christoph A Weber, Timo Hanke, J Deseigne, S Léonard, Olivier Dauchot, Erwin Frey, and Hugues Chaté. Long-range ordering of vibrated polar disks. *Physical review letters*, 110(20):208001, 2013.

[6] BM Guy, Michiel Hermes, and Wilson CK Poon. Towards a unified description of the rheology of hard-particle suspensions. *Physical review letters*, 115(8):088304, 2015.

[7] Cécile Clavaud, Antoine Bérut, Bloen Metzger, and Yoël Forterre. Revealing the frictional transition in shear-thickening suspensions. *Proceedings of the National Academy of Sciences*, 114(20):5147–5152, 2017.

[8] Chiao-Peng Hsu, Shivaprakash N Ramakrishna, Michele Zanini, Nicholas D Spencer, and Lucio Isa. Roughness-dependent tribology effects on discontinuous shear thickening. *Proceedings of the National Academy of Sciences*, 115(20):5117–5122, 2018.

[9] Takeshi Kawasaki and Ludovic Berthier. Discontinuous shear thickening in brownian suspensions. *Physical Review E*, 98(1):012609, 2018.

[10] I Theurkauff, C Cottin-Bizonne, J Palacci, C Ybert, and L Bocquet. Dynamic clustering in active colloidal suspensions with chemical signaling. *Physical review letters*, 108(26):268303, 2012.

[11] Jeremie Palacci, Stefano Sacanna, Asher Preska Steinberg, David J Pine, and Paul M Chaikin. Living crystals of light-activated colloidal surfers. *Science*, 339(6122):936–940, 2013.

[12] Ivo Buttinoni, Julian Bialké, Felix Kümmel, Hartmut Löwen, Clemens Bechinger, and Thomas Speck. Dynamical clustering and phase separation in suspensions of self-propelled colloidal particles. *Physical review letters*, 110(23):238301, 2013.

[13] Bram Schroyen, Chiao-Peng Hsu, Lucio Isa, Peter Van Puyvelde, and Jan Vermant. Stress contributions in colloidal suspensions: The smooth, the rough, and the hairy. *Physical Review Letters*, 122(21):218001, 2019.

[14] Oded Ben-David and Jay Fineberg. Static friction coefficient is not a material constant. *Physical review letters*, 106(25):254301, 2011.

[15] R.D. Mindlin. 16:259, 1949.

[16] Leonardo E Silbert, Deniz Ertaş, Gary S Grest, Thomas C Halsey, Dov Levine, and Steven J Plimpton. Granular flow down an inclined plane: Bagnold scaling and rheology. *Physical Review E*, 64(5):051302, 2001.

[17] Leonardo E Silbert. Jamming of frictional spheres and random loose packing. *Soft Matter*, 6(13):2918–2924, 2010.

[18] A Suma, G Gonnella, D Marenduzzo, and E Orlandini. Motility-induced phase separation in an active dumbbell fluid. *EPL (Europhysics Letters)*, 108(5):56004, 2014.

[19] Isabella Petrelli, Pasquale Digregorio, Leticia F Cugliandolo, Giuseppe Gonnella, and Antonio Suma. Active dumbbells: Dynamics and morphology in the coexisting region. *The European Physical Journal E*, 41(10):128, 2018.

[20] Tamás Vicsek, András Czirók, Eshel Ben-Jacob, Inon Cohen, and Ofer Shochet. Novel type of phase transition in a system of self-driven particles. *Physical review letters*, 75(6):1226, 1995.

[21] Hugues Chaté, Francesco Ginelli, Guillaume Grégoire, and Franck Raynaud. Collective motion of self-propelled particles interacting without cohesion. *Physical Review E*, 77(4):046113, 2008.

[22] Takahiro Nemoto, Étienne Fodor, Michael E Cates, Robert L Jack, and Julien Tailleur. Optimizing active work: Dynamical phase transitions, collective motion, and jamming. *Physical Review E*, 99(2):022605, 2019.

Part III

Modeling of Initial Biofilm Formation

Chapter 5

Early stage biofilm formation: review

Active matter systems are ubiquitous in the living world. Animals, like humans, are essentially active particles. At a smaller scale, active systems are also ubiquitous. Cells, for instance, are endowed by motility, which allows them to explore their surrounding environment. In addition, cells do also perform a variety of complex biological processes, including mitosis, apoptosis, movement, and have mechanical and biochemical properties depending on the external stimuli. Of course, the understanding of the features of cellular systems is way much involved than that of the schematic Brownian particles we have considered.

Stimulated by a collaboration with SCELSE, the Singapore Centre for Environmental Life Sciences Engineering, and SMART, The Singapore-MIT Alliance for Research and Technology, in my thesis I have considered the possibility of developing a particle-level description of the early-stage development of biofilms to initial microcolony formation.

In this chapter, I first very briefly describe in Sec. 5.1 what are biofilms, and why their investigation is of paramount importance. Then, I will review in Sec. 5.2 literature results on the early stage formation of biofilm. I will describe how bacteria land, explore and reproduce on a surface until they finally colonize it via the development of a biofilm. Finally, I will detail experimental results concerning the behavior of Pseudomonas aeruginosa in Sec. 5.3 and Sec. 5.4, which is a pathogenic bacteria species of our primary interest. Some conclusions are drawn in Sec. 5.5.

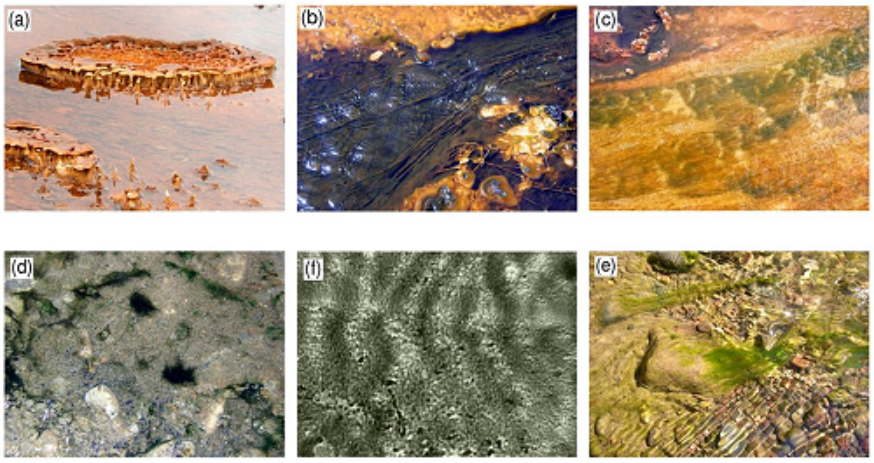

FIGURE 5.1: Examples of biofilms growing in different environments [1].

These results will guide the development of a general model for the investigation of the early-stage biofilm formation, I will introduce and discuss in the next Chapter.

5.1 Problem overview

Biofilms are self-organized bacteria communities. It also refers to bacteria and a matrix of extracellular polymeric substances (EPS) around this bacteria community [2]. They are certainly the most resilient form of life on Earth. Biofilms can survive in both hot, salty, acid and alkaline waters, as well as at extremely low temperature. Examples of biofilms growing in different environments are shown in Fig. 5.1. Biofilms colonize their host environment, including humans, in which case they are frequently the cause of persistent infections. Their resilience mainly originates from the EPS matrix, which might account for up to 90% of the dry biofilm weight. Besides allowing for a spatial and social supracellular organization [3], the matrix provides a physical scaffold that keeps the cells together and protects them from antimicrobial compounds (antibiotics) [4]. EPS also play a prominent role in the early stage biofilm formation, by promoting the attachment of bacteria on surfaces [5].

The social need for research in biofilms is huge. Biofilm grows on the surface of a tooth, causing dental plaque. More worryingly, they grow on medical devices such as prosthetic heart valves, orthopedic devices, skull implants, and might trigger virulent rejection reaction. Pseudomonas aeruginosa, for example, can enter the blood circulation through open wounds to infect organs of the urinary and respiratory systems. In a different context, biofilm cause billions of dollars in damage to metal pipes in the oil and gas industry. Sulfate-reducing bacteria, for example, transform molecular hydrogen into hydrogen sulfide which, in turn, produces sulfuric acid that destroys metal surfaces causing catastrophic failures. In the water supply system, biofilm can grow in pipes, clogging them due to their biomass [1]. It is of enormous interest to develop surfaces to which bacteria are not able to attach: to date, no surface has been discovered that will reliably inhibit the formation of biofilms [6].

On the other hand, one might also tame biofilms to benefit from them. For example, biofilms could be used in environmental biotechnology, e.g., in wastewater treatment, or for in situ immobilization of heavy metals in soil. Biofilms naturally grow by consuming organic materials in the fluid. Microorganisms (typically bacteria and fungi) can be used for microbial leaching, e.g., to metals from ores. Copper, uranium, and gold are examples of metals commercially recovered by microorganisms [1].

The life cycle of a biofilm has five phases, which are illustrated in Fig. 5.2:

1. **reversible attachment**: swimming bacteria land on a surface, and move on it. They may, however, also detach and return into the liquid. While moving on the surface, the bacteria deposit a 'conditioning-layer,' which dresses the surface that promotes the irreversible attachment.

2. **irreversible attachment**: the bacteria stick permanently to the surface. This generally occurs when bacteria form small clusters, known as microcolonies. Bacteria appear to be able to realize they are in a cluster (quorum sensing), as at this stage, they start producing EPS. Note, however, that not all bacteria produce EPS, and that it is possible to modify a bacteria to inhibit EPS production genetically.

3. **growth:** the biofilm grows as cells reproduce, new cells arrive from the liquid phase, and the EPS matrix is produced.

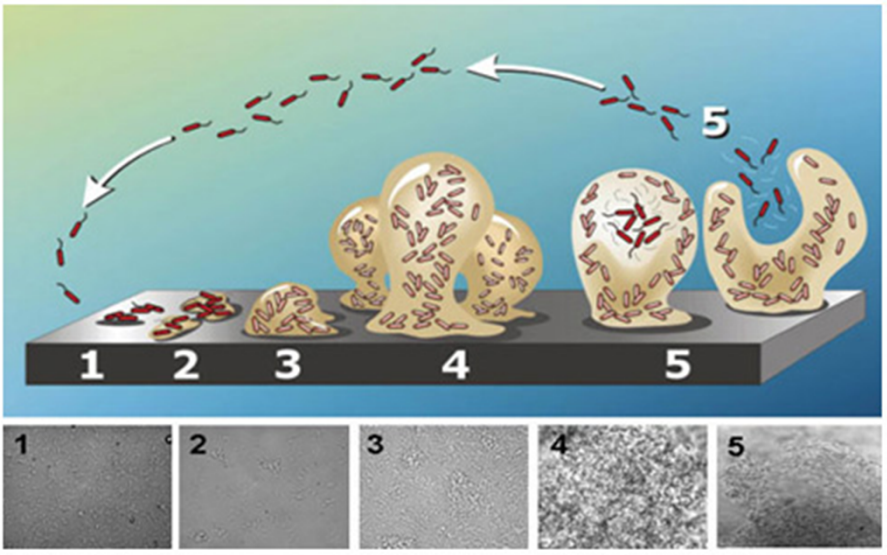

FIGURE 5.2: Schematic representation of biofilm formation. Five phase include (1) reversible attachment, (2) irreversible attachment, (3) growth, (4) maturation, (5) dispersion and their corresponding [6].

4. **maturation:** the biofilm grows further and develops a structured architecture with the assistance of EPS.

5. **dispersion:** finally, cells from the biofilm become able to detach individually. These cells move around in the medium, until they land somewhere, giving rise to the growth of a biofilm in a different location.

The growth of a biofilm from the planktonic state has two ingredients of interest. One question is how bacteria move close to a surface and attach to it. The second one is how the development of a microcolony is triggered. Such microcolony is related to the time when bacteria become irreversibly attached on the surface, marked the first stage of biofilm formation. Research in this direction is of great interest. In principle, a clear understanding of these processes might allow developing anti-microbial surfaces, where the bacteria are unable to stick. These would be extremely useful, e.g., in medical devices to stop the spreading of infections.

In the following section, I review in greater detail this early stage formation of biofilm, which will be modeled in the next chapter.

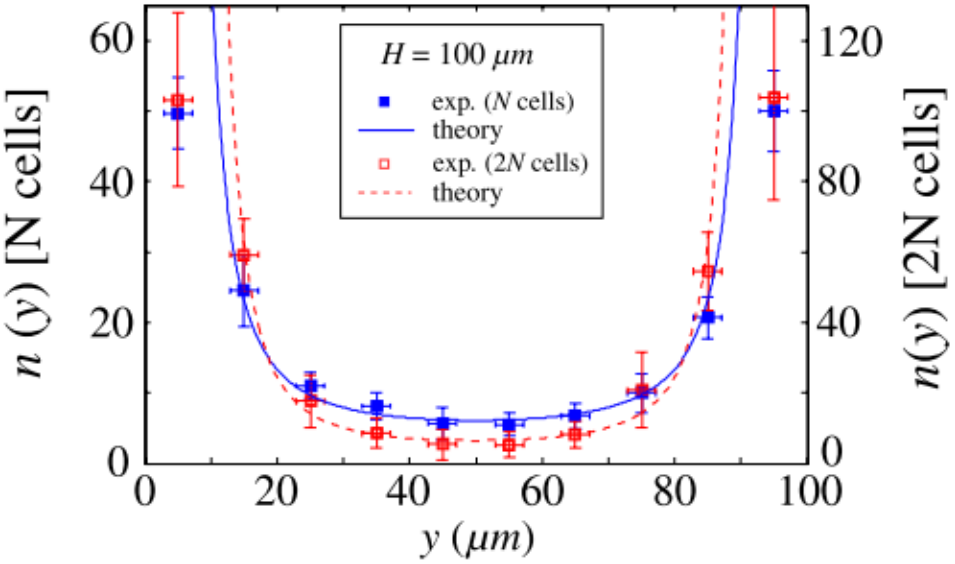

FIGURE 5.3: Number of swimming Escherichia coli bacteria as a function of the vertical coordinate y. The bacteria agglomerate at the boundary of the channel, $y = 0, 100\mu m$. Blue and red data refer to different values of the overall concentration of bacteria. Lines reproducing the steady-state concentration profile are $\frac{n(y)}{n_0} = \exp\left[L_\perp\left(\frac{1}{y} + \frac{1}{H-y}\right)\right]$ with $n_0 = 1.5$ and $L_\perp = 34.8\mu m$ (solid line) and $n_0 = 0.3$ and $L_\perp = 59.1\mu m$ (dash line). From Ref. [7].

5.2 Early stage biofilm formation

In this section, I review the early stage biofilm formation, describing how in the literature it is believed that bacteria reach a surface, move on the surface, and finally start colonizing it.

5.2.1 Reaching the surface

Bacteria in the bulk of a liquid might be assumed to move as active particles, essentially as active Brownian particles. One interesting feature of active Brownian particles is their tendency to agglomerate on surfaces. In the case of bacteria, this as been for instance investigate in Ref. [7], which studies the steady state number density distribution of swimming bacteria (Escherichia coli) between two glass plates. As they also clarify theoretically, hydrodynamic forces push the bacteria close to the surface. Their experimental results are shown in Fig. 5.3. In addition, it has been shown that biological processes such as chemotaxis, phototaxis, and rheotaxis can direct the swimming direction of the bacteria and drive them towards

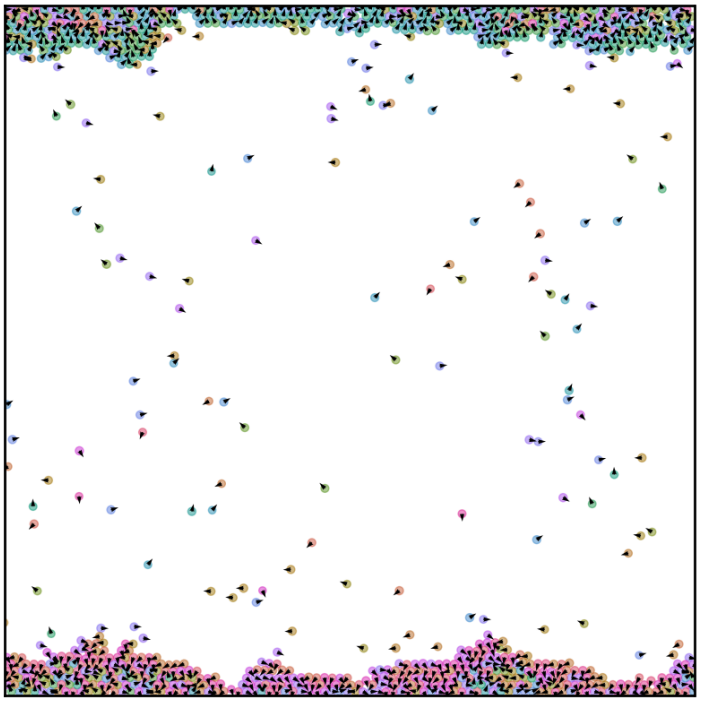

FIGURE 5.4: Snapshot of a simulations of Active Brownian particles confined between two walls. The volume fraction is $\phi = 0.1$, and the Peclet number is $\mathrm{Pe} = 500$, outside of the coexistence region. Particles are clearly seen to agglomerate on the two walls. This result clarifies that the bare presence of motility, in the absence of any hydrodynamic interaction, promotes the agglomeration of particles on a wall.

a surface [5]. The presence of other bacteria on the surface could promote Bacillus Subtilis to move towards the surface, the bacteria communicating via electrical signaling [8].

It is however to be noticed that the bare presence of motility contributes to this process. To show that this is the case, I have performed simulations of the standard active Brownian particle model, at a low density/Peclet number where phase separation is not observed, confining the particles in between two wall. As illustrated in Fig. 5.4, particles agglomerate close to the surfaces. Hence, we can safely conclude that both hydrodynamic interactions and the bare presence of motility could promote the agglomeration of bacteria on surfaces.

5.2.2 Initial attachment

Bacteria that reach a surface do not generally stay there. They explore the surface via different motility mechanisms, which differ from bacteria to bacteria and among different mutants, and may then detach from it. This detachment is extremely commonly seen in bacteria experiments [9]. This detachment is one of the major experimental problems in the study of the early stage formation via microscopy: those have the right spatial resolution to observe the bacteria and their dynamics. The trajectories are usually short as in most of cases, bacteria soon detach from the surface. Later research shows, for P. Aeruginosa, the attachment is a procedure that involves several generations of bacteria. After they notice the existence of the wall, the gene expression is changed accordingly to generate extracellular adhesion to reduced the detachment rate [9]. This is out of the scope of our research and will increase the complexity of the model. Since in the end, most of the bacteria attached to the surface do not leave, we do not model the detachment.

From a physical point of view, where a bacteria that reaches a surface and binds to it is determined by the balance of attractive and repulsive forces. Here, things become extremely complicated as these forces might be time-dependent, as the bacterium sense it is on a surface and changes its motility mechanism [10]. According to the accepted scenario [6], this complicated physical situation is described assuming the interaction to be of DLVO type. We remind that the DLVO (Derjaguin, Landau, Verwey Overbeek) is an effective interaction used in colloidal systems which is attractive at a short distance, and repulsive at longer ones. That is, the potential has a threshold so that two particles need to overcome, to feel the attraction and stick to each other. This potential combines the effects of the van der Waals attraction and of the electrostatic repulsion. The details of the surface-bacterium interaction, however, depends on the surface material and topography.

Bacteria succeed in binding to the surface by effectively changing the way they interact with the surface [6]. Specifically, within moments, bacteria feel the presence of a surface, they start producing a series of proteins and polysaccharide molecules that adsorb to the surface. Then bacteria, rather than binding directly to the surface, bind to this 'conditioning film.' The ability of the bacteria to binding to almost every surface originate from the fact that these films form on both hydrophilic (e.g., glass) and hydrophobic (e.g., plastic) surfaces.

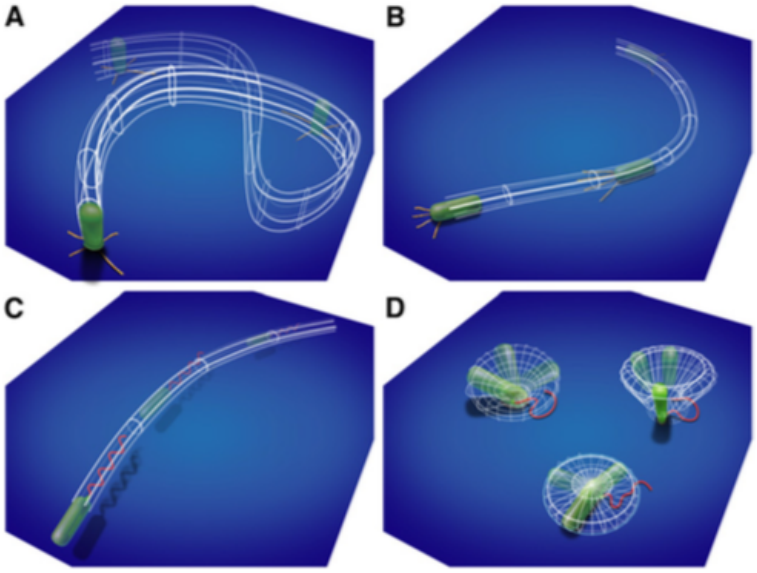

FIGURE 5.5: Surface motility mechanisms observed for P. aeruginosa: TFP-driven (A) vertical walking and (B) horizontal crawling, and flagellum-driven (C) near-surface swimming and (D) surface-bound spinning. From [13]

5.3 How do bacteria move on a surface?

The motility of bacteria on surfaces has been the subject of intense investigations. It is clear that there exist several different motility mechanisms, and that these depend on the particular species considered [11]. Interestingly, motility properties of bacteria could be experimentally controlled by using bacteria mutants whose DNA is altered. This alteration can be spontaneous or can be caused by exposure to mutation-inducing agents [12].

Here I shortly describe the mechanisms identified in the pathogen Pseudumosa Aeruginosa that I will focus in the next chapter, following a recent investigation [13]. These different motility mechanisms are illustrated in Fig. 5.5, and can be summarized as follows.

Two mechanisms are promoted by the Type Four Pili (TFP), which are appendages emanating from the body of the bacterium. These are the vertical walking and horizontal crawling mechanisms. The bacterium is self-propelled by first extending the pili and binding them to the surface. In a second step, the bacterium pulls itself on the pili. The process iterates, and it is well described as a walking process. Successive steps of a bacterium in this motility processes appears to be almost

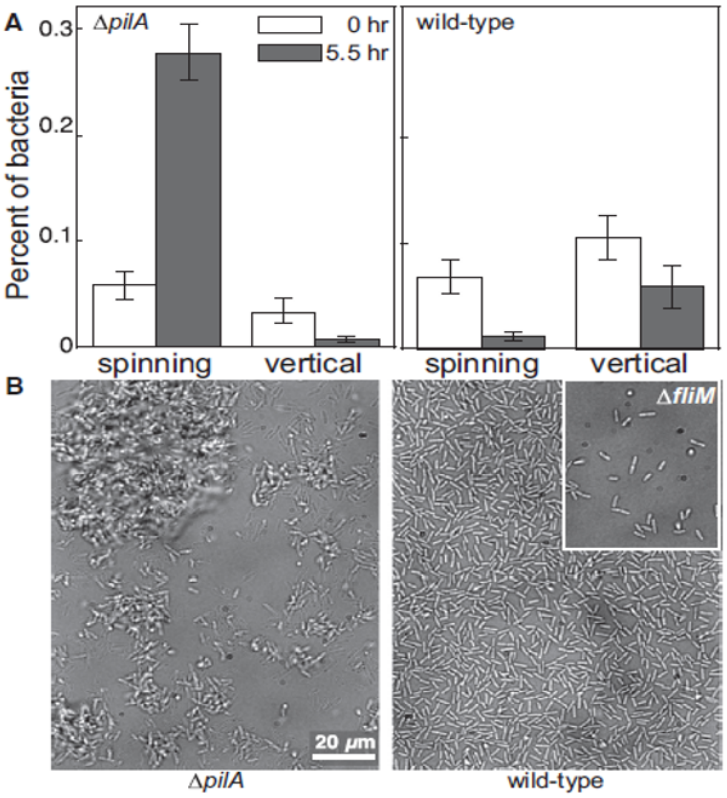

FIGURE 5.6: Lack of TFP and Flagella influence the mobility and detach rate (A) Percentage of bacteria that is in the spinning state or vertical orientation for ΔpilA (lack of TFP) and WT bacteria. (B) Representative micrographs of ΔpilA (left), WT (right), and ΔfliM (right, inset) biofilms 5.5 hours after inoculation.[13].

uncorrelated. Thus the bacterium follows normal diffusion from very short times. The diffusion coefficient is of the order of $0.1\mu m^2/\text{min}$.

The other two mechanisms are driven by the flagella. These are long appendages that protrude from the cell body. The rotation of these flagella leads to a self-propulsion force that allows the bacteria to move. This is the near-surface swimming process depicted in Fig. 5.5c. The bacterium can redistribute the flagella around its body, thus swimming in opposite directions. The near-surface swimming of bacteria is much faster than crawling or walking, and they are not actually on the surface. Thus we do not consider them.

The flagella also contribute to the spinning of surface-bounded bacteria. This is not a motility mechanism allowing the bacteria to diffuse. Most often, this spinning anticipates the detaching of the bacteria from the surface.

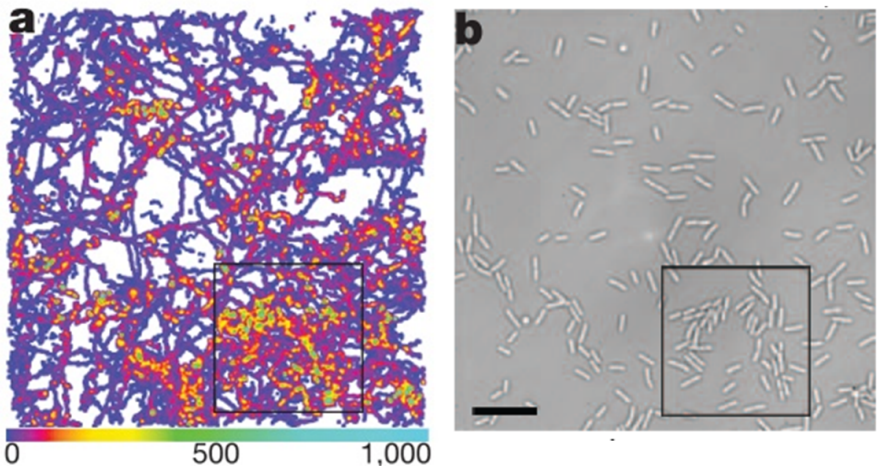

FIGURE 5.7: (a) Visit frequency map of wild type bacteria for the first 15.7 h after inoculation, when microcolonies were just starting to form (example outlined by black square). The line in panel a represent the trajectories of the bacteria, and the color-code represent the visit frequency of a particular region. (b) Bright-field image at $t < 15.7$ h. [14]

These motility mechanisms influence the development of the biofilm. This can be appreciated [13] by comparing the biofilms that are seen to evolve in so-called 'wild-type' bacteria, which are the common species, and in mutants that lack the type four pili, indicated $\Delta pilA$, and that lack the flagella, indicated with $\Delta fliM$.

Fig. 5.6A compares the fraction of bacteria that are seen in the spinning and the vertical state for the $\Delta pilA$ mutants (left-panel) and the $\Delta pilA$ (right panel), at short times and after few hours. For the $\Delta pilA$, many bacteria are found in the spinning state, because they are unable to detach from the surface. A tiny fraction is found in the vertical state. Also, since the Type-4-pili contribute to the motility, the $\Delta pilA$ strain is seen to not spread on the surface, but rather to form a large cluster. This can be appreciated by comparing the left and the right panels of Fig. 5.6B. After the same time gap, wild type didn't form cluster yet. The inset of Fig. 5.6B shows a typical microscopy image of the $\Delta fliM$ strain, after a few hours. The cell density is much lower than observed in the wild-type and in the $\Delta pilA$ strains. This indicates that the flagella play an essential role in the attachment ability of the bacteria.

When the bacteria move on a surface, they do not do it independently, and the

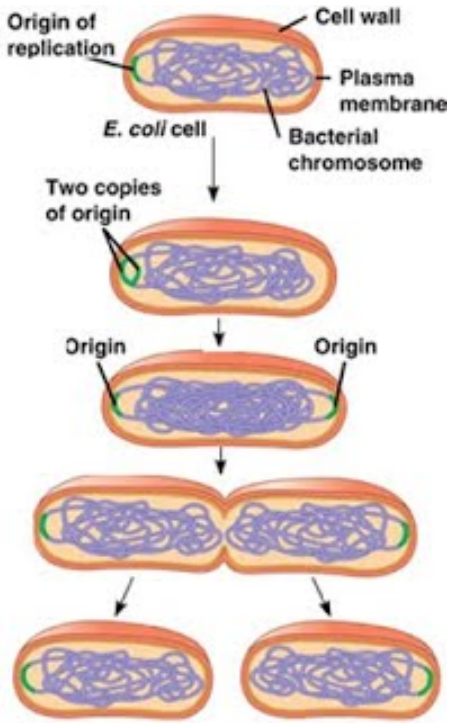

FIGURE 5.8: Schematic representation of the binary fission process of a bacterium. From the internet

correlation between their displacements is not just the result of steric effects. Indeed, bacteria such as Pseudomonas aeruginosa may produce and deposit on the surface, as they move, an exopolysaccharide, psl. Essentially, bacteria leave a trail analogous to the pheromone trail left by ants. When a bacterium moving on a surface meets a trail, it tends to move along it, reinforcing it by depositing its one psl. This gives rise to a positive feedback effect, a rich-get-richer mechanism. As a consequence, bacteria do not visit a surface homogeneously but tend to visit regions already visited by other bacteria. This is illustrated, for instance, in Fig. 5.7, taken from Ref. [14]. It is also observed that the regions where most probably microcolonies form are those with the highest frequency visits.

5.4 Reproduction

I do not to discuss here in the detail, the biological process involved in the reproduction of bacteria. This is out-of-the scope of my work. For our purposes, the modeling of biofilm formation, it is sufficient to consider that bacteria do reproduce

continuously. For P. aeruginosa, the reproduction time is roughly one hour. Of course, this depends on the external conditions, such as the availability of nutrients.

Interestingly, when reproducing by mitosis, as illustrated in Fig. 5.8, the bacteria first grow in size, and divide when their size double. This has important consequences, as in a dense assembly, it means that there is self-induced stress. Hence, bacteria may also move on a surface not because they are motile, but because other bacteria push them. The competition between the expansion of a colony due to the replication of bacteria and the motility of bacteria leads to colonies with different patterns [9, 15].

5.5 Conclusion and discussion

In this Chapter, I have reviewed the physical aspects of biofilm formation, focusing on its initial stages. How to bacteria approach a surface, explore it and finally colonize it. This is not an exhaustive review, which is beyond the scope of my work. In particular, I have not discussed the physics of the underlying biological process, which is highly debated. However, I have described what appear to be the critical ingredients needed to take into account to develop a microscopic model for the initial attachment of bacteria on surfaces. I describe this model and some of its properties in the next chapter.

References

[1] Marco G Mazza. The physics of biofilmsan introduction. *Journal of Physics D: Applied Physics*, 49(20):203001, 2016.

[2] Michel Vert, Yoshiharu Doi, Karl-Heinz Hellwich, Michael Hess, Philip Hodge, Przemyslaw Kubisa, Marguerite Rinaudo, and François Schué. Terminology for biorelated polymers and applications (iupac recommendations 2012). *Pure and Applied Chemistry*, 84(2):377–410, 2012.

[3] Hans-Curt Flemming, Jost Wingender, Ulrich Szewzyk, Peter Steinberg, Scott A Rice, and Staffan Kjelleberg. Biofilms: an emergent form of bacterial life. *Nature Reviews Microbiology*, 14(9):563, 2016.

[4] World Health Organization et al. *Antimicrobial resistance: global report on surveillance*. World Health Organization, 2014.

[5] Cecile Berne, Courtney K Ellison, Adrien Ducret, and Yves V Brun. Bacterial adhesion at the single-cell level. *Nature Reviews Microbiology*, 16(10):616, 2018.

[6] *Microbial Biofilms*. Biotechnology Research. Cambridge University Press, 1995.

[7] Allison P Berke, Linda Turner, Howard C Berg, and Eric Lauga. Hydrodynamic attraction of swimming microorganisms by surfaces. *Physical Review Letters*, 101(3):038102, 2008.

[8] Jacqueline Humphries, Liyang Xiong, Jintao Liu, Arthur Prindle, Fang Yuan, Heidi A Arjes, Lev Tsimring, and Gürol M Süel. Species-independent attraction to biofilms through electrical signaling. *Cell*, 168(1-2):200–209, 2017.

[9] Calvin K Lee, Jaime de Anda, Amy E Baker, Rachel R Bennett, Yun Luo, Ernest Y Lee, Joshua A Keefe, Joshua S Helali, Jie Ma, Kun Zhao, et al. Multigenerational memory and adaptive adhesion in early bacterial biofilm communities. *Proceedings of the National Academy of Sciences*, 115(17):4471–4476, 2018.

[10] Henk J Busscher and Henny C van der Mei. How do bacteria know they are on a surface and regulate their response to an adhering state? *PLoS pathogens*, 8(1):e1002440, 2012.

[11] Jens Elgeti and Gerhard Gompper. Run-and-tumble dynamics of self-propelled particles in confinement. *EPL (Europhysics Letters)*, 109(5):58003, 2015.

[12] Niel Woodford and Matthew J Ellington. The emergence of antibiotic resistance by mutation. *Clinical Microbiology and Infection*, 13(1):5–18, 2007.

[13] Jacinta C Conrad, Maxsim L Gibiansky, Fan Jin, Vernita D Gordon, Dominick A Motto, Margie A Mathewson, Wiktor G Stopka, Daria C Zelasko, Joshua D Shrout, and Gerard CL Wong. Flagella and pili-mediated near-surface single-cell motility mechanisms in p. aeruginosa. *Biophysical journal*, 100(7):1608–1616, 2011.

[14] Kun Zhao, Boo Shan Tseng, Bernard Beckerman, Fan Jin, Maxsim L Gibiansky, Joe J Harrison, Erik Luijten, Matthew R Parsek, and Gerard CL Wong. Psl trails guide exploration and microcolony formation in pseudomonas aeruginosa biofilms. *Nature*, 497(7449):388, 2013.

[15] Catherine R Armbruster, Calvin K Lee, Jessica Parker-Gilham, Jaime de Anda, Aiguo Xia, Kun Zhao, Keiji Murakami, Boo Shan Tseng, Lucas R Hoffman, Fan Jin, et al. Heterogeneity in surface sensing suggests a division of labor in pseudomonas aeruginosa populations. *eLife*, 8:e45084, 2019.

Chapter 6

Modeling the early stage biofilm formation

Being able to adhere and colonize every surface, biofilms are ubiquitous and most frequently harmful. They indeed have huge social costs in different fields, from medicine to engineering. The resilience of biofilms to antibiotic treatment mostly stems from the presence of the EPS matrix. This is a scaffold produced by the bacteria themselves, which protects them from chemicals, like antibiotics by slowing their diffusion. In addition, the matrix gives mechanical strength to the biofilms, protecting them from mechanical stresses. A possible strategy to mitigate the spreading of biofilms would be that to prevent their initial growth. To this end, one needs to rationalize how this growth is affected by different physical and biological processes occurring in this stage. This is a difficult task, as these processes are many, are frequently interrelated. In addition, not all of them have been characterized.

To make progress, I have developed a numerical model for the investigation of early stage biofilm formation. This model takes into account all of the processes that appears to be relevant, such as motility, reproduction, production of psl trail, production to the EPS matrix, etc. Some features, I believe to be less relevant, are for now neglected. For instance, I neglect hydrodynamic interactions, which after the initial docking of the bacteria should be minor, due to small Reynolds number. For instance, bacterial swimming speed in the bulk is around $30\mu m/s$ and its moving speed on a surface is of the order of $1\mu/s$. The Reynolds number is $\Re = \frac{\rho V L}{\nu}$,

where ρ is the density of the fluid(for water, $\rho = 10^3 kg/m^3$), ν is its viscosity(for water, $\nu = 10^{-3} Pas$),V is the relative velocity of the particle with respect to the fluid, L is the typical length of a bacterium(around $1\mu m$). Thus for bacteria swimming in the bulk, the Reynolds number is $\sim 3 \times 10^{-5}$ and for movement on the surface, the Reynolds number is $\sim 10^{-6}$. This indicates that bacterial motion is in a low Reynolds number regime where viscous forces dominate over inertial forces. Despite this and other approximations, the model is quite involved and characterised by many parameters, whose typical values are not always found in the literature. Partially, this is also because these parameters are not constants; rather, they depend on the external environment on which the biofilm develops, e.g. on the amount of food or other chemicals. Without lose in generality, the model I developed is tailored towards the pathogen *Pseudomonas aeruginosa*, for two reasons. First, because this is one of the most pathogenic bacteria, e.g. the cause of persistent infections in the medical environment. Secondly, this pathogen has been recently a subject of video-microscopy experiments. This implies that we are able to estimate from literature data reliable values for many of the parameters which characterise the model. In this aspect, consider that biofilm are seen to develop in different bacteria species, and in different external conditions, where the values of the different control parameters are certainly different. Hence, the emerging phenomenon is certainly resilient to changes in the values of the control parameters, we therefore only need to roughly estimate.

This Chapter is structure as follows. In Sec. 6.1, I introduce the numerical model. This is characterized by many parameters describing the relevance of different biological process. I, then explore the dependence of the growing properties of bacterial colony on these parameters. In Sec. 6.2, I illustrate how a colony develops from one bacteria that has no motility. In particular, I stress that the rod-like shape of bacteria introduces a local nematic ordering within the colony. Specifically, in Sec. 6.3, I demonstrate a competition between the growth rate and the motility of the bacteria. This is of interest because, as we have discussed, different mutants may have different motility properties. On the same line, in Sec. 6.4, I discuss the growth of a biofilm seeded by different mutants, that have different motility properties. In Sec 6.5, to the exploration of the role of the psl trails the bacteria leave on the surface, to investigate their impact on the frequency with which the bacteria visit different locations in space. The effect of EPS production is discussed in Sec 6.6, where we consider how the features of a microcolony changes with the

rate of production of EPS. In Sec 6.7, I demonstrate the early study of 2D to 3D transition by extending the bacteria 2D model with EPS.

6.1 Numerical model

The numerical model I have set-up, describes the development of a bacterial colony on a surface. The model assumes that bacteria move and reproduce on the surface. To reduce the number of parameters, I neglect the possibility that the bacteria move from the surface back into the liquid as well as that other bacteria land from the liquid to the surface. It would be easy to add these features, but it is conversely difficult to reliably estimate the associated adsorption and desorption rates.

I illustrate in the following, the main features of the model, which can be controlled independently. Two complex features of the model are not described here. The source code for this bacteria simulation model could be found on GitHub: Bacteria Model

First, the model is able to describe the production of psl (phospholipases) trails, and the interaction of the bacteria with psl. I describe how psl is modeled in Sec. 6.5. Second, the model is also able to describe the fact that the bacteria produce EPS (extracellular polymeric substances), and that this develop into a gel-like matrix. I describe how EPS is modeled in Sec. 6.6.

We model a bacterium as a spherocylinder, we construct by lumping together 7 point particles. The point particles of different bacteria interact via a WCA potential, with energy scale ϵ and minimum (or cutoff in the case of the purely repulsive WCA) at $D = D_{b,b} = 2^{1/6}\sigma = w = 0.6\mu$m. Accordingly, w corresponds to the width of a bacterium. The WCA potential is a LJ potential truncated at its minimum. Consecutive particles of a bacterium interact via a Harmonic spring with stiffness $k_b = 250\epsilon/w^2$ and initial rest length l_0, that is fixed such that the bacterium aspect ratio is $[(n-1)l_0 + w]/w = 3$. Using these value the size of a bacterium mimic that of *Pseudomonas aeruginosa*. Bending rigidity is provided introducing an Harmonic angular interaction, with rest angle π and stiffness $k_a = 20\epsilon$, between any three consecutive particles. This is a high enough value for the bending deformation to be negligible for the range of parameters we considered. An isolated bacterium moves by performing a run and tumble motion, whose parameters have been calibrated

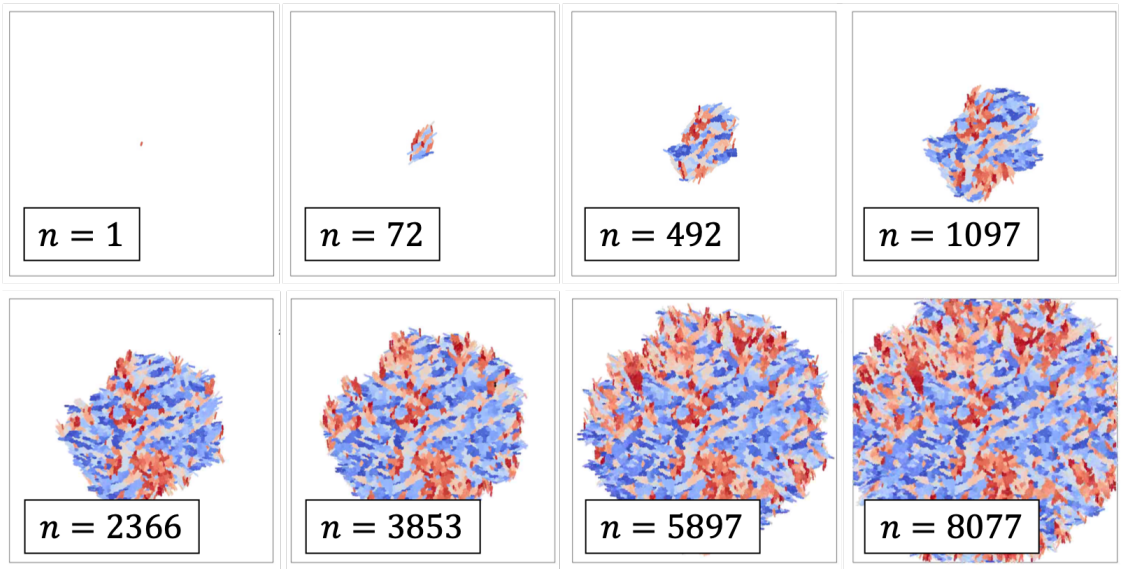

FIGURE 6.1: Growth of a colony of non-motile bacteria. The color code reflects the angle the bacteria axes forms with a fixed arbitrary direction. Hence, patches with same color correspond to regions with the same nematic director. The corresponding video of this simulation could be find in URL: https://youtu.be/_brD7-XXBLU

to mimic the dynamics of walking/crawling early stage Pseudomonas bacteria [1]. Specifically, the diffusion coefficient is $D \simeq 0.7\mu\text{m}^2/s$, while the velocity of a bacterium is $v_{\text{bact}} \simeq 0.2\mu\text{m/s}$.

Growth and reproduction: We model bacterium growth by making the rest length of the springs connecting the beads making-up the bacterium time dependent. The rest length grows linearly in $\min(t - t_b, 1.2t_r)$, where t is the actual time and t_b the time of birth of the bacterium, with a growth rate set such that an isolated bacterium doubles in length in t_r, where for each bacterium t_r, is taken from an exponential distribution with mean 1h. The maximum value of the rest length has a cutoff to avoid the unbounded growth. When a constrained bacterium experience higher pressure from the surrounding will not able to grow. Reproduction is modeled by replacing a bacterium that succeed in doubling its length with two bacteria, which occupy the same volume as the original one. The polarity of the daughter cells is identical to that of the father.

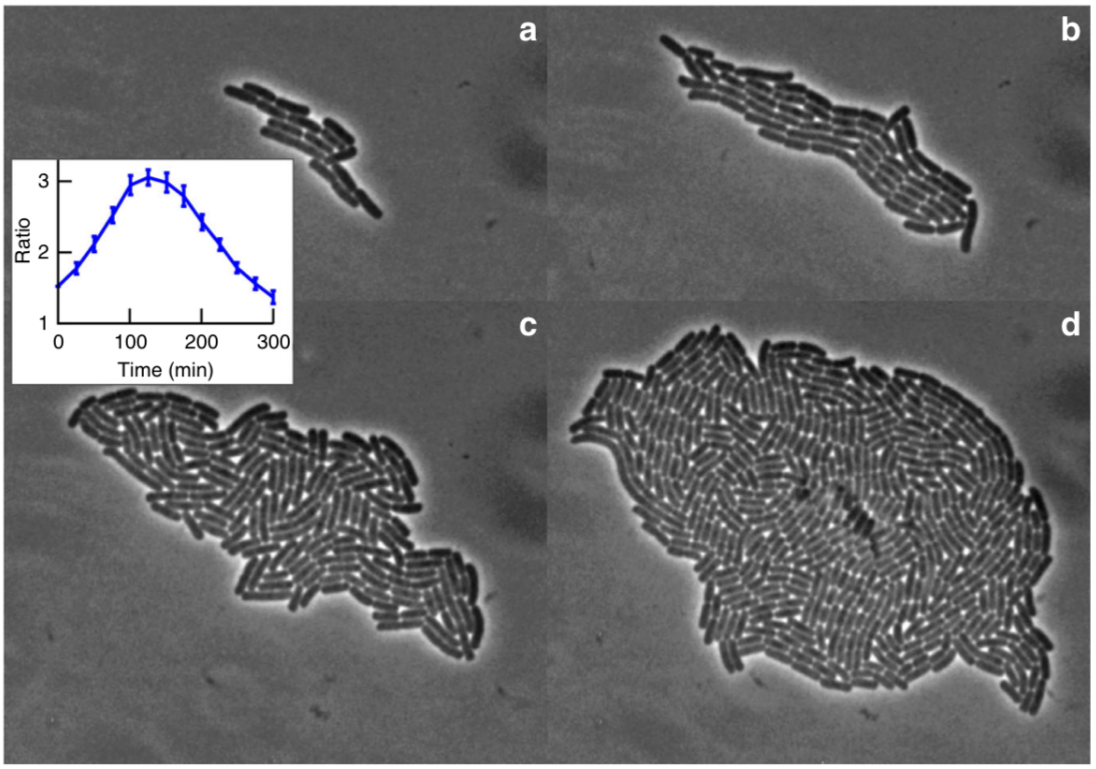

FIGURE 6.2: Experimental results for the time evolution of a growing *escherichia coli* bacteria colony. The emergence of regions with local nematic ordering is apparent. The inset illustrates the time dependence od the ratio between the major and the minor microcolony axis, averaged over 10 realisations.

6.2 Growth in the absence of motility

We begin illustrating our model at work with the simplest possible example. The growth of a colony of non-motile bacteria, in the absence of psl and eps. In this scenario, we do expect the number of bacteria to grow exponentially with time. Saturation occurs at large times due to finite size effects. This jamming transition induced by reproduction has actually been considered before [2].

We illustrate the expanding colony in Fig. 6.1, where different snapshots refer to different times, equally separated. The number of bacteria n present at each time is detailed in each panel.

The direct visualization of the colony suggests that the bacteria have a tendency to align with each other. To check whether this is really the case, we color code each bacterium according to the angle its director forms with a given axis (modulus π, given that in the absence of motility the bacteria are not polar). As the colony

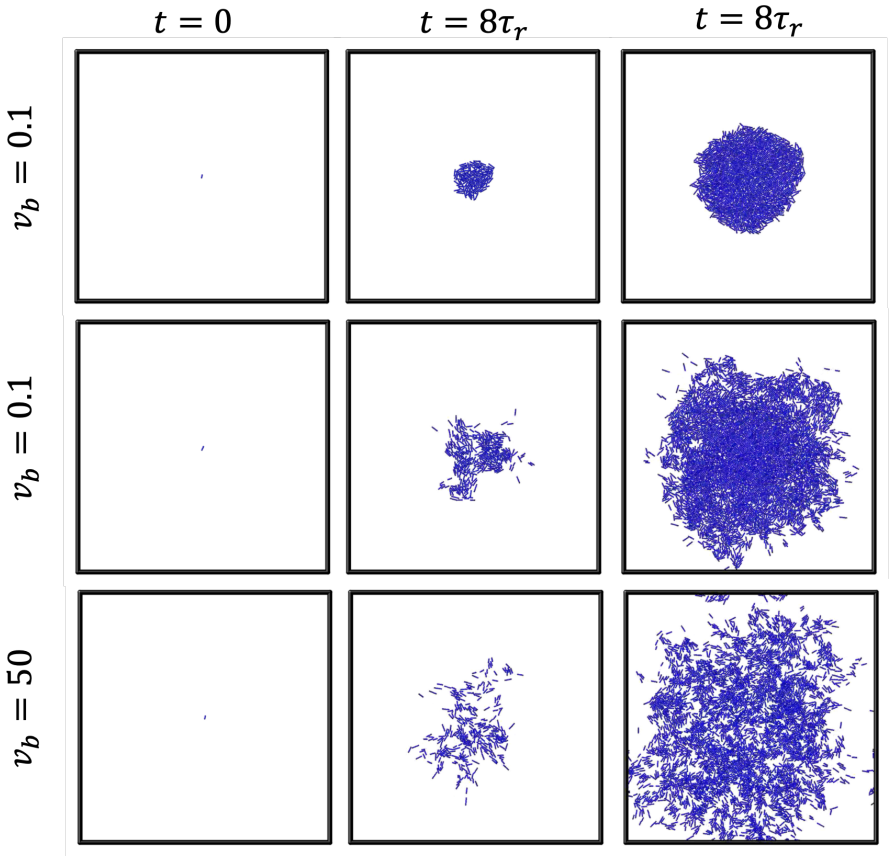

FIGURE 6.3: The evolution of three different microcolonies. The three only differ in the value of the typical bacteria velocity, which increases from top to bottom. The corresponding links for these simulations could be find in SI.

grows we clearly see the emergence of domains with a same color, which identify regions of local nematic alignment. Interestingly, such a nematic alignment in growing bacterial colonies has also been very recently experimentally reported [3, 4].

Indeed, we show in Fig. 6.2 microscopy images taking at different times during the development of a *escherichia coli* microcolony. The presence of domains with local nematic order is apparent. The inset illustrates the ratio between the major and the minor microcolony axis as a function of time.

6.3 Motility vs. growth rate

In previous chapters, we have discussed the motility mechanisms of bacteria, and also illustrated the possibility of tailoring them. In particular, different mutants, e.g. those lacking type-4 pili, or those lacking the flagella, exhibit different motility

properties. This leads to the development of biofilms with different spatial properties, as we observed in Fig. 5.6. This suggests to investigate the dependence of the spatial feature of the emerging biofilm in the numerical model on the motility.

Here we consider that, once a bacterium adheres to the surface and seeds a microcolony, the following evolution depends on the competition of two physical processes, the reproduction and the motility of the bacteria. To clarify the origin of this competition, we start by considering the time dependence of the radius of a microcolony, assuming the bacteria to have no motility. Hence, the colony expands only because the bacteria duplicate and push against each other.

To model this situation, we assume that the colony is characterised by a constant number density ρ, number of bacteria per unit area. If this is so, then the number n of bacteria in a colony of radius R is $n(R) = \rho 4\pi R^2$. How does R evolves with time? To predict $R(t)$, we assume the bacteria to reproduce with a constant rate τ_r^{-1}, so that $\frac{dn}{dt} = \frac{n}{\tau_r}$. From this assumption, we get

$$\frac{n}{\tau_r} = \frac{dn}{dt} = 8\pi\rho R\frac{dR}{dt}. \tag{6.1}$$

Hence, the radial expansion velocity of the colony is

$$v_R. = \frac{dR}{dt}. = \frac{R}{2\tau_r}. \tag{6.2}$$

Interestingly, this model predicts that the expansion velocity grows linearly with the cluster size. One might expect this to occur in the early stage development of a microcolony. At later time, the bacteria deep inside the colony will stop reproducing. From a mechanical perspective, we can consider this occurs as the bacteria are too compressed.

If we now allow for the presence of motility, another velocity enters into the problem: the typical bacteria velocity v_{bact}. It turns out that v_R and v_{bact} compete. Precisely, when $v_{\text{bact}} \gg v_R$, bacteria swim away from each other before they reproduce. Conversely, they reproduce when still close. Considering that v_R grows with the bacteria colony, we understand that for large enough colony it always happens that bacteria reproduce when in contact, pushing against each other and giving rise to the growth of a compact microcolony.

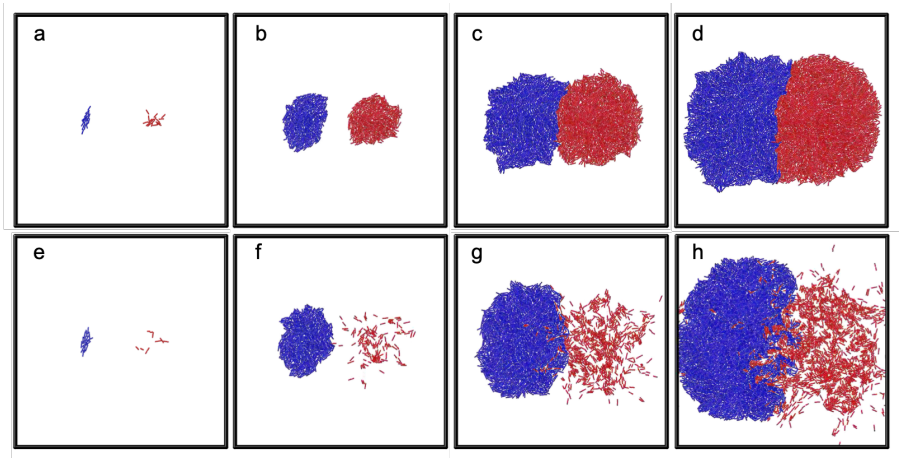

FIGURE 6.4: Considering the coexist of different species, top: two species both with small mobility, bottom: one of the species with large mobility. The corresponding simulations of these videos could be find in the SI.

As an example, I illustrate in Fig. 6.3, the developing of three different microcolonies, which only differ in magnitude of the typical velocity of bacteria. At small velocities, the microcolony is essentially compact at all times. At large velocities, bacteria are spread on the surface at short times, but then become part of a dense microcolony. This is apparent in the configuration reached after 8 reproduction times, in the case of intermediate velocities.

6.4 Coexistence of different species

During the development of a biofilm, chances are that bacteria with different motility properties will coexist. Biofilms are often multispecies [5].

Here I consider the interplay of two growing bacteria colonies, made of bacteria with different motility properties. The blue, which are immotile, and the red, which are mobile,

Fig. 6.4a-d illustrates the growth of these two colonies, in the case in which the distance between the two seeding bacteria is small compared to the radius above which the red colony becomes compact (see previous section). Indeed at short times, panel a, the red colony is spread, but at following time it is compact. Hence, when the two microcolonies enter in contact, both of them are compact. As a consequence, a sharp interface between the two colonies develops. Notice that this interface is not straight, but slightly curved. This is because the blue colony does

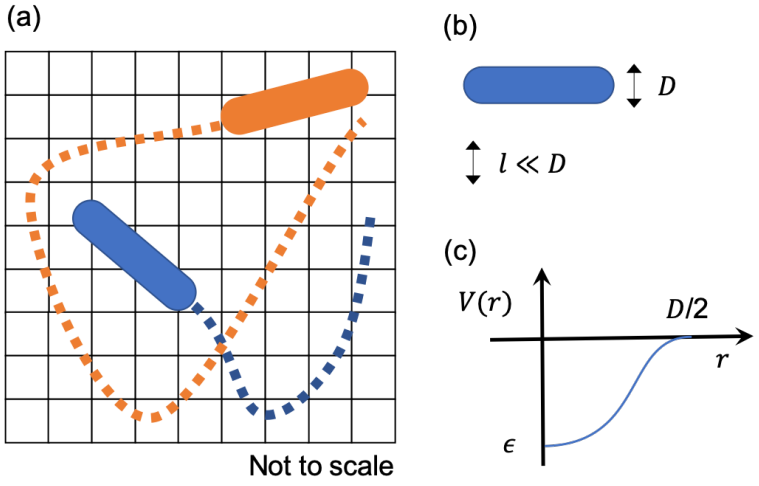

FIGURE 6.5: (a) examples of psl trail on the grid (b) the grid size is much smaller than bacteria width D (c) the psl attractive potential.

not develop as a circular one at short times. It is conversely lightly elongated, as the experimental microcolony seen in Fig. 6.2.

Fig. 6.4e-h considers a case in which the red bacteria are faster, so that when the two colonies start interacting, the red one is not yet a compact one. In this case, the interface between the two colonies is rough, and as a wavy structure as a consequence of fluid dynamics instabilities. Note, in addition, that isolated red bacteria are seen to be able to enter into the blue colony.

6.5 The role of psl

We now consider the possibility of numerically describing the role of interaction of the bacteria with their trail. To this end, the trails need to be recorded. As the psl particles are seen diffusing slowly in the experiments observations, we assume it is stationary.

From a computational viewpoint, we do that by superimposing to the computational domain a square grid, with grid size $l \simeq D/20$, with D is the width of the bacteria. As the bacteria move on the surface, we record how many times each cell is visited. Specifically, considering our coarse-grained description of the bacteria as a collection of beads, we focus on the position of the central bead. Thus when the bacteria move, we know how many times a grid cell located in position $\mathbf{r}$ has been

visited. We indicate this number as $n_v(\mathbf{r}, \mathbf{t})$. Clearly, $n_v(\mathbf{r}, \mathbf{t})$ can be seen as the superimposition of all trails left by all bacteria. We not only know if a particular location has been visited, but also how many times it has been visited. Because of this, $n_v(\mathbf{r}, \mathbf{t})$ can be thought as proportional to the amount of psl deposited by the bacteria in $\mathbf{r}$. This approach is schematically illustrated in Fig. 6.5a,b.

To model the interaction between the bacteria and the trail pattern, we add to the energy of our model the following term:

$$V_{\text{trail}}(t) = \sum_b \sum_{r_i \in b} \sum_r n_v(\mathbf{r}, t) v_{\text{Gauss}}(\mathbf{r} - \mathbf{r_i}), \tag{6.3}$$

where the first sum runs over all bacteria, the second one over all particles of bacteria b, the third one over all cells of the grid we use to record the trail pattern. The interaction between each cell element and each bead of our bacteria is given by an attractive potential, whose amplitude is proportional to the number of times the grid element has been visited. We model this attractive potential with an attractive Gaussian potential v_{Gauss}, as illustrated in Fig. 6.5c. We fix the width of the Gaussian interaction to a small value, half of the bacterial width. Notice that the trail interaction acting on each bacterium exerts an effective torque, whose net effect is that of aligning the bacteria to the trail.

In this model, the interaction potential is characterised by a typical energy scale ϵ. We do not find literature data discussing the strength of this interaction. Also, the rate of which bacteria deposit psl has not been discussed in the literature.

Nevertheless, we understand that if the bacteria deposit bacteria too frequently, and if the attraction is too strong, then the bacteria will bind to the psl deposit immediately, and will not be able to move. This appears to be unrealistic. On the order side, if the deposit rate is too infrequent, then the bacteria deposit psl in uncorrelated locations, not on a trail. This is also unrealistic. We have therefore arbitrarily chosen simulation parameters for which the concept of a trail is well defined.

In Fig. 6.6, I illustrate a representative time evolution of a bacterial colony, in the presence of psl production. Beside drawing the bacterial, I also draw the corresponding trails. These are clearly visible, particularly at short times before

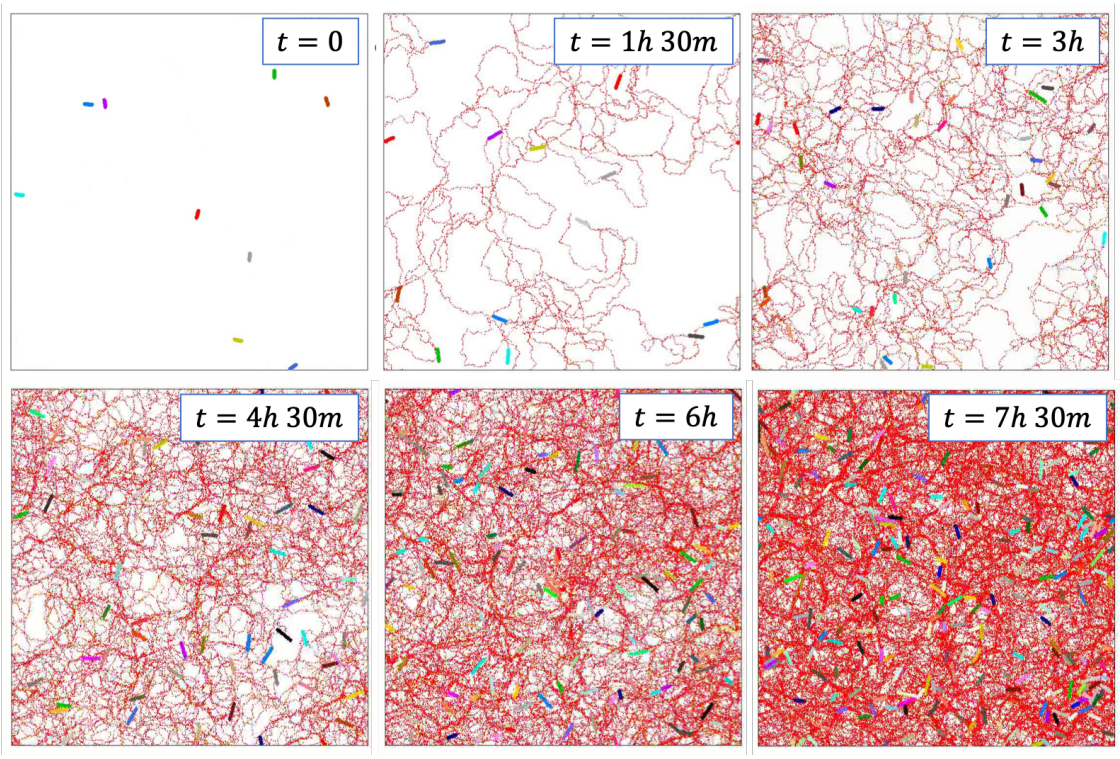

FIGURE 6.6: Early stage biofilm formation in the presence of psl production. The red lines are the trails left by the bacteria as they move around. Bacteria interact through an attractive force with the trails. The attraction to a particular location is space is proportional to the number of times this location has been visited by the bacteria. The corresponding video can be find in URL: https://youtu.be/lAYZvULn2tk.

the trails of different bacterial overlap. Qualitatively, this results are analogous to that experimentally reported in Ref. [6] (see Fig. 5.7).

To be more quantitative, we have determined the time evolution of the probability distribution of the number of times a particular grid element (pixel) has been visited. This quantity favourably compares to experimental results. Fig. 6.7a,b presents experimental results for this probability distribution, obtained (by the same group) in Ref.s [6, 7]. The probability distribution is found to decay as a power law, with a large exponent that decreases as times evolve. In panel c of the same figure, I present my numerical results for the same quantity. Clearly, the numerical model well reproduces the experimental results, both as concern the presence of a power-law decay in the probability distribution, as well as the value of the decay exponent and its time dependence.

From these studies, psl could be a promoter of the number density fluctuation in bacterial system by enhancing the visiting frequency in certain regime through

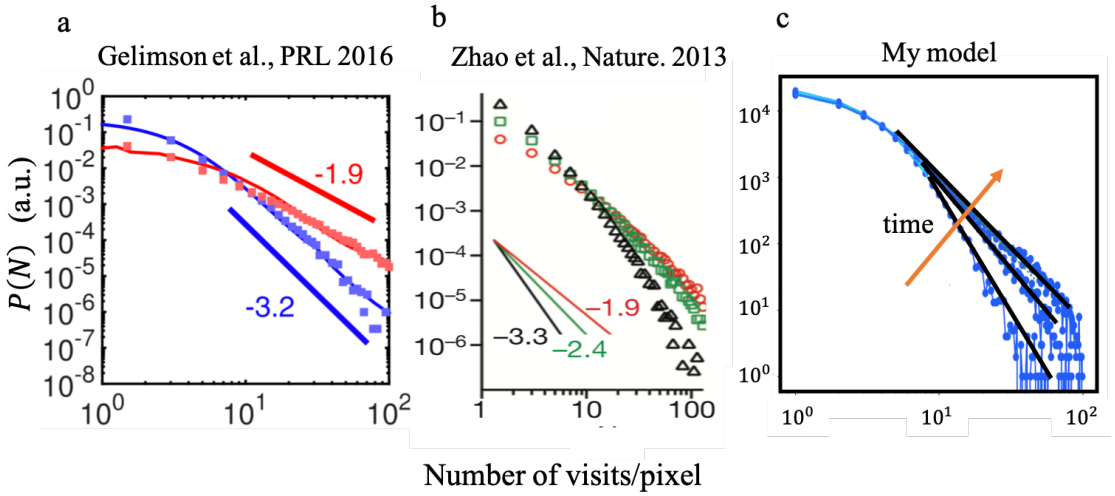

FIGURE 6.7: Experimental and numerical results for the time evolution of the probability distribution of the number of times a point (pixel) has been visited by a bacterium. Panels a and b report experimental results from Ref. [7] and Ref. [6], respectively. Panel c illustrates the results of my numerical model.

slowing down bacteria mobility speed. In some cases, if the psl deposit is rich enough to bind the bacteria locally, bacteria become stationary. Thus stationary cluster could be find in bacteria system. For this phenomena, one could check our simulation URL: https://youtu.be/TPfFfbzI850. This phenomena is similar to what we understand from the ABPs model that slow particle motion induces the formation of clustering. Those stationary bacteria could be a seed to initialize nucleation in the initial formation of biofilm.

While these results are certainly encouraging, let me mention that from a computational viewpoint, these simulations are extremely demanding, as the number of interaction centers is strongly influenced by the number of grid elements. These need to be large as the linear dimensions of the grid cell need to be smaller with respect to the size of the bacteria.

6.6 The role of EPS

One of the distinct features of biofilm, and a primary reason for their high resilience, is the presence of an EPS matrix. The Extracellular polymeric substances (EPSs) are natural polymers of high molecular weight, produced by the bacteria themselves, to which the bacteria might bond. The numerical modeling of the EPS

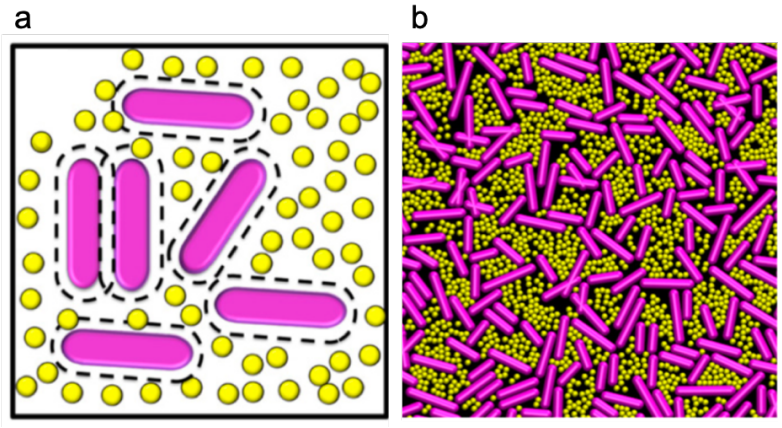

FIGURE 6.8: Ref. [8] introduced a coarse-grained description of the Extracellular polymeric substances (EPSs), which are represented as small particles, as in panel a. These EPS particles are inserted by the bacteria in their surrounding. The EPS particles interact repulsively among them and with the bacteria, and might cause a microphase separation. An example is illustrated in panel b. Adapted from Ref. [8].

matrix is certainly challenging, as one need to model the polymers, their introduction, their dynamics, and their interaction, both among themselves as well as with the bacteria. Here, we introduce a coarse-grained description of the role of EPS, and investigate its impact on the developing of a biofiolm.

6.6.1 EPS: numerical model

Our numerical model has been inspired by the only work that explicitly modeled EPS particles[8]. Here, the authors considered that EPS can be described as polymer coils. Hence, they interact among them and among each other with a purely repulsive potential, and each EPS-polymer can be represented as an EPS-particle. They also assumed that bacteria produce EPS, which means that each bacteria, with a given frequency, insert an EPS particle in its surrounding. This introduction is done only if it does not cause an increase in the energy of the system, i.e. only if the inserted particle is not in contact with any other particle, or any other bacteria. Their model is illustrated in Fig. 6.8a. In this model [8], as a colony develops, the EPS particles and the bacteria segregate, via what the authors speculate to the a depletion-like interaction. A typical phase separated configuration is illustrated in

Fig. 6.8b. Note however, that the EPS particles have no dynamics, which questions the depletion interpretation. The features of the observed phase separation depends on the rate at which EPS particles are produced [8].

While an important first step in the modeling of the role of EPS in biofilm formation, this model appears to neglect the important cohesive role of EPS. The introduced EPS particles do not bind to each other and to the bacteria, and hence the biofilm as a whole does not develop as a gel network embedding the bacteria.

Building on this previous work [8], I have therefore developed the following model:

1. Extracellular polymeric substances (EPSs) are represented as small spheres, whose size is half of the width of the bacteria, $\sigma_{\text{eps}} = D/2$.

2. EPS particles interact among them with a purely repulsive WCA potential, with energy scale ϵ (which is the energy scale of the interaction between the particles bacteria are made of). The potential goes to zero at $(\sigma_{\text{eps}} + D)/2$.

3. EPS particles are inserted by the bacteria in their surrounding, at a rate τ_{eps}^{-1}. An EPS particle is inserted only if it does not overlap with any other particle or bacteria.

4. Every Δt, where Δt is a random variable taken form an exponential distribution with average value Δ_t^*, we look for all possible pair of EPS particle that are in contact. If two EPS particles are in contact, we bond them with an harmonic bond $v(r) = 10^2\epsilon(r - \sigma_{\text{eps}})^2$, provided that they are not already bonded, with a probability p_b.

5. Similarly, every Δt we add a bond between an EPS particle and a bacteria particle in contact. In this case, the interaction energy is $v(r) = 10^2\epsilon\left[r - \left(\frac{\sigma_{\text{eps}}+D}{2}\right)\right]^2$, provided that they are not already bonded. Also in this case, the bond is added with probability p_b.

Assumption 1-3 above essentially reproduce the model of Ref. [8]. 4 & 5 on the other hand, describe the dynamics of a polymerization process. Note that the energy scale of the bond is larger than that of the interaction potential between the particle, to compensate for the fact that the harmonic interaction of the bonds is much softer than the LJ-like interaction between the particles. As for the concerned the

dynamics, we assume the EPS particle to diffuse by Brownian motion. However, we note that the typical diffusion coefficient/velocity of these particles is much smaller than that of the bacterial, which means that essentially the bacteria move in a bath of almost immobile particles.

The model has two parameters, Δ_t^* and p_b, and the rate at which bonds are formed between possible pair of particles is $p_b\Delta_t^*$. It is difficult to estimate these parameter from the experiments. In addition, we notice that the rate at which EPS is produced depends on the growing condition. Here, we decided to fix $\Delta_t^* = 1\text{min} = \tau_r/60$, and have investigated the dependence of the growing dynamics on the bond probability p_b.

6.6.2 EPS: numerical results

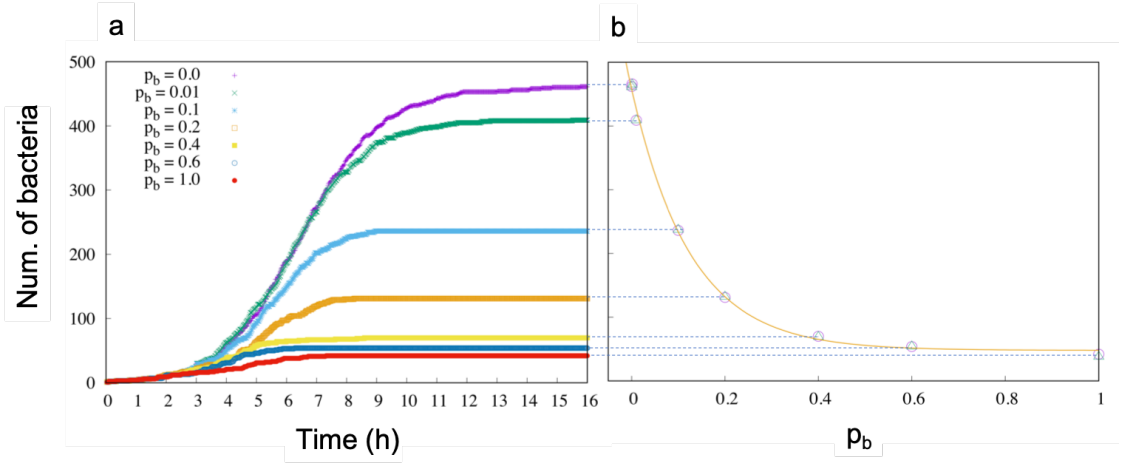

FIGURE 6.9: Effect of the bonding probability on the number of bacteria. Panel (a) illustrates the time dependence of the number of bacteria on the surface. Different curves refer to different values of the bonding probability, p_b. Panel (b) shows the dependence of the asymptotic steady state number of bacteria on the bonding probability p_b. The fitting line is an exponential one, $n_\infty + (n_0 - n_\infty)e^{-p_b/p_b^*}$.

We have investigate the dynamics and the steady state future of biofilms, as a function of the bonding probability p_b. Fig. 6.9a illustrates the time dependence of the number of bacteria, for different values of p_b. At very short times, $t < 2h$, the production of EPS does not quantitatively affects the dynamics, as different curves collapse. At larger times, the population grows exponentially, but then saturates. This saturation is not a finite size effects. This is an important results, as

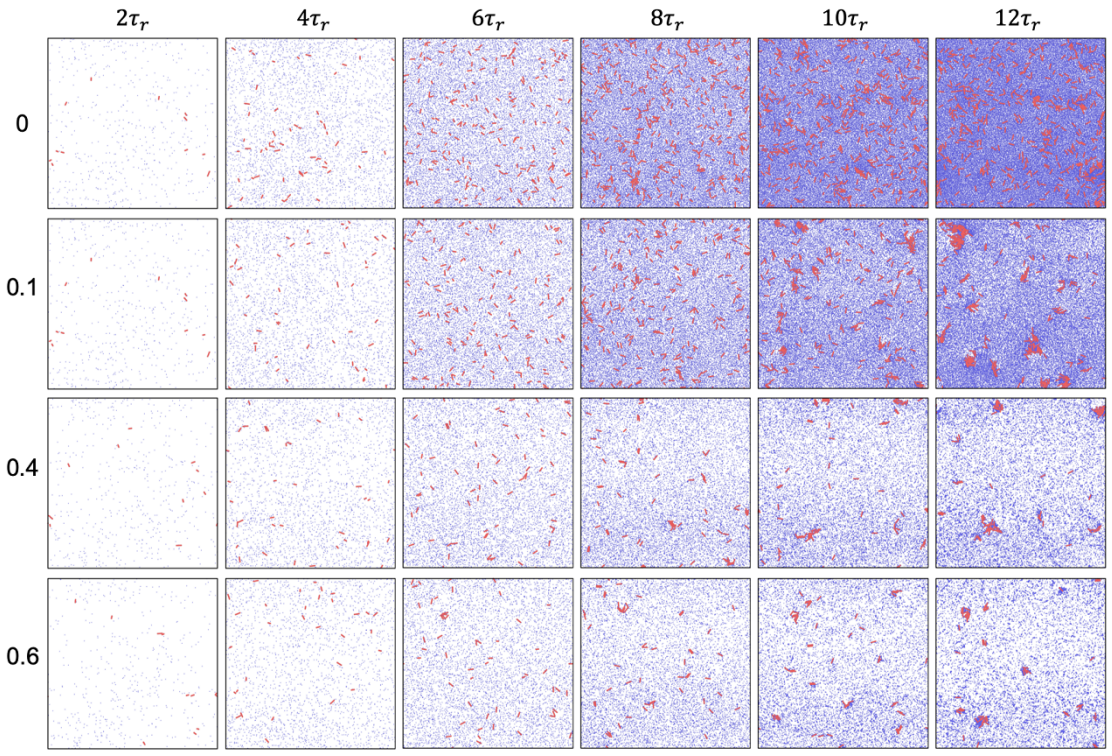

FIGURE 6.10: Evolution of system of bacteria (red) which produce EPS (blue). The EPS particles can bond to each other, and to the bacteria, with probability p_b. Different rows correspond to different values of the bonding probability p_b, as indicated.

it clarifies that in the presence of EPS a microcolony stop spreading indefinitely in two dimensions. Indeed, we do expect a transition towards a three dimensional condition. Fig. 6.9b shows that the asymptotic number of bacteria decreases exponentially with the bonding probability. If p_b is very high, growth stop with just few bacteria on the surface.

To rationalize these results, we provide snapshots illustrating the time evolution of the investigated system in Fig. 6.10. In this figure, different columns correspond to different times, and different rows to different values of the bond probability p_b, as indicated. In all case, at long times we do see the formation of small cluster of bacteria. These bacteria are glued together through the EPS particles. For small values of p_b, these cluster only form when there are many EPS particles in the systems. Conversely, for larger value of p_b, few EPS particles are able to glue the bacteria together. Bacteria are therefore self-trapped by the EPS particles the produce [9, 10].

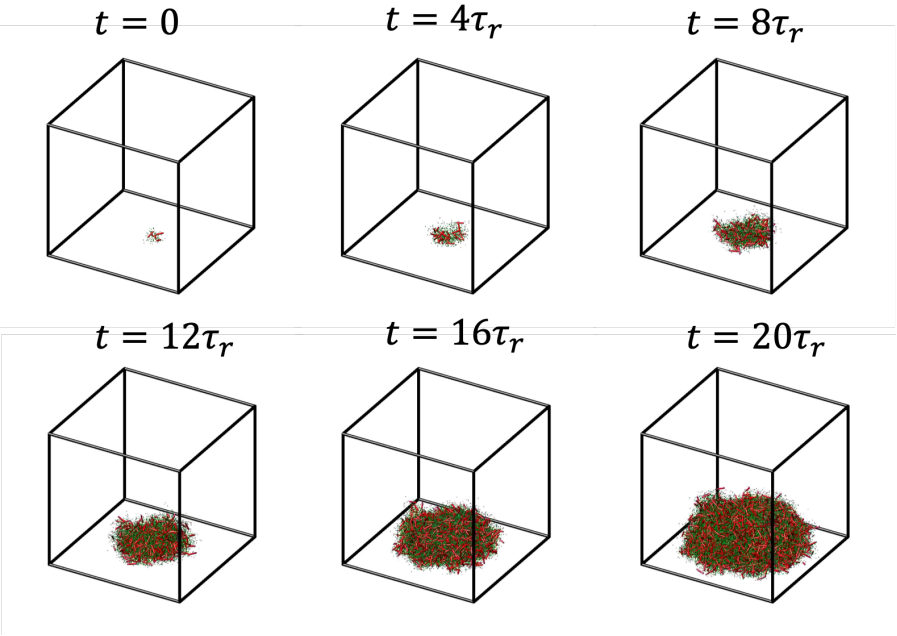

FIGURE 6.11: Evolution of a three dimensional microcolony of not-motile bacteria. The microcolony develops with the bacteria embedded in an EPS gel matrix.

6.7 From two- to three-dimensional microcolonies

All investigations reported so-far have been restricted to the early stage formation of a biofilm, which is essentially a process developing in two dimensions, on a surface. However, biofilms then develop as structured three dimensional aggregates. Here, without the aim of being quantitative, I want to demonstrate that the numerical approach I have developed is also able to describe this transition. To this end, I have extended the model to allow for the motion in the vertical direction. To drive the transition from two to three dimensions, I allow thermal noise on the EPS particles to act on the vertical coordinate. Hence, EPS particles diffuse in the whole volume. When bonded to bacterium on the surface, the thermal motion of the EPS particles may force the bacterium out of the horizontal plane. A small tilt of the bacterium is enough to seed the transition from a two to a three dimensional biofilm. Here, I assume bacteria not to be motile. Fig. 6.11 illustrates that, with these assumptions, a three dimensional biofilms develop, where the bacteria are embedded in a growing EPS matrix. I have not performed so far any quantitative investigation of these three dimensional investigation, also because of their high computational cost.

6.8 Conclusion

In this chapter, I have presented the developing of a numerical model for the investigation of the early stage biofilm formation, and few applications. This model can be considered as a toolbox for bacteria studies, as I do have implemented models for all of the biological processes that appear to be relevant: motility, reproduction, interaction with psl trails, generation of an EPS matrix. As such, the model depends on many parameters. I have calibrated some of them on the basis of experimental investigations of *Pseudomonas aeruginosa*. Other parameters have been reasonably chosen arbitrarily, in the absence of inputs from experiments.

I have first investigated the growth of a microcolony of non-motile bacteria, and then clarified the existence of a competition between reproduction rate and typical velocity of the bacteria. Asymptotically, this competition is always won by the growth rate, which makes the radius of the microcolony to grow with a velocity proportional to the ratio between the radius itself and the reproduction time. Hence, this velocity grows with the colony. As a consequence, while small microcolonies might not be compact, larger ones are compact, as the bacteria reproduce when in contact. Then, I have considered the growth of multiplies biofilms, where the two species have different motility properties. This investigation has clarified that the two species might stay spatially separated, or conversely might mix, depending on the relative typical speed of the bacteria.

I have then explored the possibility of modeling in a particle based approach, two fundamental but more complex biofilm features. First, I have considered that bacteria deposit a pls trails as they move, to which they are then attracted. I have set-up a numerical model describing trail deposition and interaction. Simulations of this model reproduce experimental results for the probability distribution of the number of times a particular location in space is visited. Then, I have developed a model to described the role of EPS. The only model describing at a particle level EPS did not consider the fact that the EPS form bonds, effectively constructing a gel network embedding the bacteria as the biofilm develop. My model does consider this important aspect. Importantly, my numerical simulations also demonstrate that this network is able to trap the bacteria, effectively inhibiting both their diffusion as well as their proliferation, as experimentally observed. This could be

the first a first stage towards the transition from a two- to a three dimensional bacterial colony.

While I was able to successfully compare the numerical model I have developed to experiments, future work ahead would require a more thorough comparison. In this respect, let me mention that the bottleneck appears on the experimental side, as systematic studies of the early stage biofilm formation process with a single particle resolution are scarce. I do have however set-up two collaborations, one within the SCELSE, the Singapore Centre for Environmental Life Sciences Engineering, and the other with the University of Madrid, Spain, and hope to get more experimental data to compare my model with in the next future.

References

[1] Jacinta C Conrad, Maxsim L Gibiansky, Fan Jin, Vernita D Gordon, Dominick A Motto, Margie A Mathewson, Wiktor G Stopka, Daria C Zelasko, Joshua D Shrout, and Gerard CL Wong. Flagella and pili-mediated near-surface single-cell motility mechanisms in p. aeruginosa. *Biophysical journal*, 100(7):1608–1616, 2011.

[2] Morgan Delarue, Jörn Hartung, Carl Schreck, Pawel Gniewek, Lucy Hu, Stephan Herminghaus, and Oskar Hallatschek. Self-driven jamming in growing microbial populations. *Nature physics*, 12(8):762, 2016.

[3] D DellArciprete, ML Blow, AT Brown, FDC Farrell, Juho S Lintuvuori, AF McVey, D Marenduzzo, and Wilson CK Poon. A growing bacterial colony in two dimensions as an active nematic. *Nature communications*, 9(1):4190, 2018.

[4] Yusuf Ilker Yaman, Esin Demir, Roman Vetter, and Askin Kocabas. Emergence of active nematics in chaining bacterial biofilms. *Nature communications*, 10(1):2285, 2019.

[5] Henriette L Røder, Søren J Sørensen, and Mette Burmølle. Studying bacterial multispecies biofilms: where to start? *Trends in microbiology*, 24(6):503–513, 2016.

[6] Kun Zhao, Boo Shan Tseng, Bernard Beckerman, Fan Jin, Maxsim L Gibiansky, Joe J Harrison, Erik Luijten, Matthew R Parsek, and Gerard CL Wong. Psl trails guide exploration and microcolony formation in pseudomonas aeruginosa biofilms. *Nature*, 497(7449):388, 2013.

[7] Anatolij Gelimson, Kun Zhao, Calvin K Lee, W Till Kranz, Gerard CL Wong, and Ramin Golestanian. Multicellular self-organization of p. aeruginosa due to interactions with secreted trails. *Physical review letters*, 117(17):178102, 2016.

[8] Pushpita Ghosh, Jagannath Mondal, Eshel Ben-Jacob, and Herbert Levine. Mechanically-driven phase separation in a growing bacterial colony. *Proceedings of the National Academy of Sciences*, 112(17):E2166–E2173, 2015.

[9] Yoav Tsori and P-G De Gennes. Self-trapping of a single bacterium in its own chemoattractant. *EPL (Europhysics Letters)*, 66(4):599, 2004.

[10] Ankush Sengupta, Sven van Teeffelen, and Hartmut Löwen. Dynamics of a microorganism moving by chemotaxis in its own secretion. *Phys. Rev. E*, 80:031122, Sep 2009.

Chapter 7

Discussion and future works

My research activity focused on the investigation of the systems of active particles, which commonly exhibit a transition from a homogeneous to a phase-separated state as the strength of their motility increases. This is an out-of-equilibrium phase transition, and examples are ubiquitous in the biological world.

While this transition might originate from common underlying physical mechanisms, there are undoubtedly many important system specific features. In my thesis, I have investigated both the active Brownian Particle model, the de facto prototypical active particle model systems, and a much more complex and refined model which I designed to describe the early stage formation of microbial biofilms.

The first part of my thesis has been devoted to the investigation of the active Brownian particles(ABPs) model. The model is reviewed in Ch. 2. In this chapter, I have also discussed the two theoretical approaches that have been put forward to rationalize the microscopic origin of the activity induced phase separation. These are the kinetic and the continuous methods. I have clearly attributed the phase separation to different microscopic processes. These theory give contrasting predictions and thus, are unable to quantitatively predict the spinodal line of ABPs in the activity, density plane. In the following Ch. 3, I have introduced a new model to predict the phase diagram of ABPs. In particular, the spinodal line is predicted by balancing physical processes that promote the growth of density fluctuations, and physical processes the suppress these fluctuations. The theoretical description of all of these processes have been refined with respect to previous attempts conducted in the literature. In addition, I have identified a new physical process responsible for

the suppression of density fluctuations, which originates from the ability of driven particles to resolve their collisions by sliding off each other. The model correctly describes numerical simulations, in both two- and three-dimensions, as well as for different values of other control parameters. See e.g. Fig. 3.4 on page 46. I believe that this is an important result, that settles a discussion in the literature by clarifying what are the physical processes at work in the prototypical model of active particles.

Chapter 4 considers an extended ABPs model, in which the interaction between the particles is frictional. This is an important modification to the model, which is relevant in experiments of dry active matter. Recent results on the behavior of sheared colloidal suspensions suggest that friction could also be relevant in the case of wet active matter, further motivating my investigation. When two frictional particles interact, they exert a torque on each other, which changes the direction of their self-propelling directions. I have demonstrated that this coupling does not promote any alignment of the self-propelling directions, e.g. as observed in the fishes school. However, friction introduces an important qualitative change in the phase diagram, as in it makes the spinodal line to diverge in the zero volume fraction limit, not at a finite volume fraction as in frictionless case. This also occurs in the experiments. I have rationalized the microscopic origin of this qualitative change, considering how friction affects the different physical processes that promote or suppress density fluctuation.

The second part of my thesis has been devoted to developing and investigating a particle based model for the study of the early stage formation of biofilm. We are again considering a system of active particles, the bacteria, that self-propel. However, the physical system is much more complex than the case of ABPs, as bacteria are alive and carry out a number of biological functions that need to be accounted for. Beside moving around, they reproduce, deposit a psl (polysaccharides) trail with which they interact, and extrude eps (extracellular polymeric substances) that form a gel-like network embedding the bacteria. These features, which I have reviewed in Ch. 5, have not been taken into consideration in previous literature works.

In Ch. 6 I have introduced the complex numerical model I have developed to simulate the early stage biofilm formation, detailing how I have modeled motility, reproduction, psl production and interaction, eps production and polymerization.

I have then presented some investigation of the effect of the different control parameters on the development of a biofilm, gradually adding to the model its different complex features. In particular, I have highlighted an interplay between the growth rate and they typical velocity of the bacteria, which controls the shape of the emerging bacterial colonies, and considered the coexistence of bacteria with different motility parameters. I have then presented results for the effect of the psl interaction, and of the eps production. Whenever possible, I compared my results with experimental ones. For instance, I have shown that my model correctly reproduces the emergence of local nematic order in growing colonies, as well as that psl makes the distribution of the number of times a region in space has been visited by a bacterium of power-law type. In addition, my model suggests that in biofilms density fluctuations are enhanced by the production of eps, which effectively acts as a glue between different bacteria. The production of extracelluar adhesion and the interplay between reproduction and mobility could be the explanation of microcolony formation.

In future, I would like to extend my research activities along the two lines I have considered. I have indeed developed a model able to rationalize the phase diagram of spherical active Brownian particles. I would like to explore how this model could be adapted to describe the phase diagram of frictional active particles, which depends on friction coefficient. The current study about frictional interaction is still more focus on the phase diagram. What's more, as we already observed in high density dynamics, friction strongly affect the particle dynamics. Study active jamming with frictional interaction could be an interesting direction. On the other hand, it would be interesting to perform a more thorough investigation of the bacteria model I have developed. In this case, the main difficulty is that of getting reliable experimental data, as microscopic investigation on the development of bacterial colonies are not common, as well as because it is difficult to carry out biological experiments in the same experimental conditions. I do have however set-up collaborations with experimental groups in this line of research, and hope to make progresses in the next future.

Appendix A

Appendix

A.1 Simulation techniques

Computer simulations have become a important tool in physics research nowadays, as Feynman's paper *Simulating physics with computers* predicted in 1981. Computer simulations can fill the gap between theoretical works and experiments, helping us to probe a problem without actually do experiment.

In soft condensed matter physics, simulations are particularly important, as the disorder which frequently characterizes this system make the developing of theoretical model arduous.

This is the same in active matter, a class of out-of-equilibrium systems lacking a description within a well established theory. Before the design of synthetic swimmers, experiments on active system were limited to the observation of the natural bird flocks, fish schooling and herd of animals. The observation method has its limit that it is hard to control the parameters, and to perform repeated experiments. Computer simulations then emerged as an essential tool in this field.

In the literature, both Monte Carlo simulations and molecular dynamic simulations have been used to model active systems. In the following, I will briefly review the molecular dynamics approach, which is the one I followed in my thesis. In the main text, I will further discuss the limitation of Monte Carlo simulations in the context of active systems.

My numerical simulations of active matter have been obtained through a customized modification of the lammps molecular dynamics simulation package. Lammps is a classical molecule dynamics simulator software [1], which can run either on single processors or parallel. We developed our own function under the structure of lammps to realise active force.

Molecular Dynamics (MD) is a type of N-body simulation for studying the physical movements of particles. It essentially consists in the numerical resolution of their equation of motion. The particles can represent individual atoms, several atoms, large molecules or even large scale objects like bacteria. The trajectories of the particles are determined resolving their Newtons equations of motion, and the forces between particles are calculated by using inter-atomic potential or other external force fields. The basic idea of MD is simple: one integrates Newtons equation $F = ma$. The steps are:

(1) Create an initial configuration

(2) Calculate forces from positions

(3) Use the velocity v, and the acceleration $a = F/m$, to determine the position and the velocities at times $t + dt$, given their values at time t.

(4) Calculate any average quantities of interest

(5) Go to 2.

The above loop is repeated until desired, or allowed by computational limitations. To update positions and velocities, the Verlet scheme is frequently used. There are many versions of the Verlet algorithm, the most common used is the 'velocity Verlet' algorithm [2], which is also used in LAMMPS:

$$\begin{aligned} \boldsymbol{p}_i\left(t+\frac{1}{2}\delta t\right) &= \boldsymbol{p}_i(t) + \frac{1}{2}\delta t \boldsymbol{f}_i(t) \\ \boldsymbol{r}_i(t+\delta t) &= \boldsymbol{r}_i(t) + \delta t \boldsymbol{p}_i\left(t+\frac{1}{2}\delta t\right)/m_i \\ \boldsymbol{p}_i(t+\delta t) &= \boldsymbol{p}_i\left(t+\frac{1}{2}\delta t\right) + \frac{1}{2}\delta t \boldsymbol{f}_i(t+\delta t) \end{aligned} \tag{A.1}$$

The choice of time integration step is a tricky problem. The time step cannot be too big and too small. Too small time steps will unnecessary slow down the simulation.

But if the time step is too big, the trajectory are not accurately reproduced and the obtained results do not have physical meaning. A good practice to fix the timestep is through the study of the timestep dependence of the energy fluctuations. If there are no growing fluctuations in energy and deviation from equipartition, the time step is suitable.

A.2 List of simulation videos

I will list the relevant videos here with the link and a short explanation.

1. Rotational instability demonstrated in small system size N=500. This video refers to a system with density ($\phi = 0.2$) and Peclet number (Pe = 500). The initial configuration is a steady state configuration reached in the presence of friction. The video shows the evolution of the cluster as friction is removed. The cluster soon dissolve. This video is correspond to the phenomenology reported in Fig. 3.7 URL: https://youtu.be/Vt66x0dsGLE

2. Rotating active cluster with friction, in a system with N=500, density $\phi = 0.2$ and Peclet number Pe = 500. The friction coefficient is $\mu = 0.9$. In this case, the cluster do not dissolve as it rotates. The corresponding phenomenology refers to Fig. 4.8 URL: https://youtu.be/b_SgM9FS8Lg

3. Mechanisms leading to the disintegration of a big cluster:

   - At small Peclet number (Pe = 200), the rotation of a cluster is not obvious. As you see in Fig. 3.8, some small clusters could break from the big cluster and then break into individual particles. URL: https://youtu.be/jjFI9tJowA8
   - Big clusters could fracture into a number of smaller clusters as seen in Fig. 3.9. These occurs, for instance, at Pe = 300. URL: https://youtu.be/EaFHmjNlebg
   - When Pe number is very large (Pe = 1000), clusters continuously break and form. URL:https://youtu.be/2mSYY1o59cg

4. Large frictional ($\mu = 0.9$) systems.

- Cluster is stable in relative at small Pe (Pe = 100) URL: https://youtu.be/7MV25b5z4aI and (Pe = 200) URL: https://youtu.be/mHtGg4JOu-k.
- Rotational instability is seen at large enough Pe number. The instability occurs after a larger timescale. URL: https://youtu.be/4rdqD6DS89k with (Pe = 500), URL: https://youtu.be/CgGJjht4eHo with (Pe = 900).

5. Video from simulations of bacteria.

   - This simulation demonstrate the emergence of nematic order in a system if reproducing non-mobile bacteria, as discussed in Fig. 6.1. URL: https://youtu.be/_brD7-XXBLU
   - Motility dependence microcolony formation processes, as in Fig. 6.3. No mobility URL: https://youtu.be/IBO6xreaKe8, small mobility URL: https://youtu.be/eZdjqvk7BSY, fast mobility URL https://youtu.be/b1epy1512As
   - Simulation with two species as shown in Fig. 6.4. One of the species could move faster,URL: https://youtu.be/754bMRzUSeE
   - Bacteria motion with psl. Stationary microcolonies are seen in the simulation. URL: https://youtu.be/lAYZvULn2tk. We also run two species simulation with psl. psl particles are not shown. URL: https://youtu.be/TPfFfbzI850

References

[1] Steve Plimpton. Fast parallel algorithms for short-range molecular dynamics. *Journal of computational physics*, 117(1):1–19, 1995.

[2] Michael P Allen et al. Introduction to molecular dynamics simulation. *Computational soft matter: from synthetic polymers to proteins*, 23:1–28, 2004.